Grado en Ingeniería Electrónica Industrial

TRABAJO FIN DE GRADO

UNIVERSIDAD DE ALMERÍA

ESCUELA SUPERIOR DE INGENIERÍA

A BIOMECHANICAL MODEL OF THE UPPER LIMB APPLIED TO THE HANDCYCLING

Curso 2015/2016

Alumno/a:

Emanuele Chiodi

Director/es:

Dr. D. Giovanni Legnani

Dr. D. José Luiz Guzmán Sánchez

UNIVERSIDAD DE ALMERÍA
Escuela Superior de Ingeniería

Trabajo Fin de Grado
Ingeniería Electrónica Industrial

UNIVERSITÀ DEGLI STUDI DI BRESCIA
Dipartimento di Ingegneria Meccanica Industriale
Corso di Laurea Magistrale in Ingegneria dell'Automazione Industriale

A BIOMECHANICAL MODEL OF THE UPPER LIMB APPLIED TO THE HANDCYCLING

Un modelo biomecánico de las extremidades superiores aplicado a una bicicleta de impulsión con las manos

Doble Título UNIBS-UAL
Mechatronics for Industrial Automation

Autor: EMANUELE CHIODI

Director: Dr.D. Giovanni Legnani
Codirector. Dr D. José Luis Guzmán Sánchez

Almería (España), Julio 2016

Curso 2015-2016

“Learn from yesterday, live for today, hope for tomorrow.

The important thing is not to stop questioning.”

(Albert Einstein)

TABLE OF CONTENTS

INDEX OF FIGURES

RESUMEN

El objetivo de este proyecto consiste en el desarrollo de un modelo biomecánico de las extremidades superiores para ser utilizado en el análisis de actividades desarrolladas en bicicletas impulsadas con las manos y brazos. Concretamente se han desarrollo dos modelos (2D y 3D respectivamente) para verificar cuál de ellos se ajustaba mejor y aportaba el mejor balance entre simplicidad y fidelidad de captura dinámica del sistema.

El modelo 2D se ha desarrollado en Matlab, mientras que el modelo 3D se ha llevado a cabo en AnyBody Modelling System, que es un entorno de modelado músculo-esqueleto para simulación de sistemas biomecánicos, el análisis de reacciones dentro del cuerpo humano o del cuerpo humano con el entorno.

Destaca que el laboratorio de trabajo *LARIN (Laboratorio di Riabilitazione Neuromuscolare e Biomeccanica delle Attività Motorie Adattate)* se ha establecido como una convenio entre "*Casa di cura Domus Salutis*" en Brescia y la Universidad de Brescia. Este laboratorio ha surgido para promover y desarrollar programas de investigación aplicados a la rehabilitación con especial énfasis en los problemas neurológicos y neurodegenerativos. Gracias a este acuerdo, ha sido posible utilizar instrumentación avanzada y toma de datos de experimentas que han sido la base de los modelos citados anteriormente.

AIM OF THE THESIS

The aim of the thesis consists in creating an upper limb biomechanical model useful for analysing the handcycling activities.

In particular two models have been realized: one 2D and one 3D, to verify which was the best compromise between simplicity and completeness of representation.

The two-dimensional model has been developed in *MATLAB* software environment; instead the 3D one has been accomplished thanks to the *The AnyBody Modeling System:* a musculo-skeletal modelling system for biomechanical simulations, that analyses the reactions within the human body or between the human body and an environment.

The *LARIN (Laboratorio di Riabilitazione Neuromuscolare e Biomeccanica delle Attività Motorie Adattate)* was established as a convention between the "*Casa di cura Domus Salutis*" in Brescia and the University of Brescia, it was born to promote and develop applied research programs dedicated to the world of rehabilitation and adapted physical activity with special emphasis on neurological and neurodegenerative problems.

Thanks to this agreement it was possible to use advanced instrumentations and collect data from experimental trials, in way to produce the models described above.

Figure 1 - LARIN and University of Brescia logos

1. INTRODUCTION

This chapter will describe the main steps developed at the base of the whole thesis:

- Thanks to the previous works developed by Ph.D. students it was possible to use the sensorized hand-bike and collect the data used in the project.
- There will be some sections dedicated to the description of the upper limb's anatomy and some other chapters used to explain the uses of hand-bike in everyday life.
- Another important part will be the summary of the instrumentations, sensors and vision system used to collect data on patients' trial at the *LARIN*.
- Then there will be the real main segment of the study, based on the realization of a 2D model using the software *Matlab* and proved with some empirical evidences on a mechanism realized in the robotics lab and used to substitute the human arm during some passive motion tests.
- Once that the 2D model has been checked through a well-know mechanism, it has been used with the data of the human tests as input, in way to obtain some good results about the kinematics and dynamics analysis of the upper limb motion.
- Finally to have analogous results on 3D movements, other softwares have been used (*OpenSim* or *AnyBody*) and were helpful to judge the validity of the 2D model and have kinematics, dynamics and muscular informations comparable with the *Matlab* project.
  Therefore it has been possible to compare the two modelizations and evaluate the precision and errors of the created model.

2. UPPER LIMB ANATOMY

This chapter gives a general anatomical description of the upper limb to introduce the role of bones, articulations and muscles. This knowledge is essential to develop a biomechanical model of the arm.

2.1 Bones of the upper limb [1] [4]

The main bones considered in in this study are the ones composing the shoulder, the arm and forearm; the bones of wrist and hand are not analysed, because the work is restricted to the movements of the shoulder and elbow articulations.
So the main bones taken into account are:

- *Scapula*: it's a triangular, flat bone, which serves as a site for attachment for many muscles. It articulates with the *humerus* at the *glenohumeral joint*, with the clavicle at the *acromioclavicular joint* and furthermore it can slide over the ribcage. In doing so, the scapula connects the upper limb to the trunk.

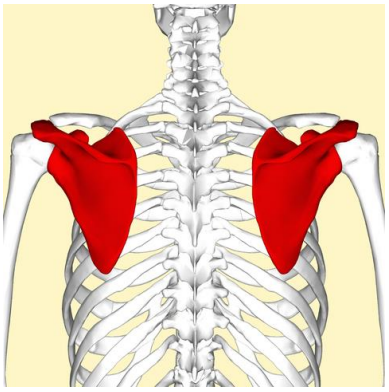

Figure 2 - Position of the scapula

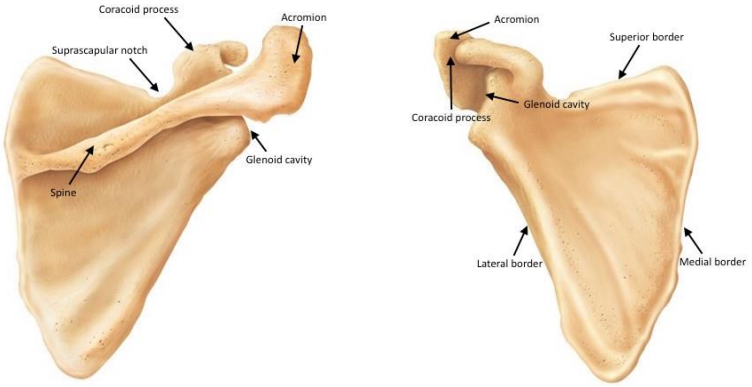

Figure 3 - Posterior and anterior view of the right scapula, with its main recognisable anatomical points

- *Clavicle*: it extends between the *sternum* and the *acromion* of the scapula. It is classed as a long bone, and can be palpated along its length. The clavicle has three main functions:

    - Attaches the upper limb to the trunk.
    - Protects the underlying neurovascular structure supplying the upper limb.
    - Transmits force from the upper limb to the axial skeleton.

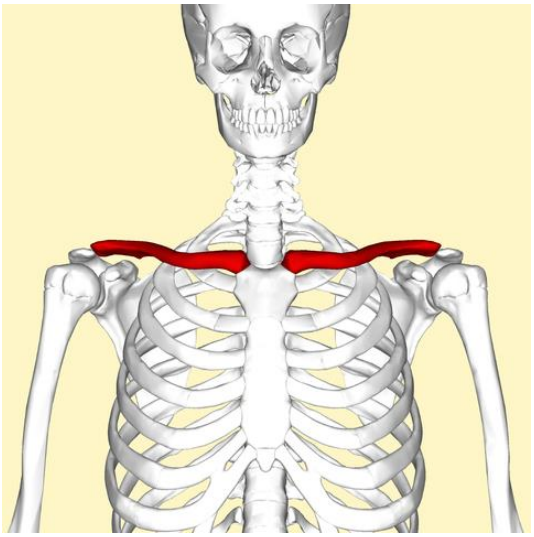

Figure 4 - Position of the clavicle

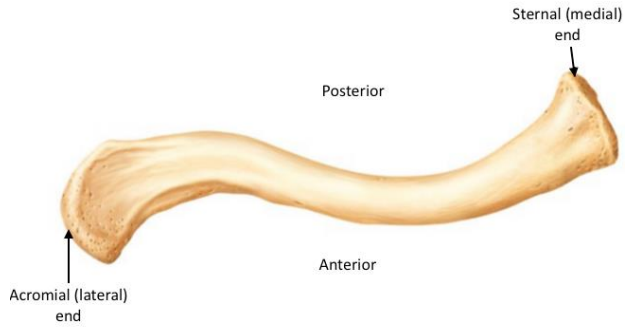

Figure 5 - Superior view of the right clavicle, with its main recognisable anatomical points

- *Humerus*: it's the bone that forms the arm, and joins it to the shoulder and forearm. The *proximal region* articulates with the scapula and clavicle, forming part of the shoulder joint. Distally, the *humerus* articulates with the forearm bones (*radius* and *ulna*), to form the elbow joint.

  The important anatomical features of the *proximal region* of the humerus are the *head* that projects medially and superiorly to articulate with the *glenoid cavity* of the scapula and the *tubercles* and the *intertubercular sulcus* that serve as sites of attachment of muscles like the *rotator cuff muscles* and *biceps brachii*.

  The *shaft* of the *humerus* contains several *tuberosities* that are sites of attachment of many muscles of the shoulder and arm.

The *distal part* of the humerus articulates with the *ulna* and *radius* at the elbow joint; the lateral and medial borders of the humerus form *medial* and *lateral supraepicondylar ridges*, rough zones that are sites of many of the *extensor muscles* in the posterior forearm. Close to these there are the *lateral* and *medial epicondyles*, that can be easily palpated at the elbow and used as *bony landmarks*.

Finally located medially there is the *trochlea* that articulates with the *ulna* and beside it there is the *capitulum* which articulates with the *radius*.

Also found on the distal portion of the humerus are three depressions, known as *coronoid*, *radial* and *olecranon fossae*, that accommodate the forearm bones during the movement at the elbow.

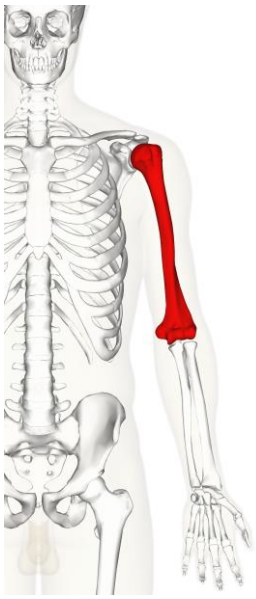

Figure 6 - Position of the humerus

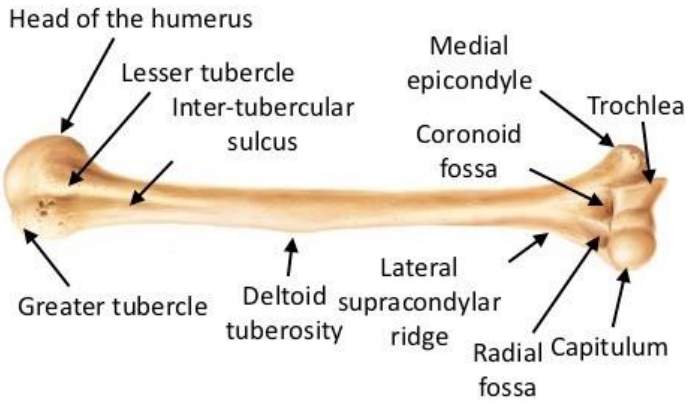

Figure 7 - Right humerus view, with its main recognisable anatomical points (Proximal region on the right, distal region on the left)

- *Ulna*: it is a long bone in the forearm. It lies medially and parallel to the *radius*, the second of the forearm bones. The ulna is stuck, with the radius pivoting to produce movement, and acting the prono-supination. Proximally, the ulna articulates with the *trochlea* of the humerus at the elbow joint. Distally, the end of the ulna is much smaller in diameter than the proximal end and terminates in a rounded head that articulates with the *ulnar notch* of radius, forming the distal radio-ulnar joint.

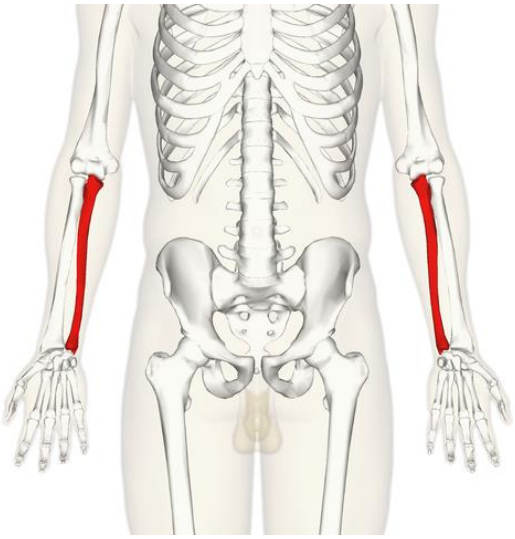

Figure 8 - Position of the ulna

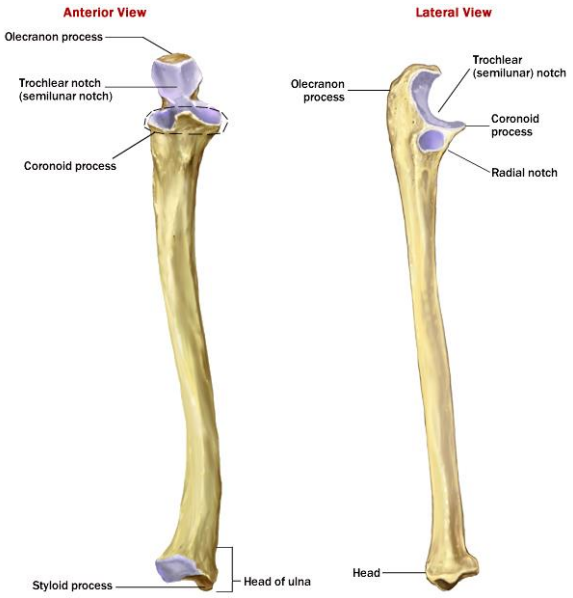

Figure 9 - Right ulna frontal and lateral views, with its main recognisable anatomical points

- *Radius*: it's a long bone in the forearm. It lies laterally and parallel to ulna, it pivots around the ulna to produce movement at the proximal and distal radio-ulnar joints.

  The radius articulates in four places:

  - Elbow Joint: partly formed by an articulation between the head of the radius, and the *capitulum* of the humerus.
  - Proximal Radioulnar Joint: an articulation between the radial head, and the *radial notch* of the ulna.
  - Wrist Joint: an articulation between the distal end of the radius and the carpal bones.
  - Distal Radioulnar Joint: an articulation between the *ulnar notch* and the head of the ulna.

  The proximal end of the radius articulates with both the elbow and proximal radio-ulnar joints; contrary to the ulna, the radial shaft expands in diameter in the distal part, it is triangular in shape (similar to ulna), with three borders and three surfaces.

  In the distal region, the radial shaft expands to form a rectangular end. The lateral side projects distally as the *styloid process*. In the medial surface, there is a concavity, called the *ulnar notch*, which articulates with the head of ulna, forming the distal radio-ulnar joint.

The distal surface of the radius has two facets, for articulation with the *scaphoid* and *lunatecarpal* bones, this makes up the wrist joint.

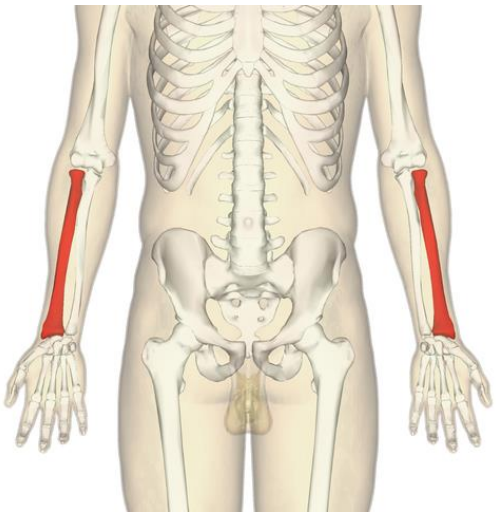

Figure 10 - Position of the radius

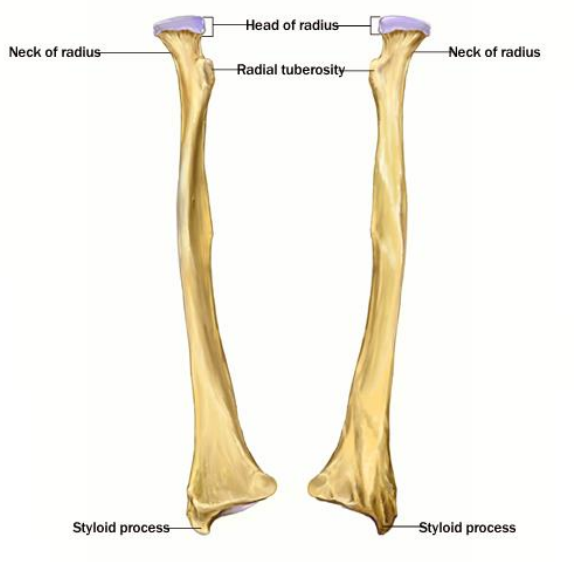

Figure 11 - Right and left radius frontal view, with its main recognisable anatomical points

As explained before we'll focus on the analysis of the movements and features of arm and forearm, therefore of the shoulder and elbow joints, not taking into account the wrist and hand and their relative bones, muscles and joints.

2.2 Articulations of the upper limb [3]

The contact region between two adjacent bones is called *articulation*, from a functional point of view it's possible to classify articulations in three main different groups:

- *Synarthrosis*: bones are connected by an interposed layer of dense fibrous connective tissue or cartilage that don't allow mobility (e.g. junctions of skull bones)
- *Amphiarthrosis*: bone surfaces are covered with a layer of *hyaline cartilage* and are joined by a disc of fibrous cartilage, limited movements are allowed (e.g. some bones of the pelvis)
- *Diarthrosis*: these joints allow significant movements of the limbs, the joint surfaces are covered with *hyaline cartilage*, and enclosed in the *synovial cavity* (e.g. elbow, shoulder, and in wider terms the most part of limbs articulations).

The type of articulation we need to consider for our study is the last one: *diarthrosis articulation*, in particular the joints we want to define are elbow and shoulder ones.
In general this kind of articulation is classified based on the shape of the bones ends and on the possible movements of the joint itself.
In our case the shoulder and elbow are defined by two different *diarthrosis*:

- The shoulder and its *glenohumeral joint* are defined as *enarthrosis*, it can be modelled as a ball and socket joint, and it admits three rotational degrees of freedom: *flexion/extension*, *abduction/adduction* and *rotation*.

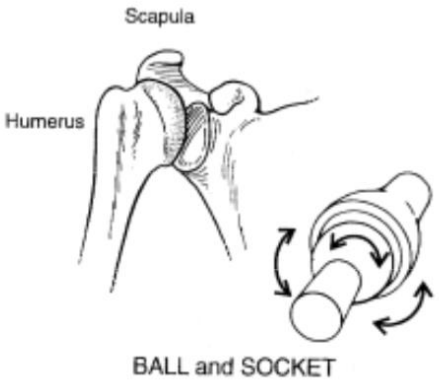

Figure 12 - Approximation of the shoulder joint as a ball and socket joint

- The elbow is a *trochlear articulation*, it's composed by two surfaces: a *trochlea* (shaped like a pulley), that in our case is the distal part of the humerus, and a notch traversed longitudinally by a ride that fits the throat of the trochlea (ulna). This articulation admits, for what concerns our study, just one rotational degree of freedom: *flexion/extension*.
  Actually the axis of the humerus and ulna present a deviation angle of about 10-15° depending on the extended or flexed articulation, this variation is small and it will not be taken into account in the modelization used in this thesis.

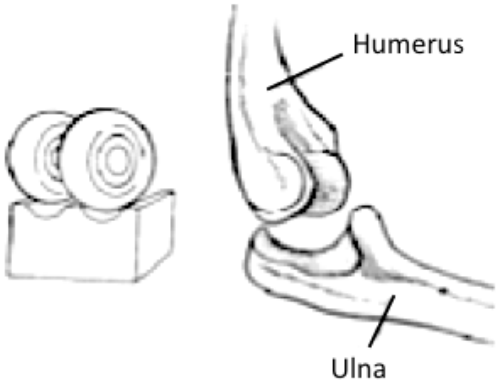

Figure 13 - Approximation of the elbow joint as a pulley and a notch joint

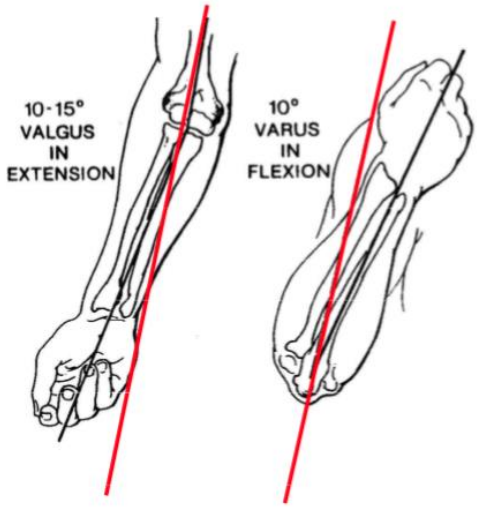

Figure 14 - Deviation angle of the humerus and ulna axis

Actually there is another type of movement generated in the elbow: the *prono-supination* of the hand, that consist in a rotation of the radius around the fixed ulna bone.
This degree of freedom is generally assigned to the wrist articulation, so it's not treated in this study.

Once defined the types of articulation we need to work with, it's also important to give e brief report on possible ranges of motion of these two joints in each degree of freedom in which they can move; it is also important to show the convention for measuring each angle.

Let's start analysing the motion of the shoulder, as written above, it has 3 different degree of freedom:

- *Shoulder Flexion/(Hyper)Extension*: it's in the sagittal plane and it has an amplitude of about [+180°, -50°], the zero is considered as the resting position with the arm laying vertical along the body side.

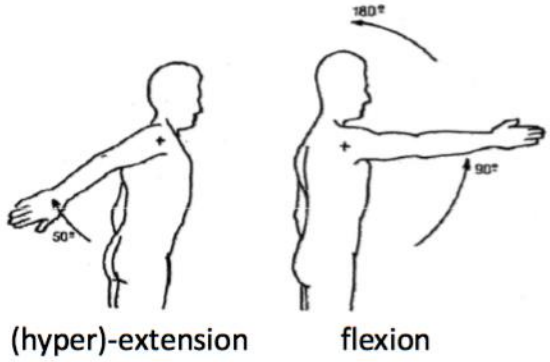

Figure 15 - Shoulder Flexion/(Hyper)Extension range of motion

- *Shoulder Adduction/Abduction*: it's in the frontal plane. *Adduction* is really weak in *protraction* (i.e. through the scapula-thoracic articulation, the shoulder is moving back) and about 30°/40° in *retraction* (i.e. the shoulder is moving ahead); on the contrary *abduction* has a bigger amplitude of motion (about 180°).

  Also in this case the zero is considered as the resting position with the arm laying vertical along the body side.

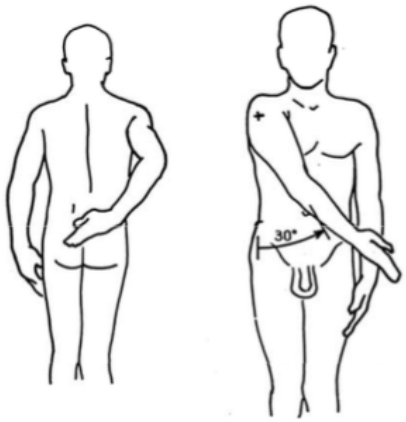

Figure 16 - Shoulder Adduction range of motion

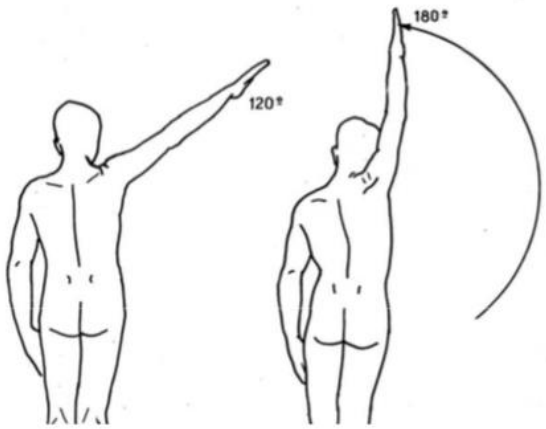

Figure 17 - Shoulder Abduction range of motion

- *Shoulder Axial rotation*: it's about the longitudinal axis of the humerus and with the elbow flexed at 90°, it has a range of motion of about 80° in *external rotation* and 90° in *internal rotation*. The zero is considered as the position with the arm laying vertical along the body side, and the forearm straight in the sagittal plane, with the elbow at 90°.

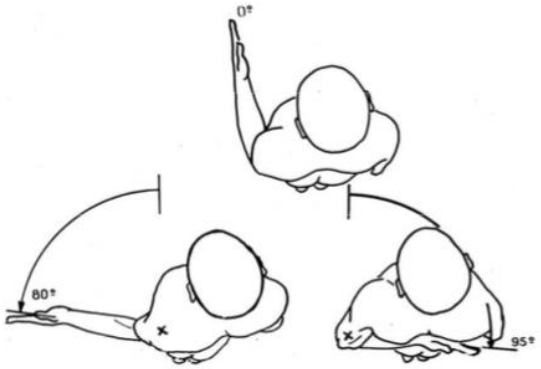

Figure 18 - Shoulder Axial rotation range of motion

The elbow allows *flexion/extension* of the forearm but also the *prono-supination* movement of the hand, but in our case we'll associate this last articular motion with the wrist degrees of freedom. So the elbow joint can be described as follows:

- *Elbow Flexion/Extension*: the axis of the humerus and forearm don't pass through the centre of rotation of the elbow, so that the flexion can reach about 150°. The zero position is considered as the position with the forearm aligned with the arm.

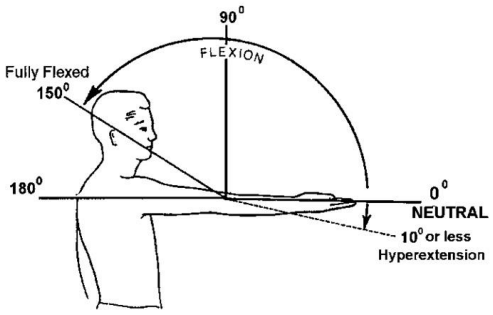

Figure 19 - Elbow Flexion/Extension range of motion

So after having defined all these simplifications of the articulations, the kinematic model of the upper limb can be simplified as these images (Figure 20 and Figure 21) show:

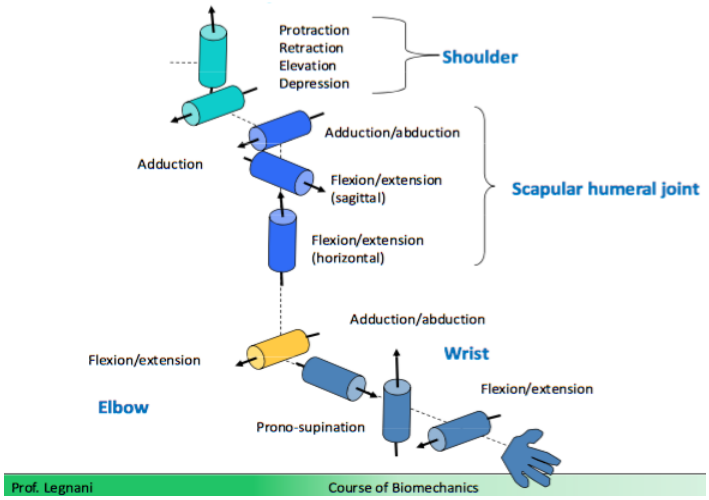

Figure 20 - Simplified kinematic model of the upper limb

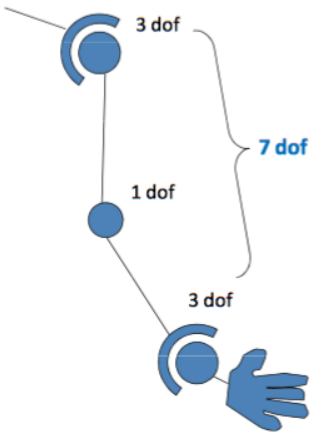

Figure 21 - 7 total degrees of freedom

It's easy to see that we'll consider from now the shoulder as a combination of 3 d.o.f. and the elbow with just 1, putting the remaining 3 d.o.f. at the wrist joint.

2.3 Muscles of the upper limb [1] [4]

For the study that concerns this thesis we'll consider just the main muscles that, from previous publications and thanks to the results of EMG analysis and 3D softwares utilised here, we know as the most used in hand-cycling activity.

2.3.1 Shoulder muscles

The muscles of the shoulder are associated with movements of the upper limb. They produce the characteristic shape of the shoulder, and can be divided into two groups:

- *Extrinsic*: originate from the torso (a.k.a. the superficial back muscles), and attach to the bones of the shoulder (clavicle, scapula or humerus).
- *Intrinsic*: originate from the scapula and/or clavicle, and attach to the humerus.

There are also three muscles that lie in the pectoral region and exert a force on the upper limb, they are the *pectoralis major*, *pectoralis minor*, and the *serratus anterior*:

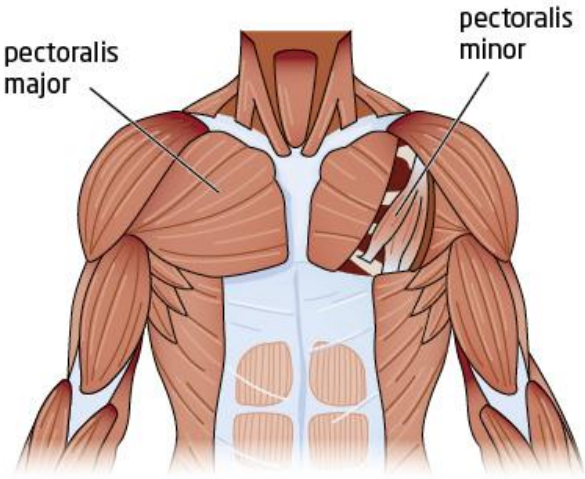

Figure 22 - Position and shape of pectoralis major and pectoralis minor

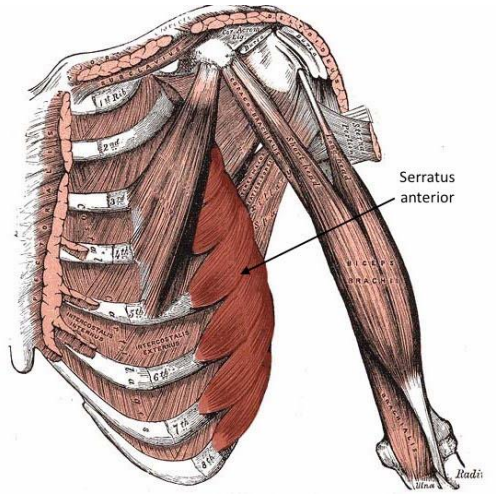

Figure 23 - Position and shape of serratus anterior

The *extrinsic muscles* are organised into two layers the superficial and deep ones, for our study we'll describe just the most superficial muscles because they are used more during hand-cycling:

- The *trapezius* is a broad, flat and has a triangular shape, the muscles on each side form a trapezoid shape and it's the most superficial of all the back muscles.
  Originates from the skull, *ligamentum nuchae* and the *spinous processes of C7-T12 vertebras*. The fibres attach to the *clavicle*, *acromion* and the *scapula spine*.
  The upper fibres of the trapezius elevates the scapula and rotates it during abduction of the arm. The middle fibres retract the scapula and the lower fibres pull the scapula inferiorly.

- The *latissimus dorsi* originates from the lower part of the back, where it covers a wide area. It has a broad origin, arising from the *spinous processes of T6-T12 vertebras*, *iliac crest* and the inferior three *ribs*. The fibres converge into a tendon that attaches to the *intertubecular sulcus* of the humerus. The main actions are to extend, adduct and medially rotate the upper limb.

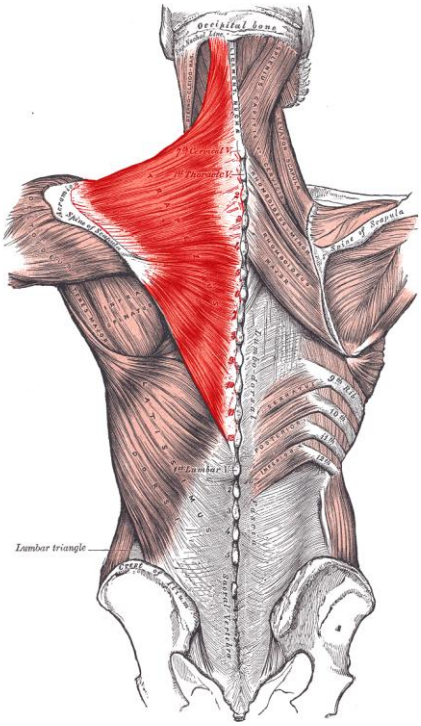

Figure 24 - Position and shape of trapezius

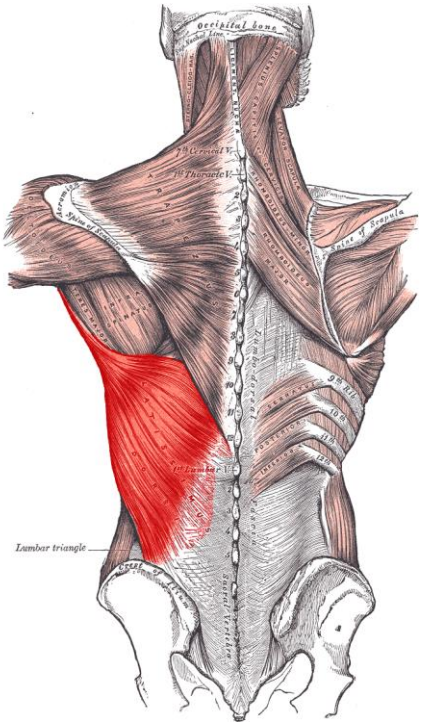

Figure 25 - Position and shape of latissimus dorsi

The *intrinsic muscles* originate from the scapula and/or clavicle, and attach to the humerus; there are six muscles in this group: the *deltoid*, *teres major, supraspinatus*, *infraspinatus*, *subscapularis* and *teres minor*.

We'll describe just four of them because they are the most activated during cycling activity:

- The *deltoid* muscle is shaped like the Greek letter delta (Δ), from which its name derives. It can be divided into an anterior, medial and posterior part; it originates from the scapula and clavicle and attaches to the *deltoid tuberosity* on the lateral surface of the humerus. The anterior fibres produce a flexion movement of the shoulder, the posterior fibres an extension and the middle fibres are the major abductor of the arm.

- The *teres major* originates from the posterior surface of the inferior angle of the scapula and attaches to the *intertubecular groove* of the humerus; it adducts the shoulder and medially rotates the arm.

The following two muscles are part of the so called *rotator cuff muscles*, a group of four muscles that in the resting phase has the function to give to the *glenohumeral* joint an additional stability:

- The *infraspinatus* originates from the scapula, attaches to the greater *tubercle* of the humerus and laterally rotates the arm.

- The *subscapularis* originates from the costal surface of the scapula, attaches to the lesser *tubercle* of the humerus and like *teres major* medially rotates the arm.

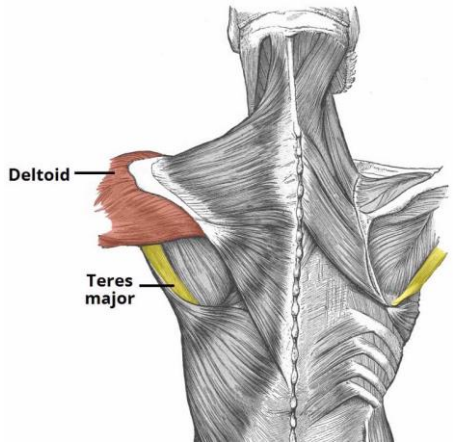

Figure 26 - Position and shape of deltoid and teres major

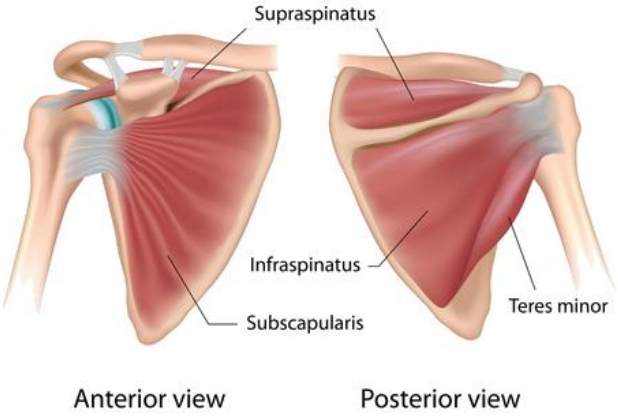

Figure 27 - Position and shape of the 4 rotator cuff muscles

2.3.2 Arm muscles

In this subchapter we'll focus on the muscles that are in the arm, even if there are a lot of other muscles that attach there, for the sake of simplicity we'll describe just the main three.
It's possible to divide the arm into two sections, the anterior compartment and the posterior one; the first two muscles shown below are located in the first compartment, the third muscle in the back part:

- The *biceps brachii* is a two headed muscle and although nearly all of the muscle mass is located anterior to the humerus, it has no attachment to it. Both the long and the short heads originate from parts of the scapula and at the level of the humeral shaft they combine forming the belly of the biceps brachii. Distally, the biceps attaches to the *radial tuberosity*, in a unique tendon.
  The main action of the biceps brachii is *supination* of the forearm, but it also flexes the arm at the elbow and at the shoulder.

- The *brachialis* muscle is positioned deep to the biceps brachii, it originates from the medial and lateral surfaces of the humeral shaft, and inserts into the *tuberosity* of ulna, very close to the elbow joint.
  It's the main *flexor* muscle of the elbow.

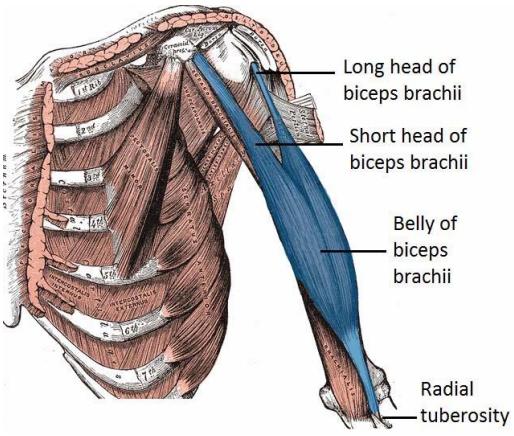

Figure 28 - Position and shape of biceps brachii

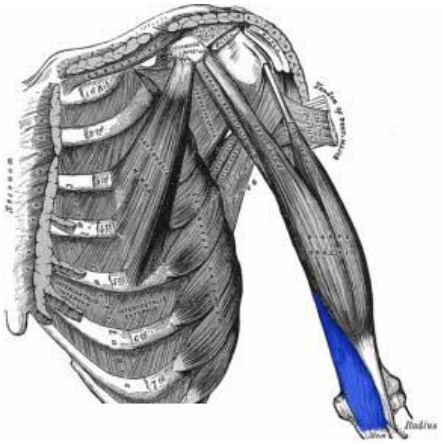

Figure 29 - Position and shape of brachialis

- The *triceps brachii* is the only muscle in the posterior compartment, with three different heads**:** its medial one lies deeper than the other two, which cover it. The long head originates from the scapula (*infraglenoid tubercle*), the other two from the humerus; like in case of *biceps brachii* the three heads converge to make one muscle that attaches to the ulna (*olecranon*). The activity performed by the triceps is to *extend* the arm at the elbow.

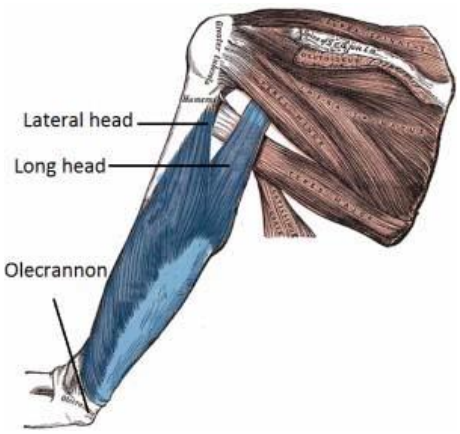

Figure 30 - Position and shape of triceps brachii

2.3.3 Forearm muscles

Also in this case, like the previous one, the forearm can be considered as divided into two compartments: anterior and posterior.
For the aim of our study we are not going to analyse every muscle present in this area, because like outlined before we'll not consider the movements of wrist nor the fingers' motion.
So there will be just a presentation of the ones useful for our analysis.

The muscles in the posterior compartment of the forearm are commonly known as the *extensor* muscles, anatomically they can be divided into two layers: deep and superficial.
The general function of these muscles is to produce *extension* at the wrist and fingers.
We are going to take into account just two of those:

- The *brachioradialis* is a flexor muscle at the elbow, it is most visible when the forearm is half pronated, and the elbow is flexed against resistance.
  It originates from the proximal part of the humerus, and attaches to the distal end of the radius, just before the radial *styloid process*.

- The *extensor carpi ulnaris* originates from the lateral *epicondyle* of the humerus, and attaches to the base of *metacarpal V.* Its main function is to produce adduction as well as extension at the wrist.

The muscles in the anterior part of the forearm are, on the contrary, *flexor* of the wrist and fingers; also in this case we'll dwell on the description of few muscles, in comparison to the number of total located in this zone.
The two muscles considered originates from a common tendon that arises from the *medial epicondyle* of the humerus:

- The *flexor carpi radialis* attaches to the base of *metacarpals II* and *III*, its function is to flex and abduct the wrist.

- The *pronator teres* attaches laterally to the mid-shaft of the radius and it's an important muscle in the *pronation* of the forearm.

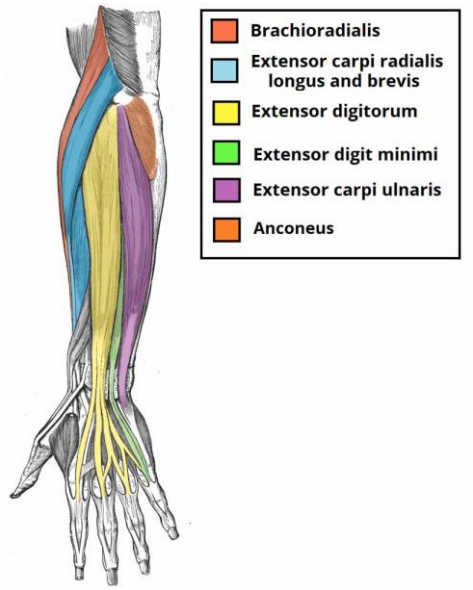

Figure 31 - Muscles of the posterior forearm

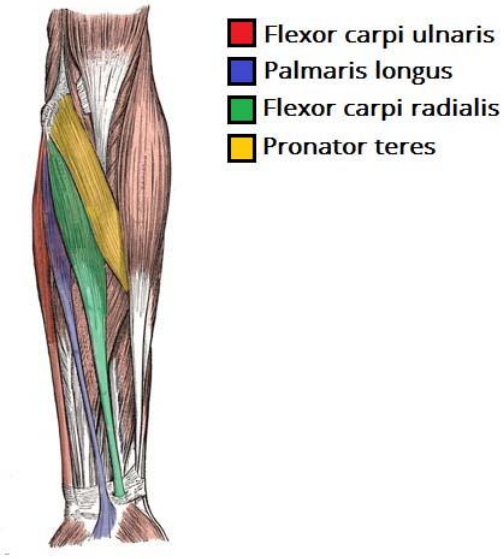

Figure 32 - Muscles of the anterior forearm

3. THE HANDBIKE [8]

This chapter describes the main characteristics of the handbike. A *handcycle* is a type of human-powered land vehicle driven by the action of the arms, for that it is often used by people with limited mobility in the lower limbs. This device is constituted by a rigid frame to which are connected three wheels: two driven posterior wheels and a frontal one, that provides the traction and steering. Despite usually having three wheels, they are also known as *handbikes*.

Figure 33 - Paralympics handcycle race

The motion is transmitted from the arms to the ground through a system of two cranks, which are connected to the driving wheel through a chain. The handbikes are equipped with braking and gearing systems similar to the classical bicycles' ones.

Once the cranks were *asynchronous* as on normal bicycles, but currently the solution of *synchronous* pedalling is preferred, because it has the advantage that the cyclist has to tolerate balanced efforts in the arms, so it's going to load more evenly the bust and back; also with regard to the march stability, it has good effects minimizing the swings due to the cranking asynchrony.

As it regards the materials, also on handbikes, like for the conventional bicycles, it has passed from the steel to the experimental titanium alloys, from aluminium up to the current carbon fibre that has remained now the only material employed.

Handcycling is becoming increasingly popular for recreation and sport. Studies have shown that the handbikes are more mechanically efficient than propelling a hand-rim wheelchair system, because the handcycling system provides for more continuous arm motion and power transfer.
Physical demands are decreased as larger and more muscles are used in the upper extremities; cranking a handbike typically results in higher speeds or longer durations than propelling a manual wheelchair.
There are three different types of handbike that are classified according to the user's sitting position:

- *Upright handcycle*: is for recreation only. It's relatively slow because the upright sitting position creates greater wind resistance and lower mechanical efficiency. These handcycles have a higher risk of tipping compared with the other types of handbikes because their centre of gravity is higher. However, upright handcycling is a good first step to learn the synchronized propelling pattern. Steering and getting in and out of it are more manageable.

  Generally the cranking system should be set up below the shoulder height of the rider to allow gravity to assist propulsion, but not so low that the pedals and the steering system bump into the user's legs.

Figure 34 - An example of the upright handcycle

- *Recumbent handcycle*: can be propelled fast enough for racing and are used in the *Paralympics*. Users lie back in a highly reclined position with the legs forward. The seat position is lower than the previous type of handbikes described, with the seat just a few centimetres off of the ground. The cranks are brought close to the trunk to make greater use of the pectoral muscles, which provides better ergonomics in the cranking movement. Similar to upright handcycles, a lower-positioned cranking system provides gravity assist with propulsion. There are two types of recumbent handbikes:

    - A *fork-steering* handcycle that turns via rotation of a shaft connected to the fork holding the front wheel.
    - A *lean-steering* handcycle has the steering axis in the middle of the frame and turning is accomplished by the user shifting his own body weight.

  It may take longer time to learn how to operate a lean-steering handbike than a fork-steering one, but the first one has the advantages to be more efficient and smoother in turning compared to the second described. However, the lean-steering system is less stable at high speeds and requires better trunk control and balance.
  The handbike used in our study belong to this group of devices.

Figure 35 - An example of the recumbent handcycle

- *Kneeling handcycles*: are essentially for racing. The rider assumes a position where the legs are hidden under a small seat. This positioning is similar to that used in racing wheelchairs. The user leans forward to turn the cranks, allowing the rider to use body weight as well as upper-body strength to propel the handcycle. The centre of the cranks should be about at the middle of the abdomen to allow the user to use the trunk movement to push the cranks forward and then use the shoulder muscles and biceps to pull the cranks.

Figure 36 - An example of the kneeling handcycle

Several studies about the comparison between the different types of handcycles have been published during these years, especially on the effects of these different configurations on the loads applied to the shoulder (a critical factor in wheelchair use) and on the different ranges of motion of each articulation. In particular these analysis were comparing different types of devices but also different configurations on the same handbike, to evaluate the effects and the importance of the changes of the backrest and of the cranks hub positions. [9] [10]

4. LABORATORY WORKPLACE

This chapter contains the description of the workplace in which the experimental data used in this study have been collected, in particular we'll focus on three main parts:

- The system (ergometer) through which it's possible to apply a resistance on the driving wheel, so as to set the intensity of the training and the power produced.
- The force sensor positioned in the left handle of the handbike, to capture the exchanged forces between the subject and the crank.
- The vision system and the superficial EMG, thanks to which it's possible to have information about the kinematics of the patients and the muscles utilized during the tests.

This instrumentation and devices are located in the rehabilitation centre of *LARIN* in Brescia.
All the system described below was created and tested in a previous work of master thesis and Ph.D., it has only been used to obtain the data to use as input of our whole analysis; for this reason we'll limit ourselves to a concise report of the work previously conducted.

4.1 Generation of the work: the ergometer [11]

The power produced by the pedalling test is controlled by the way of a system called *ergometer* that is able to adjust the required power by the examined subject, in certain posture and speed conditions.
This system consists in a chain connected to an unused pinion of the driving wheel, through which the motion is transmitted to an inertial and resistant load.

The system that allows to adjust the workload uses a *brushless* motor controlled in torque uswd as a *brake*. The value of the resistant torque is calculated based on the value of power that has been established during the initial setting part of the test.

The motor is connected to two free wheels that give to the test an important security aspect: they prevent the back rotation caused by the engine and/or the entrainment of the handles.

The system must be activated by the same action that moves a handcycle, therefore a handbike with no wheels was mounted on a structure made of aluminium bars on which was also fixed the system for the generation of braking power. The driving action developed by the subjects is transmitted to the brake system by means of a chain and gear wheels.

The electronic controller that drives the motor is programmed and monitored by a computer using a software.

The commercial systems typically use mechanical or magnetic brakes, on the contrary the innovation here consists in using a brushless motor, appropriately controlled in torque; this gives high flexibility to the system, first of all because the resistant torque applied doesn't depend on the engine rotational speed, as it happens for the traditional brakes; secondly, exploiting the operating possibilities of the brushless motor, it is possible to set several functionalities, also related to the safety of tests.

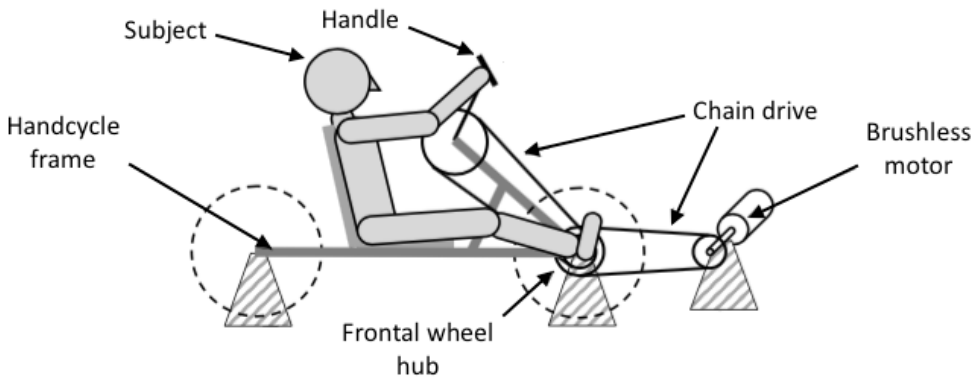

Figure 37 - Scheme of the system

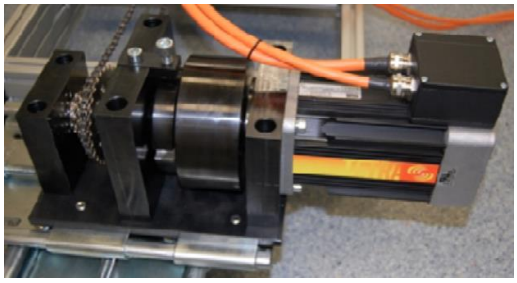

Figure 38 - Detail of the brushless motor

In order to make everything as usable as possible, a control panel has been created using LabVIEW. The user works on the panel shown below, utilized to set and monitor all the parameters of the experimental protocol. It's easy to see that some indicators show the instantaneous cranking speed, the power and the time of the test, facilitating the subject to maintain a regular movement, and the supervisor to set the desired power:

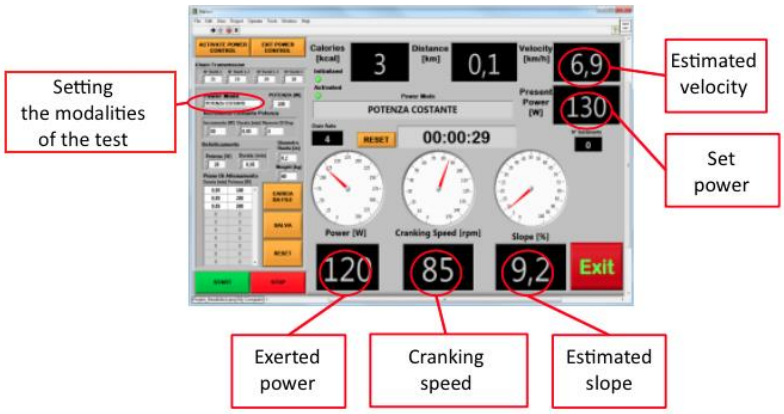

Figure 39 - LabVIEW control panel

4.2 Vision system and superficial EMG

The vision system installed at the *LARIN* laboratory, located at *'Casa di cura Domus Salutis'* in Brescia, is a professional system of the BTS Bioengineering named *BTS SMART-DX 100,* it's used by doctors and researchers all around the world due to the high definitions of the cameras and a great computing power.

It's based on digital cameras that use high sensibility sensors and illuminators with a great radiation power that allows capturing even the smallest movements.

BTS SMART-DX 100 integrates, synchronises and manages all the real-time kinematic, kinetic, electromyographic and video data from connected devices; thanks to the possibility to create a calculation *protocol*, it's easy to reconstruct the movement of the subject just from the data deriving from few markers. [6]

The markers are placed on the patient body in easily recognisable anatomical points, normally they are some *bony landmarks*, that are parts of the bones that protrude and can be palpated under the skin.

In our case we'll have three markers on the subject body: two on the arm, one defining the position of shoulder joint (placed on *acromion*) and another one to identify the elbow (placed on *humerus epicondyle*); the third one's placed on the hip that in our case it's fixed, considering that the laboratory handcycle belongs to the *recumbent* type and the patient is fastened to the backrest with a belt.

Other two markers are placed on the fixed frame of the system (one behind the seat and another one in front) to have landmarks of the reference frame of the vision system.

Last three markers are placed to define the position of the hub of the crank, and of the handle, in particular the second two are place on the top and on the bottom of the handle, so as to make possible the calculation of the inclination angle of it, and derive the forces component like explained in the following subchapter (4.3 Forces exerted on the handle [11]).

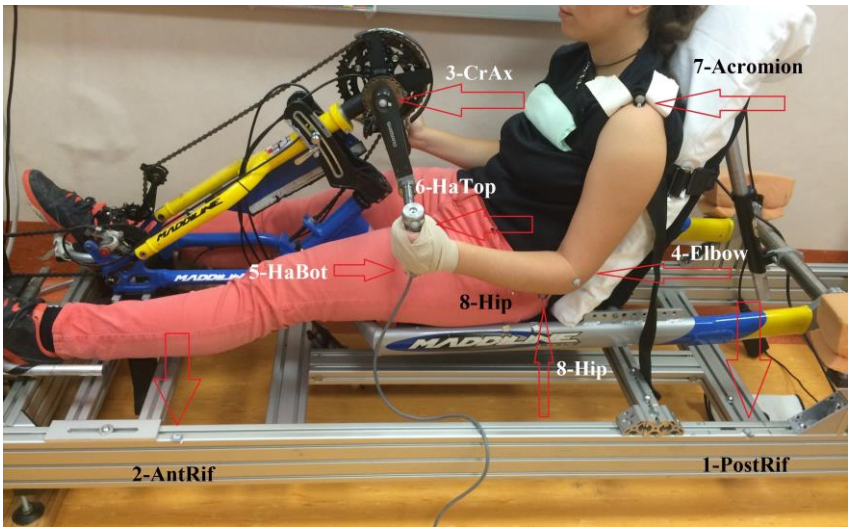

Figure 40 - Markers used during the acquisition

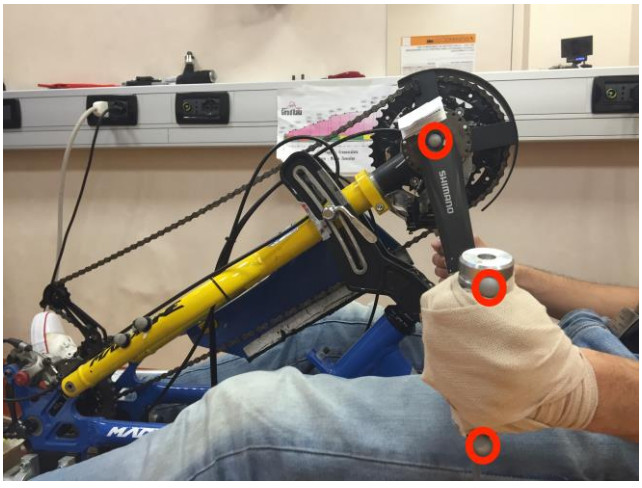

Figure 41 - A detail of the markers used to define the angle of the handle and of the crank

The *BTS SMART-DX 100*, like outlined before, provides also the possibility of analysing the data of *electromyography*; thanks to this potentiality, it was decided to place, with the help of the physiotherapist of *LARIN* laboratory, some surface EMG sensors to investigate the activity of the main exterior muscles of the upper limb.

These sensors are *electrodes* able to provide only a limited assessment of the muscle activity, referred just to the most superficial muscles, but anyway it's a good way to have information about the muscular activation during the tests.

In this case 5 EMG electrodes have been placed: the first one for the *biceps brachii*, the second for the *triceps brachii*, the third, fourth and fifth ones, respectively for the *anterior*, *middle* and *posterior deltoid*.

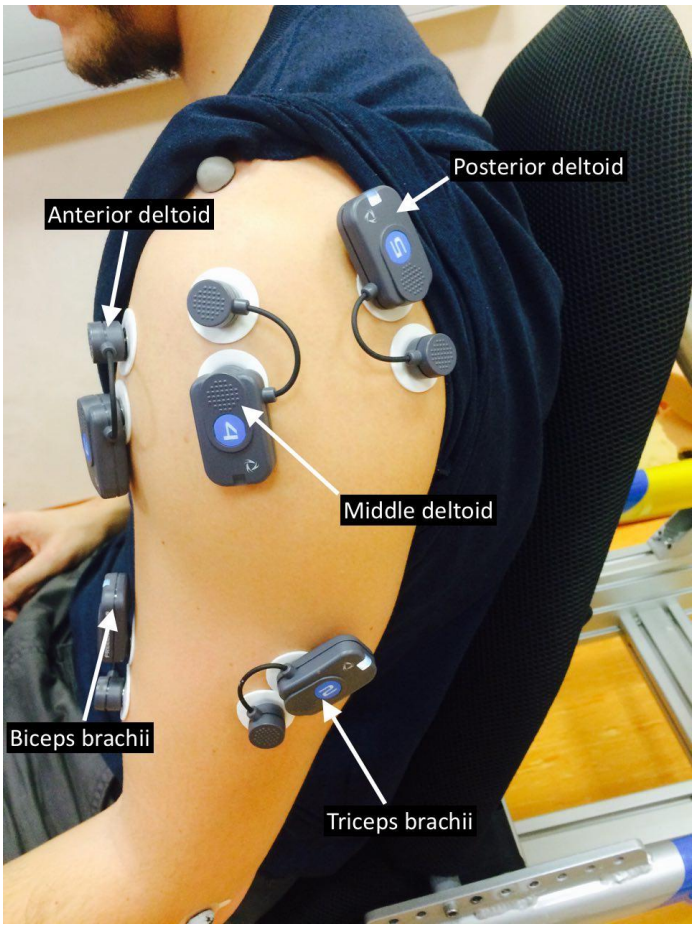

Figure 42 - 5 EMG electrodes used on the main superficial upper limb muscles

4.3 Forces exerted on the handle [11]

All the models of motion and dynamic analysis use data derived from systems analysis and acquisitions: these data contain information on the kinematics, on the forces exerted by the person under examination or on the surrounding environment reactions. Therefore the information on forces exchanged during the pedalling tests is collected through a load cell and strain gauges installed on the left handle of the handcycle, in order to obtain two components of forces: the axial (f_A) to the handle and the normal (f_N) to it.

Then from the two components measured by the force sensor we can find the *tangential* and *radial* component of the forces with respect to the crank; two markers are positioned on the top and the bottom of the handle, by means of the vision system it's possible to establish what is the angle of inclination of the handle compared to the crank one.

Once we obtain the value of those angles we can easily find the component that we prefer to analyse: F_T and F_R of the crank, or F_X and F_Y based on the x and y axis of the vision system reference frame.

In the Figure 43 the force components are shown: in red the axial and normal to the handle, in blue the tangential and normal to the crank and in black F_X and F_Y. α and β are respectively the crank angle and the handle angle obtained through the vision system.

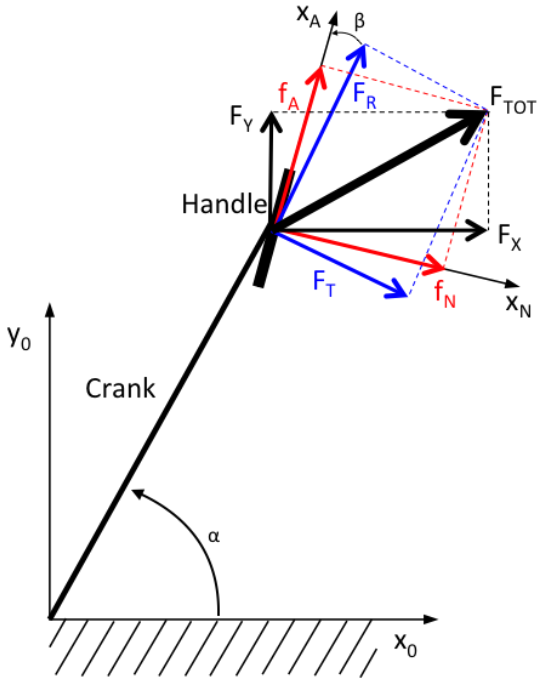

Figure 43 - Force components

Figure 44 - The sensorized handle

5. MATLAB 2D MODEL

Once collected the data of some subjects at different powers, the real part of the work of this thesis started. In this chapter we'll describe rather thoroughly the main parts of the analysis effectuated: starting from the forces and the positions of the markers gathered in the laboratory, a *2D model* of the upper limb have been created using the interactive technical environment *MATLAB*. The main purpose is generally to generate a methodology applicable to several subjects, the following studies are therefore an example of analysis of a healthy young man (25 years old), 1,86 cm tall and with a weight of 80 kg. His cranking activity generates an average power of 40 W.

5.1 Modelization of the upper limb

To use our data in *MATLAB* in a 2D context, we needed to realize an approximation of the upper limb considering it like a combination of two rigid links with a rotational joint between them (elbow joint) and connected to the ground with another rotational joint (shoulder joint).
The lengths of these links have been set from experimental measurement on the patient body parts:

- The length of the link between shoulder and elbow joint has been set as the measured length of arm.
- The length of the second link (after the elbow joint) has been fixed as the distance between the elbow and the mid-hand; we don't study the wrist articulation, for that our forearm is considered until more or less the position of the middle point of the handle (the midpoint of the segment joining the top and bottom handle markers).
- The forearm link is connected with another rotational joint to the crank, the length of which has been experimentally measured.

After these considerations we can consider the whole upper limb and the crank connected like a *four-bar linkage* (Figure 45).

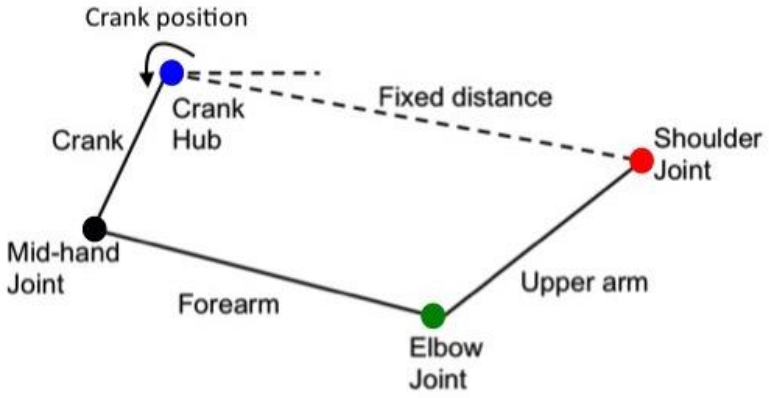

Figure 45 - Approximation as a four-bar linkage

In the Figure 45 we can clearly see that the hub of the crank and the shoulder are supposed as positioned at a fixed distance; that's not true in reality, because the shoulder (identified by the *acromial maker*) makes small movements during the tests, but for the aim of our study we assume the shoulder position as completely stuck, and so the distance set as the mean of the experimentally measures (from markers positions).

The masses and inertias of each part have been estimated using the *anthropometric tables* [5]: measuring the total weight of the subject and his height, they provide an approximation of the weights of the single parts, that are particularly difficult to measure experimentally. Furthermore the anthropometric relations allow to find out the positions of the centres of mass of each body part and their *radius* of *gyration*, in order to calculate the moment of inertia referred to each axis of rotation, and then to each joint.

The approximations of the anthropometry are more valid in case of healthy patients, but when the subjects are disabled the distribution of mass is not like estimated by the tables, so the relations of the masses of each part can't be adequately evaluated.

The people utilized as subjects of this study are non-disabled, therefore the approach described to estimate the physical parameters can be considered valid.

Anyway the real proportion of masses depends on each patient's past history, especially in sports activities, nobody has the same characteristics, particularly trained people in which case some body parts can be more trained and consequently massive than others. The Figure 46 shows the anthropometry scheme commonly used [3] [5].

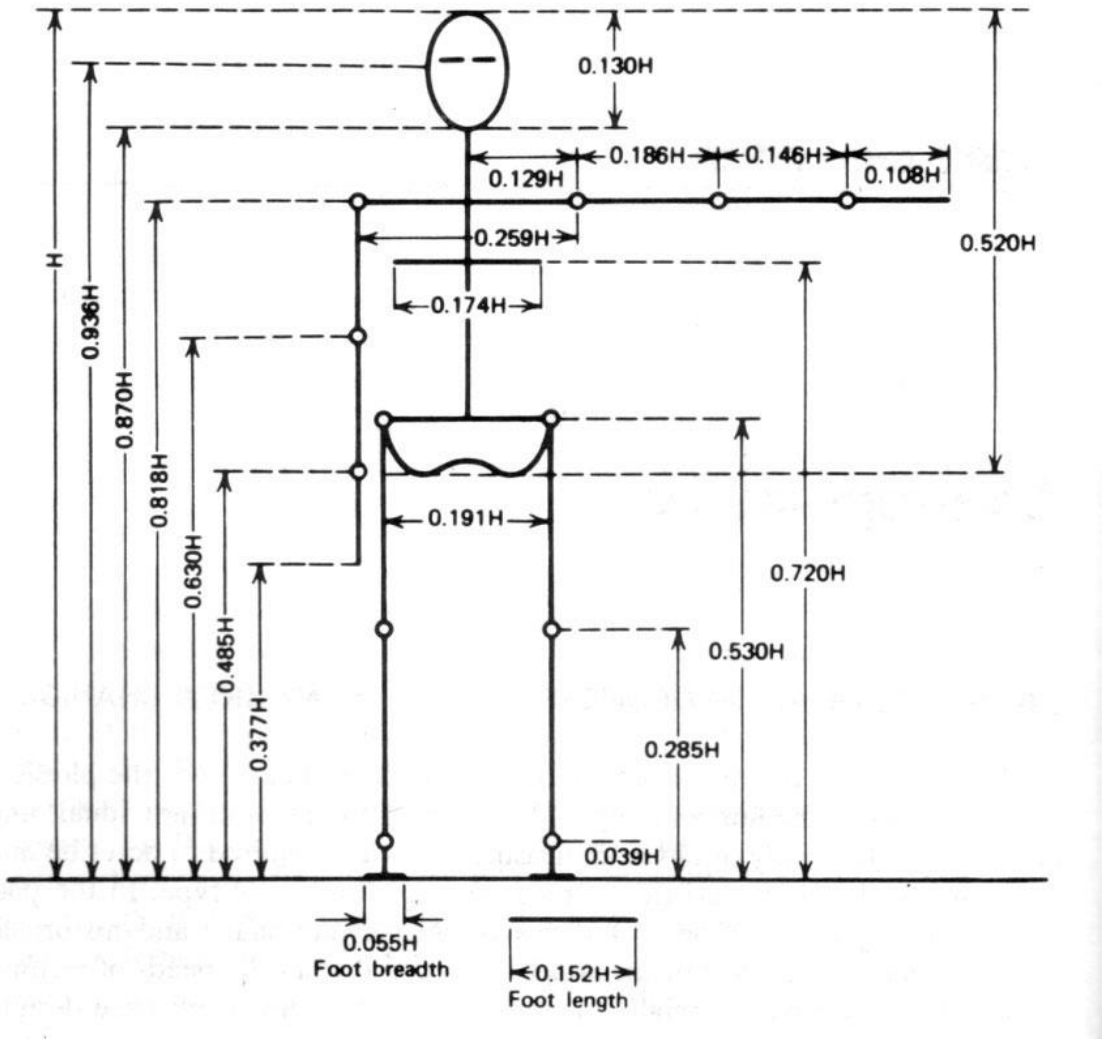

Figure 46 - Anthropometry of the segments lengths

5.2 Data approximation

The data gathered during a single test contained a lot of cranking rotations, analysing a single cycle of pedalling is not very useful in order to obtain a general trend of the motion periodicity.

Therefore it was decided to consider only the data in which the motion had a periodic behaviour, namely, the time interval that can be considered at *operating speed*, not taking into account the *transient* part.

Plotting in *MATLAB* the crank velocity as a function of the crank position we can easily define the cycle, from which we can start considering the data (Figure 47).

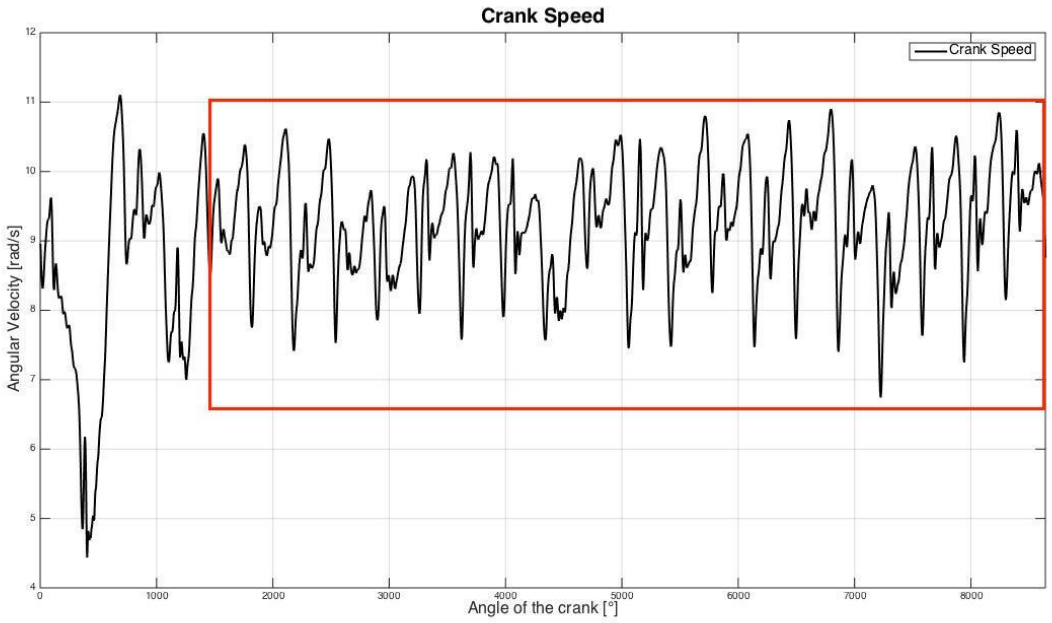

Figure 47 - Crank speed depending on crank position

The Figure 47 shows the evolution of the crank speed during the whole test, the part highlights with the red square is the one at operating speed, in which a periodic stabilization of the velocity is clear. The first 4 cycles are then discarded, the others (in red) considered as input data in the model for the variables: crank position, forces and time.

Once defined the data interval, we decided to approximate the forces and position records with a *'smoothingspline'* using the *MATLAB* function *fit* [13]. The *smoothingspline* produces an approximation of a set of data depending on a parameter that defines the level of smoothing from 0 to 1: the minimum produces a least-squares straight-line fit to the data, the maximum creates instead a cubic spline interpolant. If you do not specify the smoothing parameter, it is automatically setted as 0.99, the best approximating but not interpolating curve (case of this study). Smoothing splines are piecewise polynomials like cubic spline that minimizes the distance from the data with a least square method.

We use this function order to create a new curve, where we don't have a pre-set *sample rate* imposed by the acquisition frequency, but from which we can extrapolate the data with a frequency of our choice. In this way we can easily obtain an average value comparing the records, cycle after cycle, at the same crank position with a discretization step of one degree.

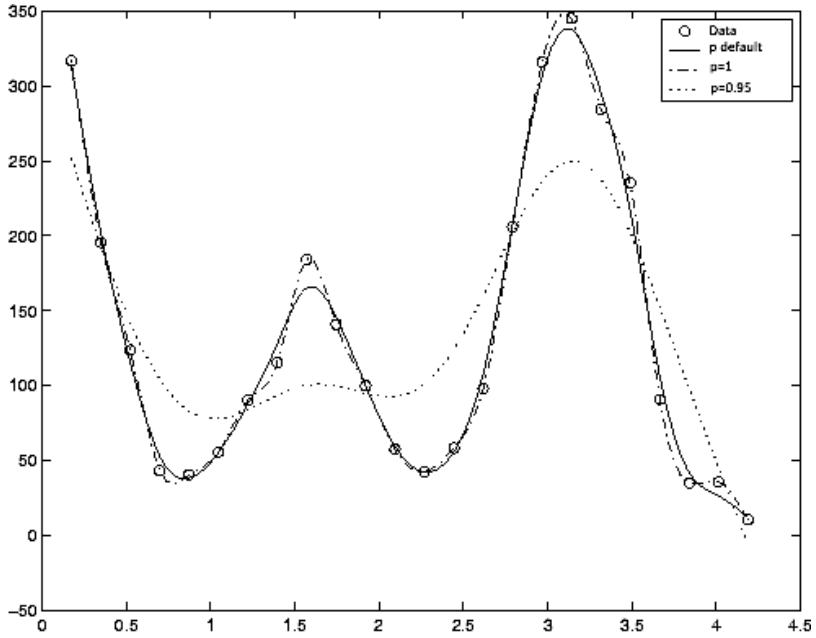

Figure 48 - Example of approximation using the smoothing spline: the dots stand for the data to fit, the dashed line is an approximating spline with a smoothing parameter (p) of 0.95, the point-line curve is the interpolating spline with p=1 and the full line is the approximating spline with p=0.99 (default value)

This solution is also a good method to get an idea of the variability of data during the test, the following figures (Figure 49 Figure 50 Figure 51) we'll shows the variability of crank velocity, F_X and F_Y during the analysed cycles at operating speed.

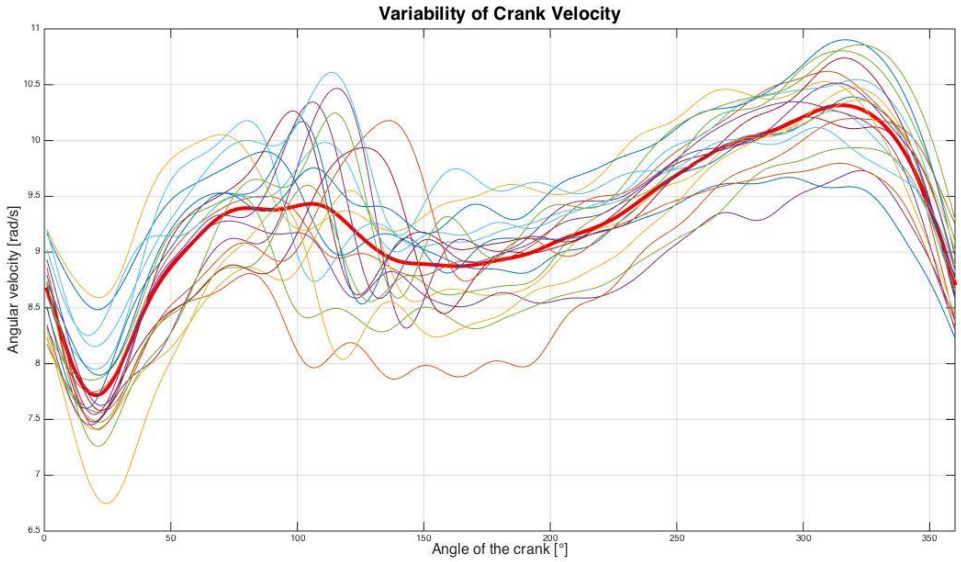

Figure 49 - Variability of crank velocity

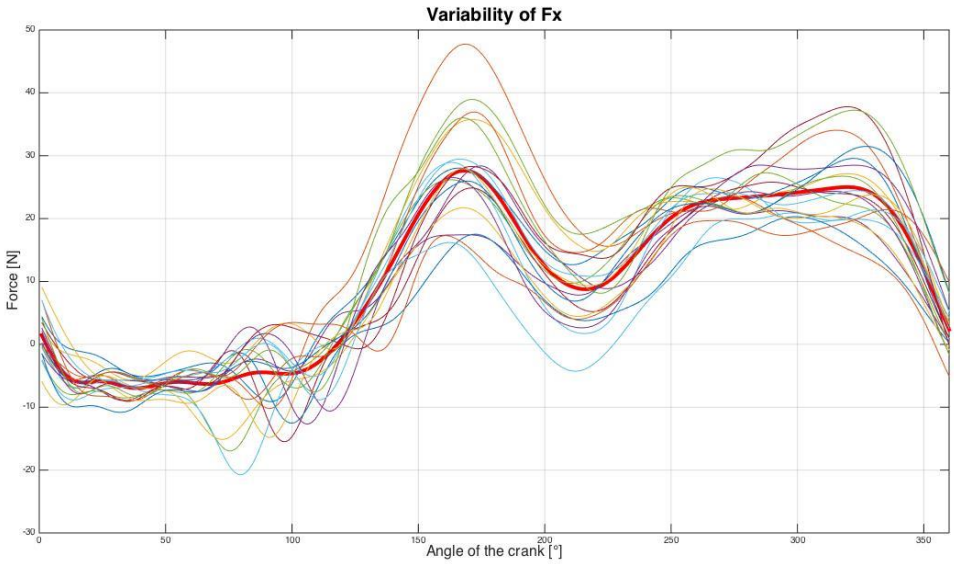

Figure 50 - Variability of F_X

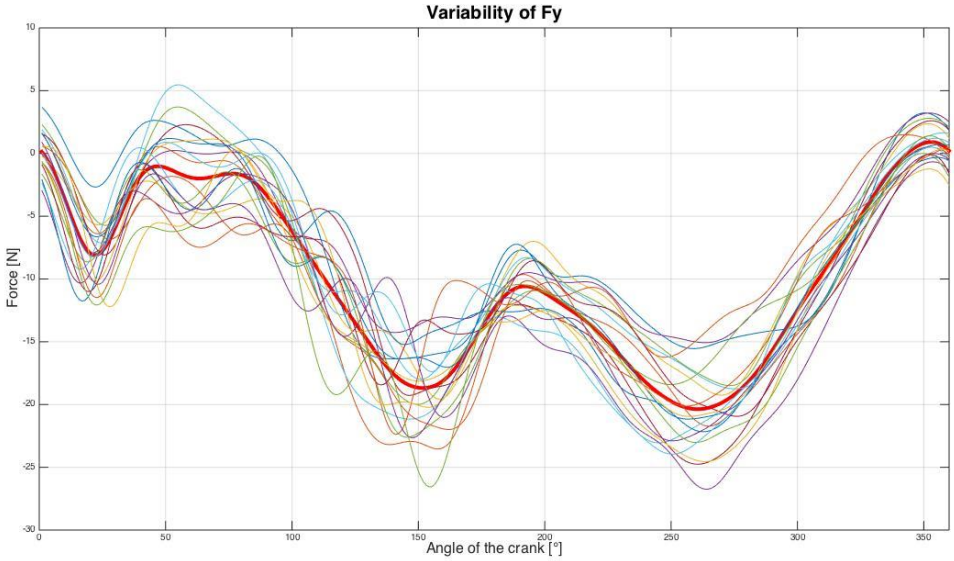

Figure 51 - Variability of F_Y

The average of each variable (crank speed, F_X and F_Y) is represented in red, whereas the approximated data referred to each cycle have been plotted in a different colour.

The mean values of these three smoothed parameters will be from this moment the inputs of the *MATLAB* model described in the next subchapters.

5.3 Kinematic 2D analysis

The procedure described in this subchapter has the aim to solve the *kinematics* of the modelized upper limb.

We decided to use the kinematic equations used in the case of the *SCARA robot* to find the joint coordinates at the shoulder and elbow, we'll call them respectively α and β.

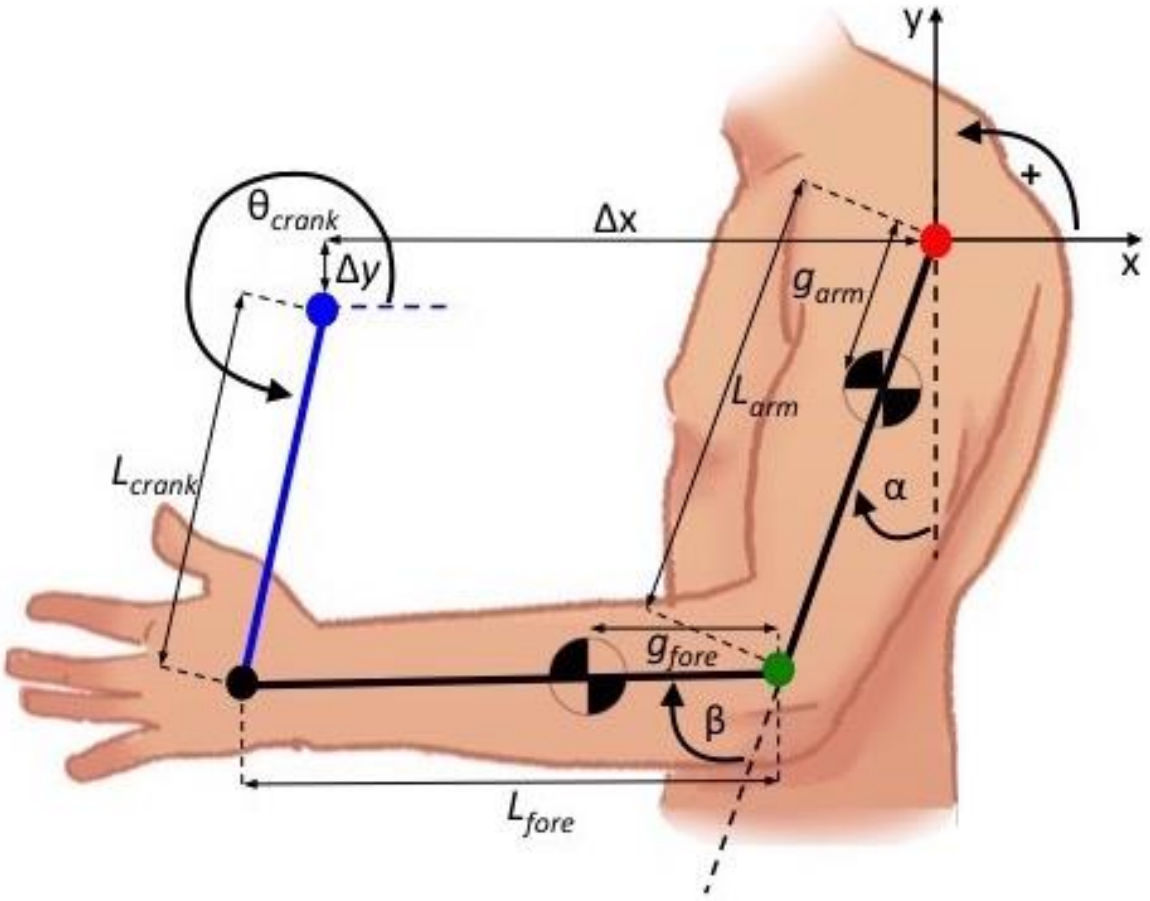

Figure 52 - The parameters of the model created

The Figure 52 defines the variables of the kinematic analysis (α and β), the lengths of the forearm, arm and crank (respectively L_{arm}, L_{fore} and L_{crank}), the angular position of the crank θ_{crank}, g_{arm} and g_{fore}: the proximal distances of the centres of gravity of arm and forearm, and finally Δx and Δy which stand for the fixed distances along x and y axis between the shoulder and the crank hub.

The model reference frame has the sign convention shown in the Figure 52 and its origin is in the shoulder point (red dot), that we assumed as stuck.

Starting from these data we can easily find the handle position in function of the crank angle:

$$\begin{cases} x_h = L_{crank} \cdot cos(\theta_{crank}) - \Delta x \\ y_h = L_{crank} \cdot sin(\theta_{crank}) + \Delta y \end{cases} \tag{5.3.1}$$

Once we have obtained the position of the handle in the main reference frame, we can apply the equations that define the inverse kinematics of the *SCARA robot* [12]:

$$\begin{cases} \beta = \pm acos\left(\dfrac{{x_h}^2 + {y_h}^2 - {L_{arm}}^2 - {L_{fore}}^2}{2 \cdot L_{arm} \cdot L_{fore}}\right) \\ \alpha = atan2(y_h\,, x_h) - atan2\big(L_{fore} \cdot \sin(\beta)\,, L_{arm} + L_{fore} \cdot \cos(\beta)\big) \end{cases} \tag{5.3.2}$$

L_{arm} and L_{fore} are the arm and forearm lengths; x_h and y_h the handle positions; α and β the angles at the shoulder and elbow respectively.

The values of those two coordinates can be graphed in *MATLAB*, in function of the crank position θ_{crank}, Figure 53.

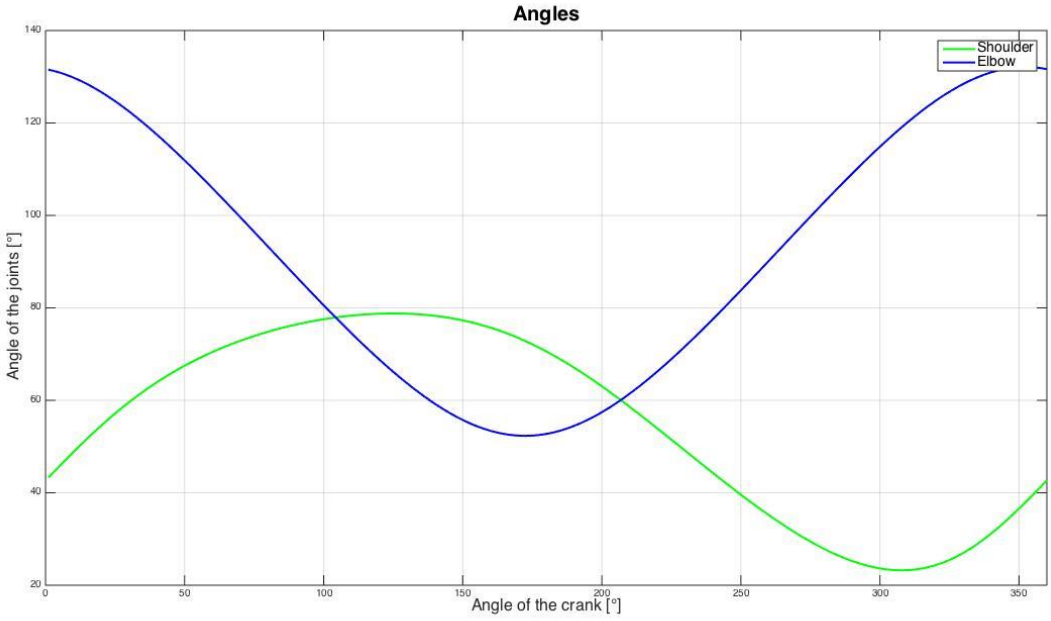

Figure 53 - Calculated α (in green) and β (in blue)

We will show now, in contrast with these calculated data, the experimental angles projected in 2D from the real acquired markers position (Figure 54-Figure 55-Figure 56).

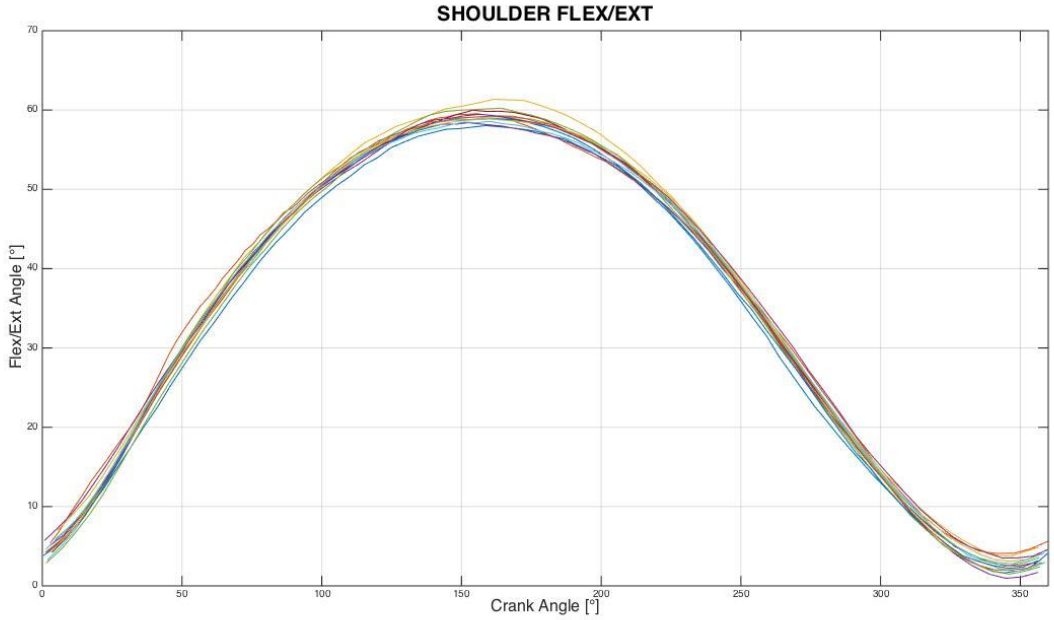

Figure 54 - Variability of the projection in 2D of the shoulder angle of flexion (α)

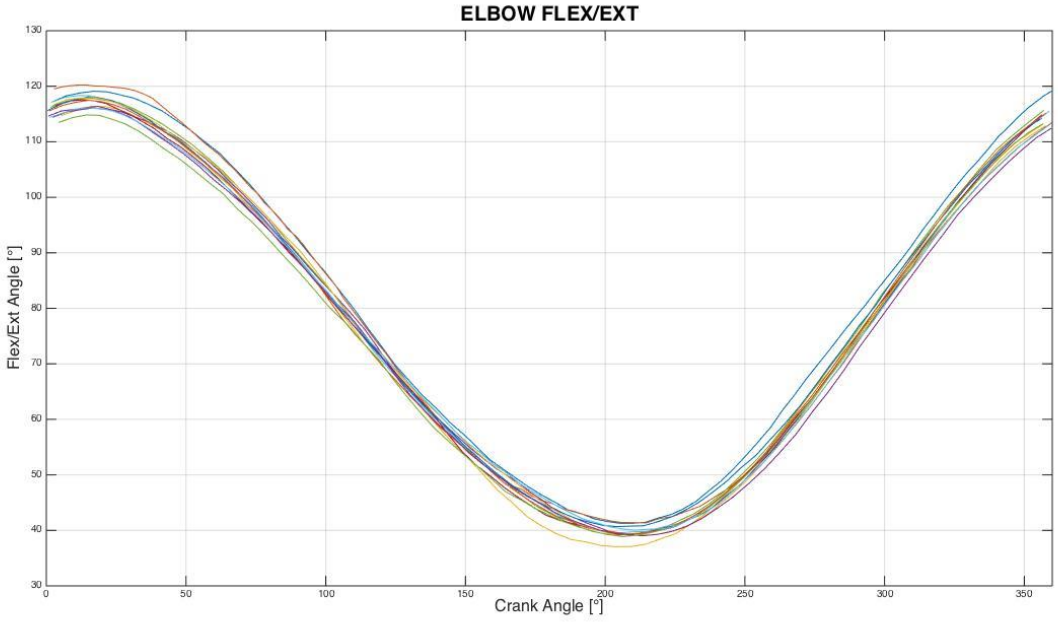

Figure 55 - Variability of the projection in 2D of the elbow angle of flexion (β)

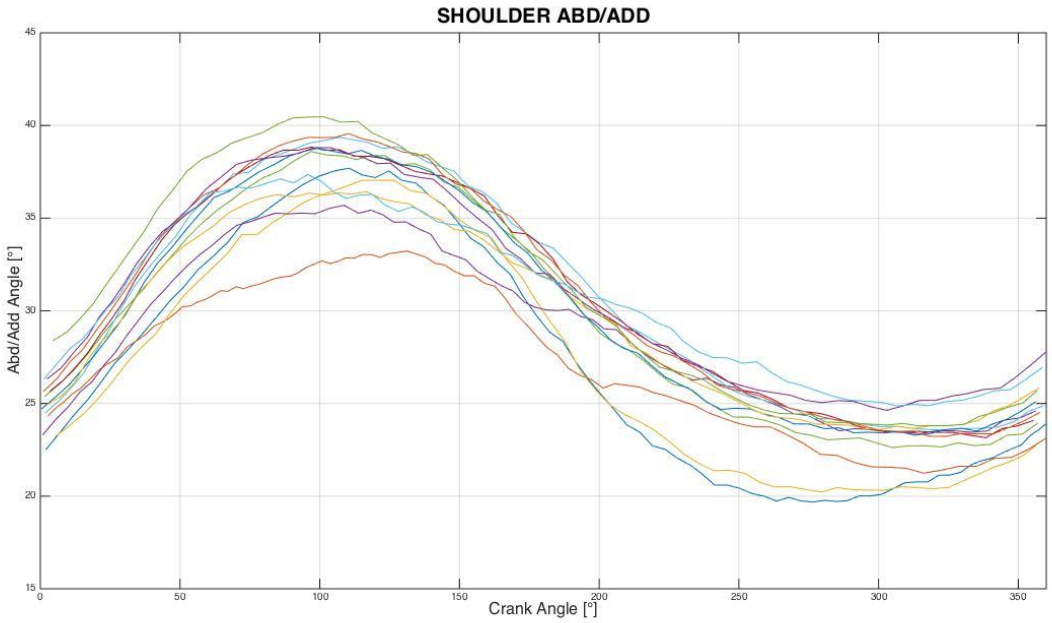

Figure 56 - Variability of the projection in 2D of the shoulder angle of abduction

These figures show that there is a low variability in shoulder and elbow flexion during the cycles analysed, but we can't say the same thing about the shoulder abduction, that is evidently harder to control.

From the experimental data we found the angles, projecting the markers position, along the axis of the reference frame, like shown in Figure 57 and Figure 58.

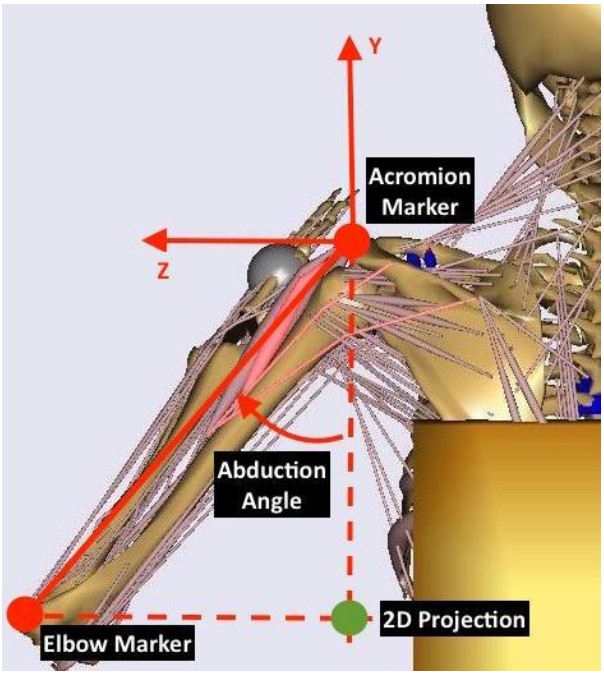

Figure 57 - Projection of markers to find abduction angle

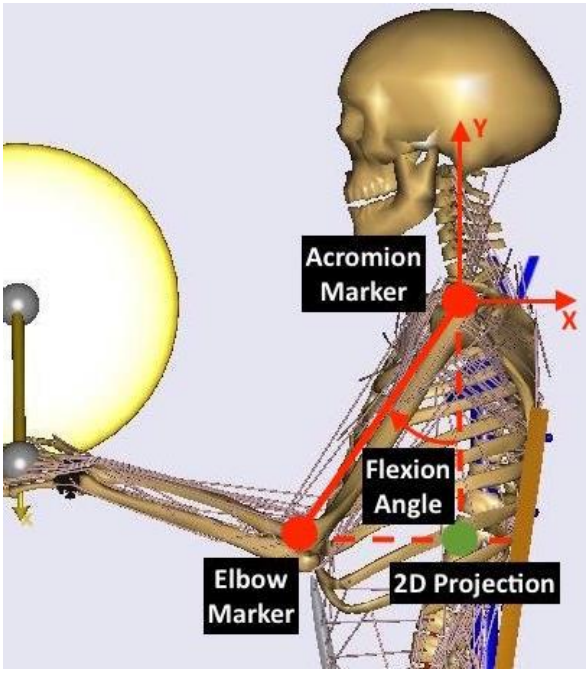

Figure 58 - Projection of markers to find flexion angle

Figure 57 and Figure 58 show what we meant when we talked about projections, starting from the coordinates of the acromion and elbow markers, we could project the movement in 2D in Y-Z plane in case of abduction or in X-Y plane in case of shoulder flexion, in order to easily find the angles with trigonometry.

The assumption that the shoulder has to be fixed, can affect the total result of inverse kinematic, because actually the *acromial marker* is moving like the Figure 59 display.

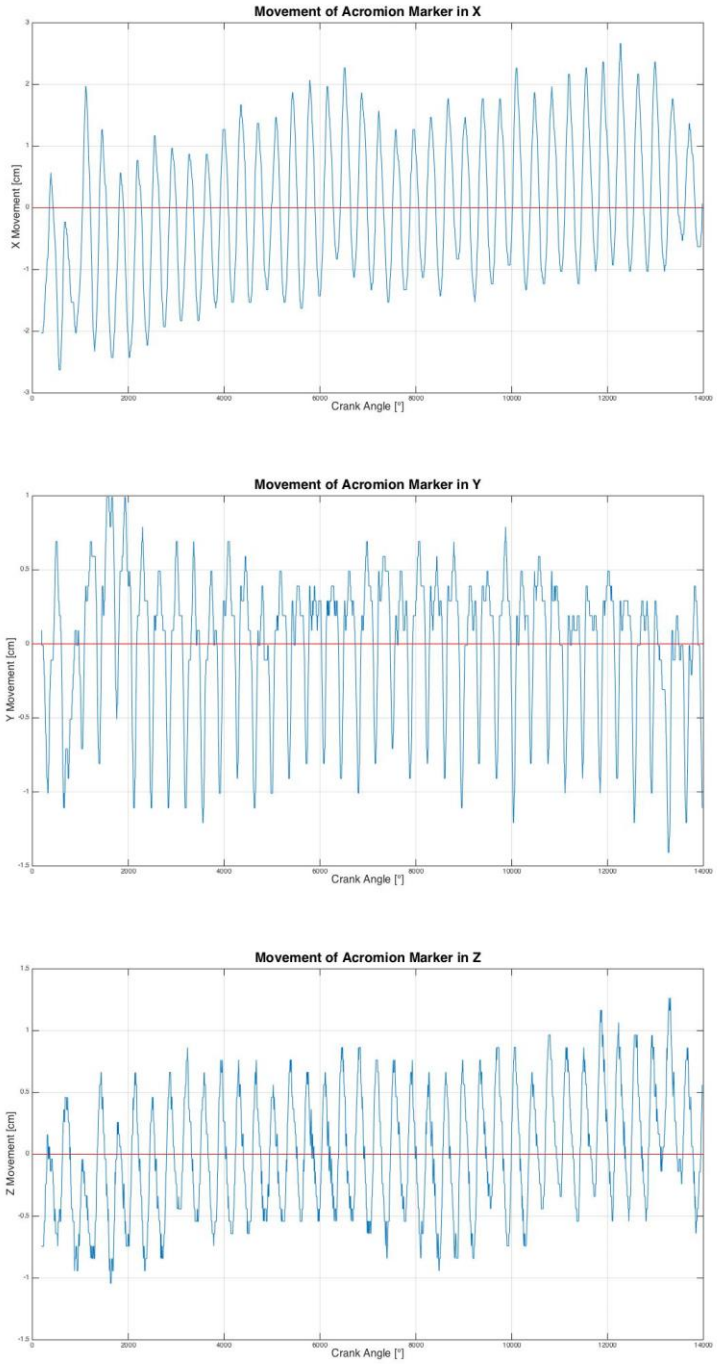

Figure 59 - X-Y Z movement of the acromial marker

The X-Y-Z movements of the acromial marker are plotted with respect to the average motion value. From the graphs it's easy to evaluate the mean amount of motion in each direction: in X the marker moves of about 2.5 cm per cycle, in Y 1.5 cm and in Z 1 cm.

In the motion just highlighted we have anyway to take into account the intrinsic error of the vision system, displayed in Figure 60: the crank length should be constant during the test, but actually it varies of about 1 cm.

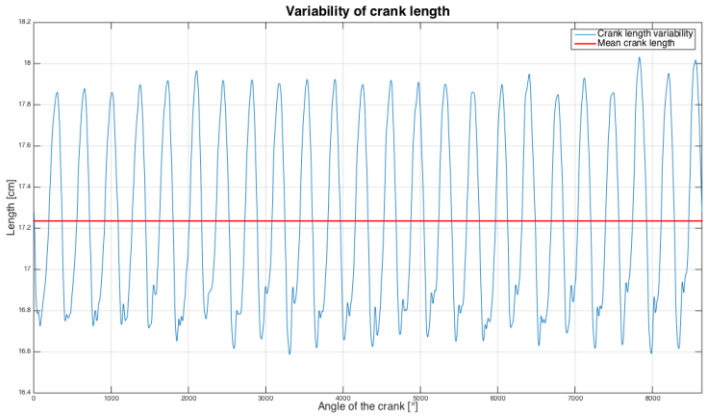

Figure 60 – Variability of the crank length

For the 2D *MATLAB* study that concern this part of the thesis we can in any case utilize the angles α and β calculated, because we'll consider just a 2D motion, even if this is not the real behaviour of the subject during the tests.

Once solved the kinematic problem we can also plot a stylised representation of the whole system, during the cranking activity (Figure 61).

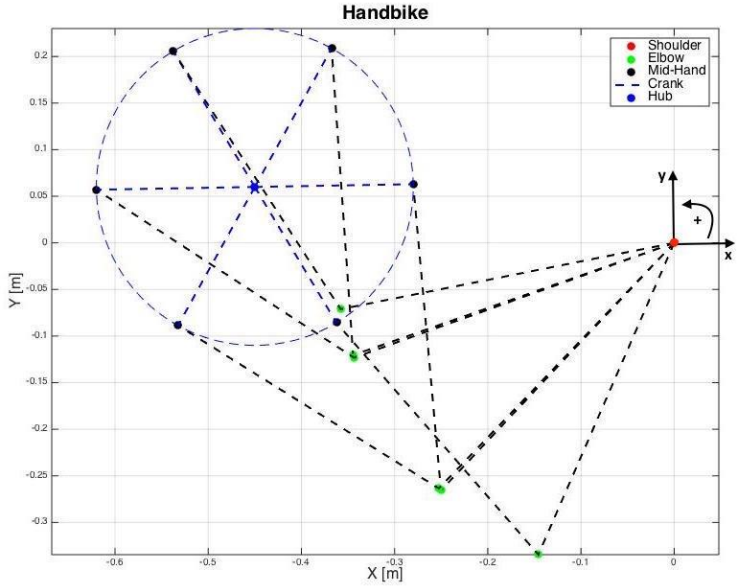

Figure 61 - Handbike representation: in red the shoulder (centre of the reference system), in green the elbow, in black the mid-hand joint and in blue the crank hub

5.4 Dynamic 2D analysis

In this subchapter we'll describe the equations, calculations and results of the *dynamic analysis* carried out to obtain the generated *torques* at the shoulder and elbow joint, starting from the forces experimental data. The subject is the same of the previous chapter and the data refer to the test at power of 40 W.

Similarly to the kinematic analysis (chapter 5.3 Kinematic 2D analysis), we'll adopt the approach of resolution of the dynamic problem treating the modelized upper limb like a *SCARA robot*.

First of all, starting from the results of kinematics (α and β), we wanted to numerically approximate the derivatives in order to obtain the velocities and accelerations of the joint coordinates:

$$\dot{\alpha}(i) = \frac{\alpha(i+1) - \alpha(i)}{t(i+1) - t(i)}$$
$$\ddot{\alpha}(i) = \frac{\dot{\alpha}(i+1) - \dot{\alpha}(i)}{t(i+1) - t(i)} \tag{5.4.1}$$

Like shown in the equations above we derived the angular positions (α and β) the first time to find the velocities (α̇ and β̇) and the second to obtain accelerations (α̈ and β̈); the index *i* stands for the *i*th *sample* considered to calculate two consecutive positions and the interval of time passed between them.

Now we can define the *extended Jacobian matrix (J)* of the system: it's generally the matrix containing the coordinates of the end effector (*mid-hand*) and of the joints, derived with respect to each parameter that defines the degrees of freedom (in this case α and β).

In our case we have to consider not only the joints positions, but also the positions of centres of gravity of both links, because the inertial and gravity effects have to be taken into account.

The vector of the positions extended S_e is defined like follows [12]:

$$S_e = \begin{bmatrix} x_h \\ y_h \\ x_{g_{fore}} \\ y_{g_{fore}} \\ \alpha + \beta \\ x_{g_{arm}} \\ y_{g_{arm}} \\ \alpha \end{bmatrix} = \begin{bmatrix} L_{arm} \cdot cos(\alpha) + L_{fore} \cdot cos(\alpha + \beta) \\ L_{arm} \cdot sin(\alpha) + L_{fore} \cdot sin(\alpha + \beta) \\ L_{arm} \cdot cos(\alpha) + g_{fore} \cdot cos(\alpha + \beta) \\ L_{arm} \cdot sin(\alpha) + g_{fore} \cdot sin(\alpha + \beta) \\ \alpha + \beta \\ g_{arm} \cdot cos(\alpha) \\ g_{arm} \cdot sin(\alpha) \\ \alpha \end{bmatrix} \tag{5.4.2}$$

From the positions we can now calculate the *extended Jacobian matrix* [12]:

$$J_e = \frac{\partial S_e}{\partial Q_i} = \begin{bmatrix} -L_{arm} \cdot sin(\alpha) - L_{fore} \cdot sin(\alpha+\beta) & -L_{fore} \cdot sin(\alpha+\beta) \\ L_{arm} \cdot cos(\alpha) + L_{fore} \cdot cos(\alpha+\beta) & L_{fore} \cdot cos(\alpha+\beta) \\ -L_{arm} \cdot sin(\alpha) - g_{fore} \cdot sin(\alpha+\beta) & -g_{fore} \cdot sin(\alpha+\beta) \\ L_{arm} \cdot cos(\alpha) + g_{fore} \cdot cos(\alpha+\beta) & g_{fore} \cdot cos(\alpha+\beta) \\ 1 & 1 \\ -g_{arm} \cdot sin(\alpha) & 0 \\ g_{arm} \cdot cos(\alpha) & 0 \\ 1 & 0 \end{bmatrix} \quad (5.4.3)$$

The equations contained in this matrix consist in the positions (S_e) derived with respect to α and β; like in the inverse kinematics the parameters L_{arm} and L_{fore} stands for the arm and forearm lengths, g_{arm} and g_{fore} are the proximal distances of the centres of gravity of arm and forearm.

It's also important, like outlined in the previous page, to evaluate the effect of inertia and gravity, the inertial diagonal matrix (M) and the gravity vector are defined like follows[12]:

$$M = diag\left[m_{hand}, m_{hand}, m_{fore}, m_{fore}, J_{g_{fore}}, m_{arm}, m_{arm}, J_{g_{arm}}\right]$$
$$A_g = [0\,, g\,, 0\,, g\,, 0\,, 0\,, g\,, 0] \quad (5.4.4)$$

m_{hand}, m_{fore} and m_{arm} are respectively the masses of the hand, forearm and arm; $J_{g_{fore}}$ and $J_{g_{arm}}$ stands for the inertial barycentric moment of forearm and arm calculated as the mass of each part multiplied by the square of radius of gyration referred to each body length. The variable g is the gravity acceleration 9.81 m/s^2.

We can now define the inverse dynamic equation [12]:

$$C_q = \underbrace{\left(J_e{}^T M J_e\right)\ddot{Q} + \left(J_e{}^T M \dot{J_e}\right)\dot{Q}}_{\text{Inertia}} + \underbrace{J_e{}^T M A_g}_{\text{Gravity}} - \underbrace{J_e{}^T F_e}_{\text{External Forces}} \quad (5.4.5)$$

C_q is the result of the inverse dynamics, it's the vector containing the torques at shoulder and elbow: $C_q = \begin{bmatrix} C_{shoulder} \\ C_{elbow} \end{bmatrix}$; J_e is the Jacobian matrix, ${J_e}^T$ the transpose of it, $\dot{J}_e$ its temporal derivative, M the inertial matrix, A_g the gravity vector, $\ddot{Q} = \begin{bmatrix} \ddot{\alpha} \\ \ddot{\beta} \end{bmatrix}$ and $\dot{Q} = \begin{bmatrix} \dot{\alpha} \\ \dot{\beta} \end{bmatrix}$ the vectors containing the angular velocities ($\dot{\alpha}$ and $\dot{\beta}$) and accelerations ($\ddot{\alpha}$ and $\ddot{\beta}$), finally $F_e = \begin{bmatrix} F_x \\ F_y \end{bmatrix}$ the vector containing the external forces measured (F_x and F_y).

In the equation (5.4.5) it's easy to verify the influence of each component (inertial, gravity and external forces) in the total value of the produced torque, thanks to *MATLAB* it's possible to solve the matrix equation (5.4.5) and plot the total torque and also the torque deprived of inertial effects, to evaluate the influence of the latter.

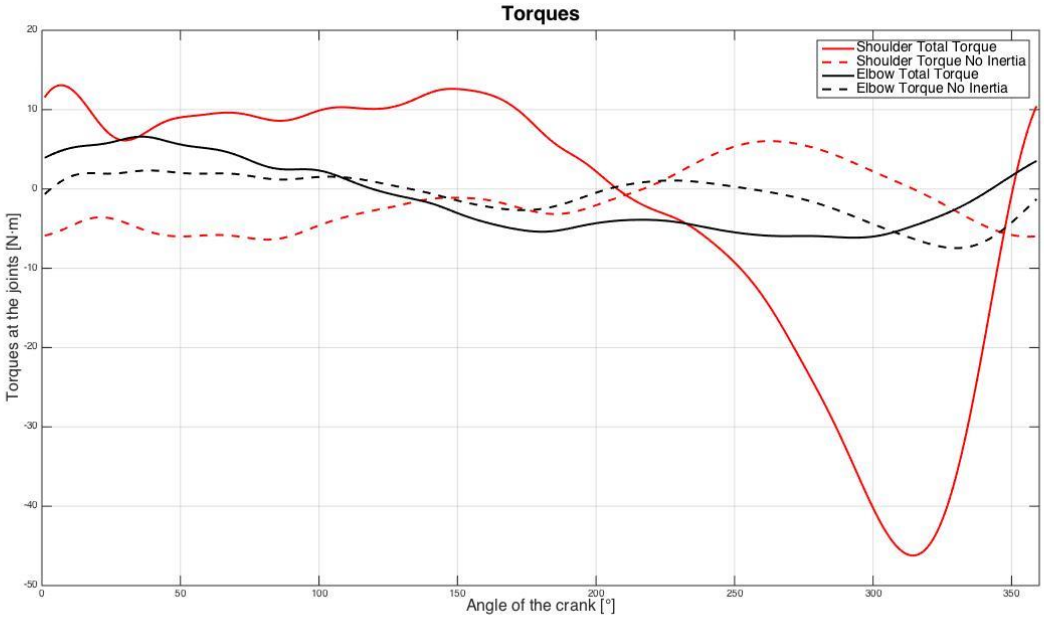

Figure 62 - Torques resulted from the inverse dynamic analysis: in red the shoulder and in black the elbow. The continuous lines represent the total torques, the dashed ones the values neglecting the inertial effects but still considering the weight

From the Figure 62 it's evident how the inertial components composing the torques are important in the total amount generated, especially for the shoulder in which it's a consistent part of the whole torque.

It's interesting also to show how the total force exchanged at the handle changes during the cranking activity [15] (Figure 63).

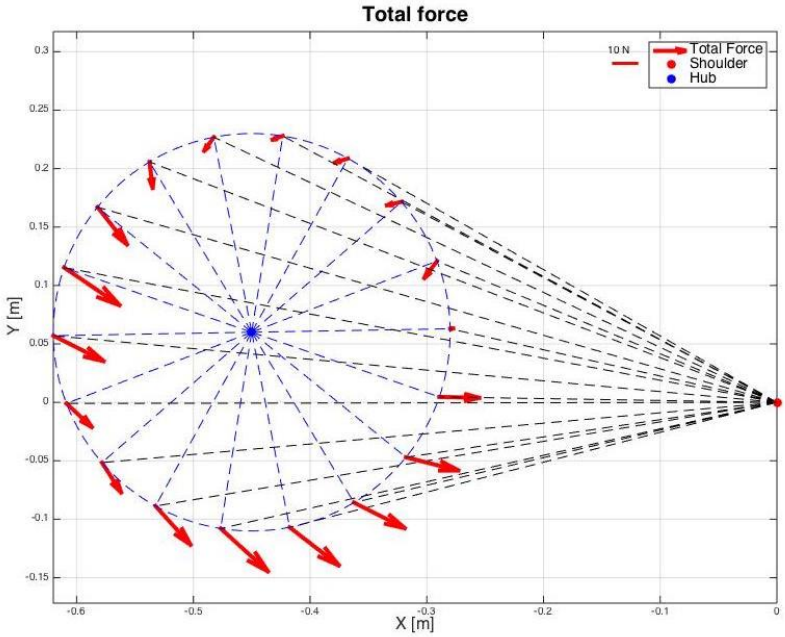

Figure 63 - Total force measured during 360° of cranking

The red dot shows the shoulder position, the blue one the crank hub, whereas the total forces at the handle are represented like red *vectors*.

Another useful graph produced in *MATLAB* similar to the previous one (Figure 63) shows the changes of the different components, described in the equation (5.4.5), composing the total force.

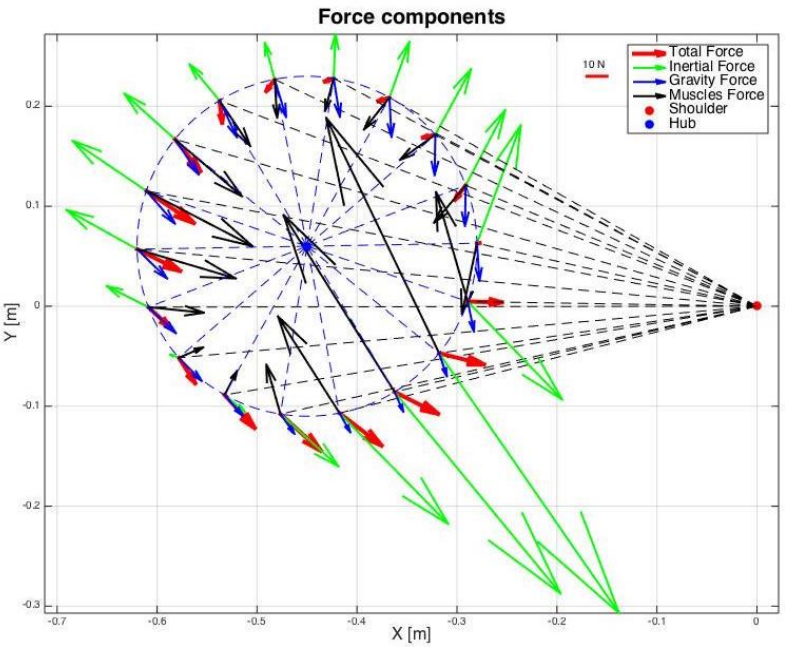

Figure 64 - Force components calculated during 360° of cranking

Also in this case the red and blue spots stand for the shoulder and the crank hub, respectively. The different components are represented with coloured *vectors*: the red arrows are the total forces

measured, the blue ones the gravity components of the force, the green ones the inertial parts of it and finally the black ones the muscle forces generated to compensate and contrast all the other components.

Furthermore, another interesting idea comes from the polar diagram of the tangential and radial forces (F_T and F_R) at the crank, here in the Figure 65 it's possible to identify, from the forces distribution along the 360°, the efficiency of the cranking activity [11] (Figure 65).

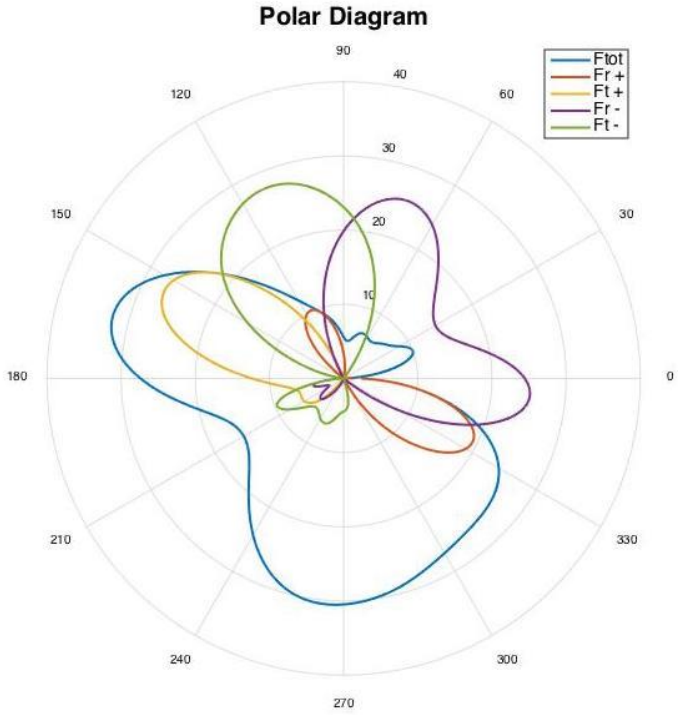

Figure 65 - Polar diagram of F_T and F_R, in red and purple the positive and negative radial force, in yellow and in green the positive and negative tangential force, in light blue the total force

The efficiency coefficient is evaluated like the portion of the tangential force (F_T) on the total amount of force (F_{TOT}) instant per instant. The angle used for the Figure 65 is the crank angle, the 0° position is the closest position with the horizontal crank.

5.5 Power verification

For each test the mean power generated has been set as a discriminating parameter. Like explained in the chapter 4.1 Generation of the work: the ergometer [11], thanks to the *LabVIEW* control panel, used as a feedback, it was possible for the patient to maintain as much as possible the power to a constant level controlling the cranking speed.

From the dynamic analysis results we could calculate the power generated and compare it to the pre-set value, in the case in exam the mean power was set at 40 W:

$$P_{shoulder} = C_{q_{shoulder}} \cdot \dot{\alpha}$$
$$P_{elbow} = C_{q_{elbow}} \cdot \dot{\beta} \qquad (5.5.1)$$

$$P_{total} = P_{shoulder} + P_{elbow}$$
$$P_{handle} = F_T \cdot \dot{\theta} \cdot L_{crank} \qquad (5.5.2)$$

The equations 5.5.1 describe how the values of the shoulder and elbow powers have been calculated: the torques, obtained from inverse dynamics, times the angular velocities ($\dot{\alpha}$ and $\dot{\beta}$) of shoulder and elbow joints respectively.

The equations 5.5.2 represent the total power as the sum of the powers generated at the elbow and shoulder; the power transmitted to the handle is instead the multiplication of the crank tangential force (F_T) to the cranking speed ($\dot{\theta}$) and the crank length (L_{crank}).

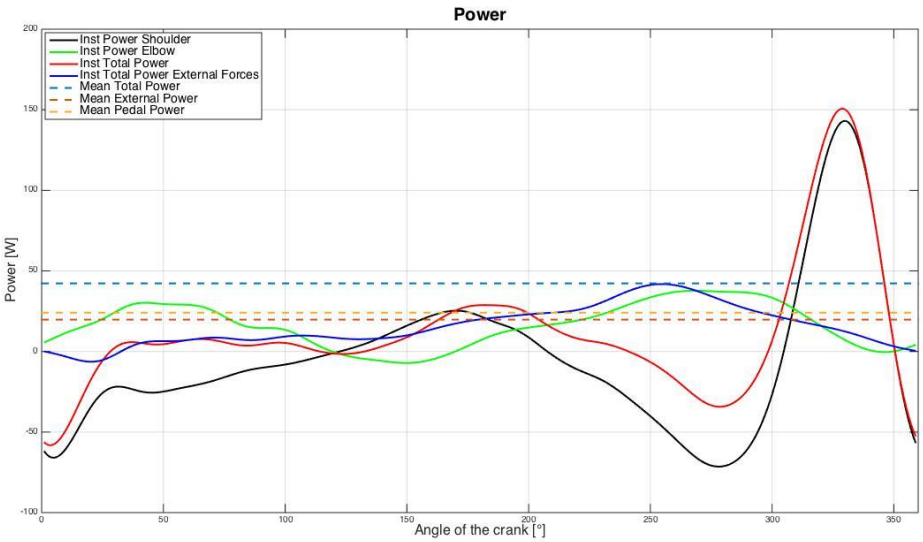

Figure 66 - Power generated during a cranking cycle

The Figure 66 shows how the power generated changes during the handcycling activity: the black curve stands for the power exerted at the shoulder, the green graph instead represent the power generated in the elbow joint.
The last two charts show the total power generated (red) and the total power caused just by the external forces (blue).

The mean values calculated are plotted as dashed lines: in light blue the average value of the total power generated, in orange the mean of the power due to the external forces and in yellow just the power transmitted to the pedal.
Examining the results, we can easily notice that the power at the handle (yellow) it's about 20 W (exactly 24.0969 W); it's more or less the half of the value chosen at the beginning of the test (40 W) because the pedalling activity has been done with both limbs, the fact that it is not equally divided into right and left parts can be due to a non-perfect symmetry of the subject.
The total average power (light blue), on the contrary, it's much more than the requested value (it's about 42.2216 W for just a limb), this is due to the fact that the inertial and gravity effects are not symmetrical on a single cycle like they should be normally (e.g. in a robot), because of the speed and acceleration profiles, that aren't symmetrical neither.
The last dashed line (orange) shows the value of the power given by just the external forces (its value is 19.7701 W), it may be considered the real effective power produced by the subject in a theoretical case, similar to a robot, in which the other components of the generated torques (equation 5.4.5) should have a null effect on the 360°.

5.6 Muscles forces

The last analysis carried out in the two-dimensional study in *MATLAB* concerns the investigation of plausible forces produced by the muscles of the elbow joint.

The shoulder articulation is too complex to be simplified in a 2D study, in particular the muscles that act on it aren't fusiform like most of the ones operating at the elbow.

Once we've obtained the torques at the elbow from the inverse dynamics, thanks to anatomical studies [4] [7] we can select the main muscles that can be considered as flexor and extensor of the elbow.

In our case we have chosen as the most important:

- The *triceps brachii* as the only *extensor* muscle considered.

- The *biceps brachii*, the *brachioradialis* and the *brachialis* as the flexor muscles.

It has been decided to use the graphics contained in a publication [14], that found experimentally on ten corpses the values of the moment arms of the muscles listed above; another reason that doesn't make possible the muscles analysis in the shoulder is that there aren't in-depth studies, like the one just outlined, about the moment arms of the articulation muscles.

The article [14] shows plots in which the lever arm of each muscle [cm] is figured in function of the flexion angle of the elbow [°]:

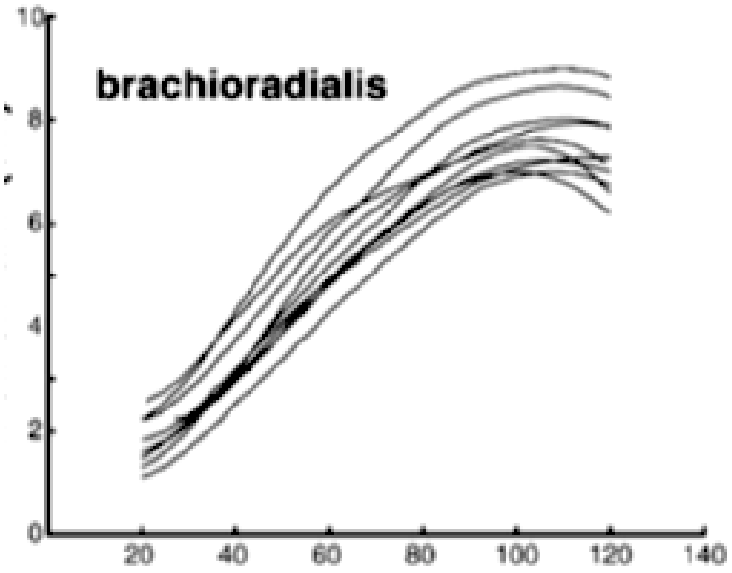

Figure 67 - Example of a chart from the [14]

We imported in *MATLAB* these charts using a graphic software that assigning to the images the range of the x and y axis gives in output the position of the point that we selected on the curves.
In this way we could interpolate these points in *MATLAB* obtaining the functions that describe the trend of each moment arm.

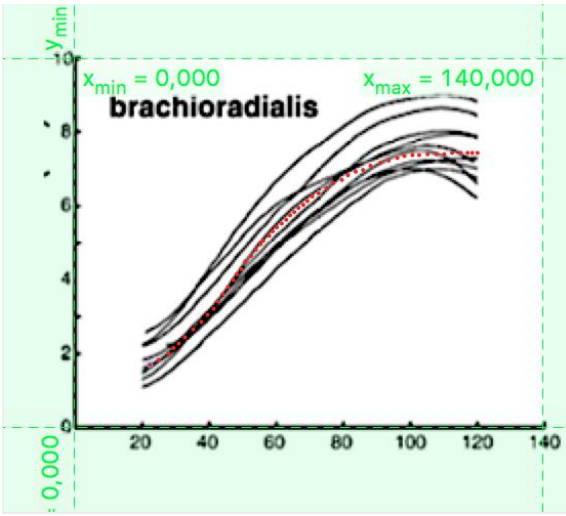

Figure 68 - Example of point interpolation

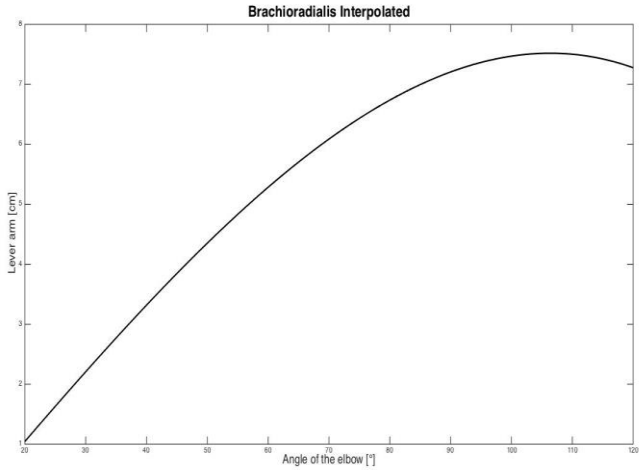

Figure 69 - Interpolated brachioradialis moment arm

Once obtained these functions, we began to analyse the possible solutions for finding the forces of each muscle; we needed to find a recapitulatory equation in order to obtain the values of forces comparable with the ones in the real human body. Thanks to the preceding biomedical and medical studies [3], we know how in general the human body divides the external loads on the several muscles usable to accomplish a task.
Normally there is a function that has to be minimized, called from now the *overload function* [3]:

$$f(F_{m_1}, F_{m_2}, \dots, F_{m_n}) = \left(\frac{F_{m_1}}{F_{m_{1MAX}}}\right)^2 + \left(\frac{F_{m_2}}{F_{m_{2MAX}}}\right)^2 + \dots + \left(\frac{F_{m_n}}{F_{m_{nMAX}}}\right)^2 \quad (5.6.1)$$

The equation (5.6.1) defines the overload function *f*; F_{m_1}, F_{m_2} stands for the muscular forces and $F_{m_{1MAX}}, F_{m_{MAX2}}$ are the maximum forces that each muscle can generate.
These maximum forces are evaluated in this way:

$$F_{m_{1MAX}} = PCSA_{m_1} \cdot k \quad (5.6.2)$$

Where $PCSA_{m_1}$ is the *Physical Cross Section Area* that, in other words, is the average section of each muscle; *k* stands for the highest traction generable by a muscular fibres area of one cm^2.

We assigned at the *PCSA* and *k* of each muscle, values that have been experimentally found as the averages in human bodies.
In particular we set the *k* at the measure of 80 N/cm^2 for all the muscles, that's not always true in reality but in the theoretical studies it's often considered like that.
We assigned to the cross sectional areas these values found in literature [3]:

- $PCSA_{triceps} = 14.9\ cm^2$
- $PCSA_{biceps} = 4.6\ cm^2$
- $PCSA_{brachialis} = 7.0\ cm^2$
- $PCSA_{brachioradialis} = 1.5\ cm^2$

Consequently the maximum force deliverable for each muscle is:

- $F_{tricepsMAX} = 1192\ N$
- $F_{bicepsMAX} = 368\ N$
- $F_{brachialisMAX} = 560\ N$
- $F_{brachioradialisMAX} = 120\ N$

The previous values listed are just approximately estimations of the real *PCSAs* and maximum forces generable by elbow muscles. For example, in case of trained people, these values normally increase, but it's not easy to evaluate them; anyway for the aim of this thesis we can consider these measures a valid approximatio.
For the minimization of the *overload function* it's necessary to define some constraints, in the case in exam we have selected:

- The rotation equilibrium equation: in which the torques produced by the muscles have to balance the total calculated torque (from inverse dynamics), composed by the components described in the equation 5.4.5.
- The sign of the muscle force: can be just positive because the muscles can only pull and not push.
- The exerted force: has to be from a null value until the upper limit set by each $F_{m_{1MAX}}$.

In *MATLAB* it's possible to find the minimum of constrained nonlinear multivariable functions thanks to the function *fmincon* [13].

In case of the elbow flexion the overload function obtained is:

$$f(F_{bic}, F_{brac}, F_{bracrad}) = \left(\frac{F_{bic}}{F_{bicMAX}}\right)^2 + \left(\frac{F_{brac}}{F_{bracMAX}}\right)^2 + \left(\frac{F_{bracrad}}{F_{bracradMAX}}\right)^2 \quad (5.6.3)$$

The constraint about the equilibrium at rotation is:

$$C_{elbow} - F_{bic} \cdot L_{bic} - F_{brac} \cdot L_{brac} - F_{bracrad} \cdot L_{bracrad} = 0 \quad (5.6.4)$$

Where C_{elbow} *is the calculated torque,* F_* the force and L_* the lever arm of each muscle.

The results obtained in *MATLAB* have been plotted in the Figure 70.

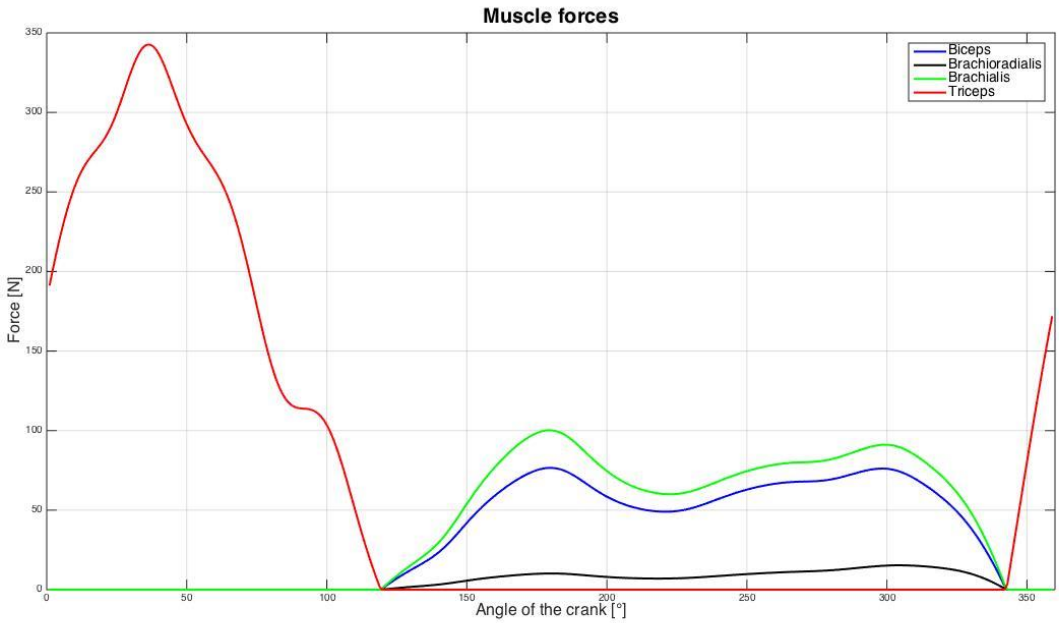

Figure 70 - Muscle analysis: in red the force generated at triceps, in green at brachialis, in blue at biceps and in black at brachioradialis muscle

The shape of the curves represented in Figure 70, are coherent with the flexion-extension alternation that the elbow should have in a cycle of pedalling, considering the zero of the crank angle as the horizontal closest position of the handle.

The *MATLAB* function *fmincon* guarantees that the forces generated are positive and under the saturation value (F_{max}), like outlined before.

The forces plotted are just an estimation of the real forces that should be generated during a handcycling movement: first of all because we considered just some of the muscle crossing the elbow (there are more muscles that should be taken into account), but in our case we didn't have information about their *PCSA* and *moment arms*.

Secondly some of the muscles mentioned are bi-articular (*biceps brachii* and *triceps brachii*), so we should consider them not just acting on the elbow but also on the shoulder, in this case the approximation can be considered valid because these two muscles are actually each one merging in a single tendon at the elbow. Finally, the *PCSA* and *k* we assumed, are average values based on experimental data collected, but they aren't the exact cross sectional areas and specific force of the subject, whose data we're analysing.

Last, but not least, the forces we gathered are generated in a 3D movement that is much more complex and particularly different from the two-dimensional taken into account.

For this reason in the next chapter (6. ANYBODY 3D MODEL) we'll describe the 3D analysis executed and the results of it.

One last analysis, comparable to the one shown in the Figure 65, it's constituted by the evaluation of the muscular forces on a polar diagram [21] (Figure 71).

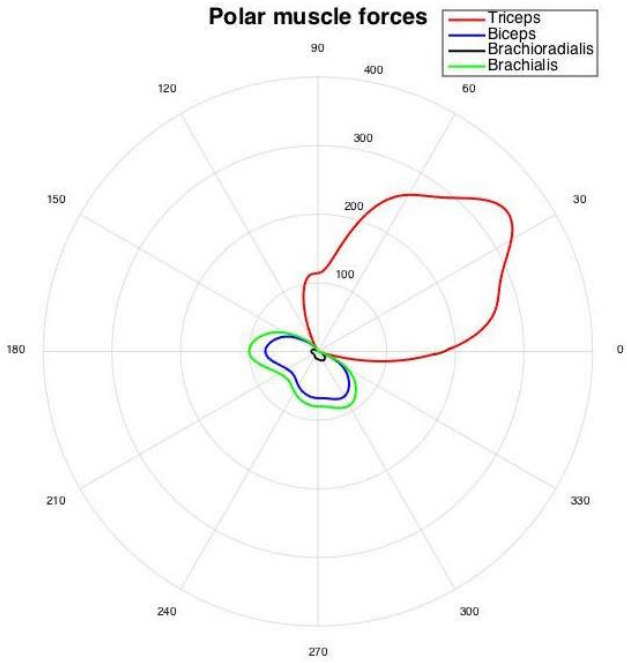

Figure 71 - Polar plot of muscles forces: in red the force of the triceps, in blue the biceps one, in black the brachioradialis and in green the brachialis

This graph can be useful for analysing the period of activation of each muscle, and usable in a comparison with the results that will be obtained in the successive 3D analysis study.

6. ANYBODY 3D MODEL

In this chapter we'll describe similarly to the previous one (5. MATLAB 2D MODEL), the software used: *AnyBody*, the features of the 3D model created and the results obtained with this in-depth analysis.

6.1 The AnyBody Technology

With a proven and validated technical knowledge, AnyBody Technology is the undisputed global leader in applied musculoskeletal analysis [20]. We worked in particular with *The AnyBody Modeling System*, a software that allows the users:

- To analyse in a musculoskeletal way the daily activities;
- To apply inverse kinematics and dynamics analyses, starting from markers positions and measured forces;
- To predict the posture and motion of the human body interacting with instruments or environment;
- To use models already present in the *Modelling Repository*, that can be freely modified and simulated with imported CAD models of the interacting environment.

Figure 72 - AnyBody Logo

More in details, the *AnyBody Modeling System* is a *MusculoSkeletal Modeling System* for biomechanical simulations analysing reactions within the human body or between the human body and an environment. Environments can be [23]:

- something within (implant, e.g. knee or hip device);
- something attached to (exoskeleton, e.g. knee brace or space-suit);
- something interacting (e.g. automotive seat, wheelchair, handbike) with the human body.

AnyBody uses the input (*motion* and *external forces*) and calculates the activations of the individual muscles responsible for this motion: this process is called in the software simulation *Inverse Dynamics*.
AnyBody uses for skilled motions in an optimization process, a muscle recruitment solver to solve what muscles (each single fascicle) will be used; that means you get muscle forces, activations and joint reaction forces and moments during this motion. Additionally, each model can be setup to obtain forces and moments in any point of interest.
In our case we'll use for the 3D analysis: the motion of the crank (position, velocity) and the forces exchanged at handle/palms of the hands (F_X,F_Y and F_Z).
There are several fields of application:

- In *orthopaedics*: it's possible to develop new *implant* design simulating accurate reaction forces to minimize loads on joints and implants.
- In *automotive ergonomics*: the user may optimize the seat design, pedal steering wheel and handle positions.
- In *sports* and *high performance*: new designs of sport equipment can be analysed or developed.
- In *aeronautics* or *aerospace*: devices for use in space can be developed and optimized to maximize activations on certain muscles to train them in the most efficient way.

6.2 The model developed

Thanks to the *Repository* that *AnyBody* makes available to every user, a lot of models of the complete human body or of its parts are freely downloadable and modifiable.
In particular there wasn't a pre-created model of the handcycle, so taking information and ideas from the several models present in the library we could create our own *Handbike model*.
Specifically we used two different models to design the one utilized in this study:

- *Hand Pump Model*: A model of a person operating an old-fashioned asynchronous pump by hand, it's based on a standing model of the complete human body.

- *Wheel Chair Model*: A model of a person sitting in a wheelchair, with the seat and the wheels of the wheelchair contained in the interacting environment, it's based on a human body model without lower limbs.

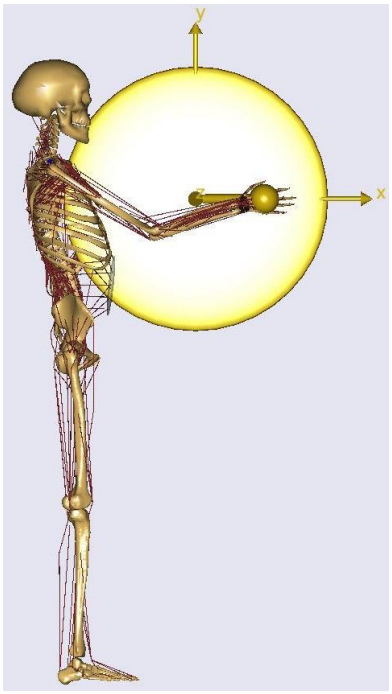

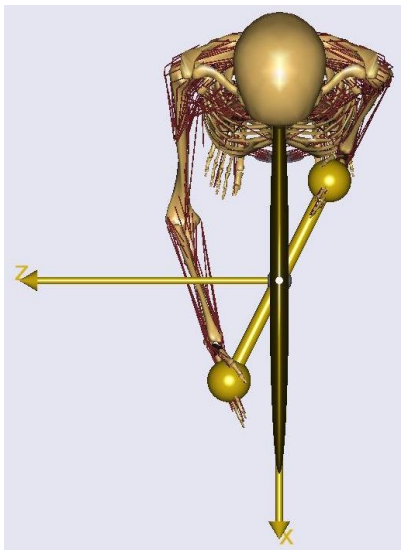

Figure 73 - Hand Pump standing model: views from the side and from above

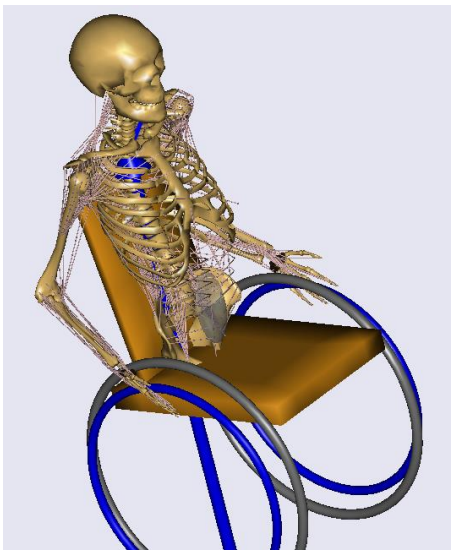

Figure 74 - Wheelchair sitting model

Thanks to the programming environment that *AnyBody* provides, it's easy to combine different codes deriving from various models.
In order to create a handbike model as similar as possible to the real handcycle in the *LARIN* laboratory, we merged the two models described before into one; particularly we took from the

Hand Pump Model the interacting environment of the wheel changing the position of the handles in way to obtain a synchronous pedalling; from the *Wheelchair Model* we took the human body with no legs and the seat, neglecting the wheels and the push rims.

The result obtained is a nice approximation of the real handcycle configuration:

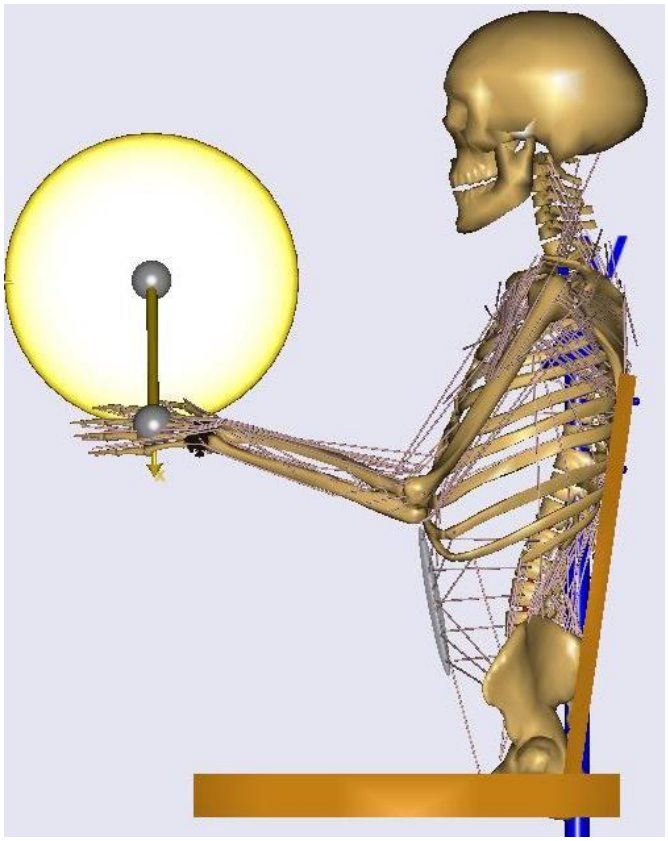

Figure 75 - Created handcycle model in AnyBody

Figure 76 - Real configuration of handcycle

From the Figure 75 and Figure 76 we can compare respectively the obtained result with the real configuration, we decided to not consider the lower parts of the body because, for what concerns the aim of our study, they would have had just more unused degrees of freedom. In the reality the subject was fastened to the backrest with a belt, in the 3D model there was already in the *Wheelchair* a way to maintain the body bonded to the seat: it has been done adding some constraints on the spine, in order to obtain a good adherence between the support and the back.

6.3 Setting the designed model

Once designed the new model, we needed to set it properly in order to achieve a configuration totally comparable with the real situation analysed in the lab.

First of all we had to scale the human body model using the physical parameters of the subject of the test; *AnyBody* normally follows the relationships described by the anthropometry, in particular starting from the total mass and the height of the patient, it automatically scales the body parts considered.

It's possible for advanced users also to define a new scaling law, but in our case it has been decided to use the uniform scaling law already present in the standard repository model, because like explained in a previous chapter, we had just non-disabled subjects, consequently the anthropometric tables are a good approximation in evaluating the physical parameters.

Other features that have been set are the position and dimension of the cranking wheel. Starting from the *hand pump* we had to change the handles position and put them in a synchronous way to simulate the handcycle properly; the length of the cranks has been set at the value measured on the laboratory handbike and the position of the hub has been positioned using the coordinates derived from the vision system data.

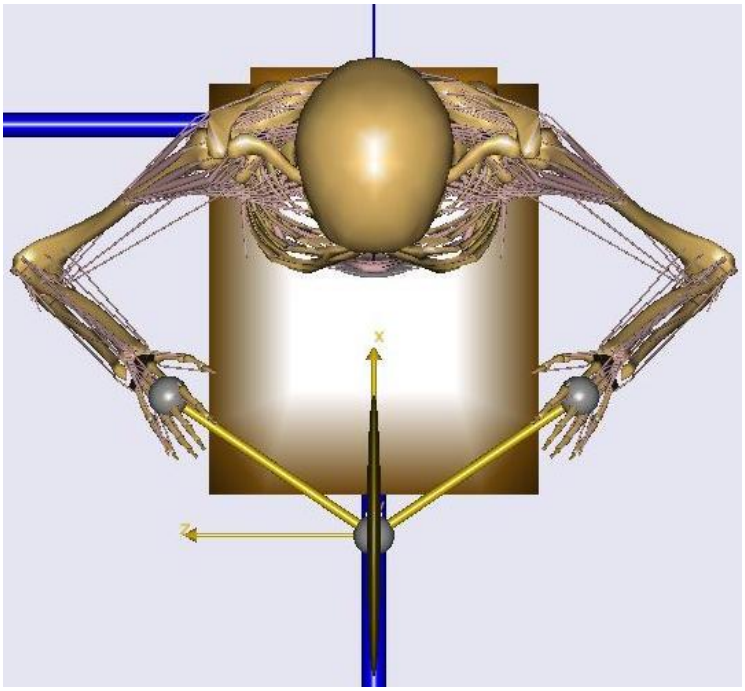

Figure 77 - View from above of the cranking wheel and handles positions

6.4 Moving the handbike

Like outlined in the chapter 6.1 The AnyBody Technology, there are several ways to move the model:

- It's possible to associate to a device in the environment a certain motion law and so achieve the desired movement of the whole model.
- From the forces exchanged between the human body and the environment and the movement associated, the software can solve the kinematic and dynamic problems.
- The most complete way to move the whole model is using markers position and data coming from a vision system acquisition.

Unfortunately in the case of study, the number of markers that were positioned on the subjects of the tests, weren't enough to move in a proper way the bones of the human model in *AnyBody*, that is to say that to achieve an apparently plausible movement we needed to fix some degree of freedom, especially on the shoulder.
The main problem was that we had just two markers directly applied on the patients bony landmarks, one on the *humerus epicondyle* and the other on the *acromion*, but actually the latter could define just the position of the *scapula* but not its rotation; furthermore there were no information on the *clavicle* and so the shoulder's several degree of freedom couldn't be defined in a proper way.
To solve this problem we decided to recreate, thanks to the potentiality of the software, the movement of the body starting from the rotation of the crank, that we reproduce thanks to the data collected in the laboratory. Specifically we linked the palm of both hands to the handles with a spherical joint (called *palm node*); then we passed to the *driver* (*AnyBody* technical language), located in the wheel hub, the angular position of the crank associated with the time, in this way we could make it rotate with the real motion law observed in the laboratory test.
We set also the starting position of the crank as the one considered of the real handbike (0° the horizontal closest position of the handle).
After this we could run the kinematic analysis, from the motion just described, we obtained the movements of the body: such as the angle of motion of each degree of freedom of the human model in function of time (duration of the test) or, added by us, also the possibility to choose, as

abscissa of the graphs, the crank position in degree, in order to easily find a correlation between human body behaviours (kinematic results) and the crank position during a pedalling cycle.

The next step to complete the analysis was to apply, in the aforementioned *palm node,* the forces measured with the load cell on the handle, in particular the F_X and F_Y components.

We had to add also the F_Z, being the model three-dimensional, but not having information related to it (the sensor gave us just 2D forces components), we assigned to it a null value during the whole test (from precedent studies it has been tested that the force component direct to the centre of the wheel has a small value compared with the others, so we neglected it).

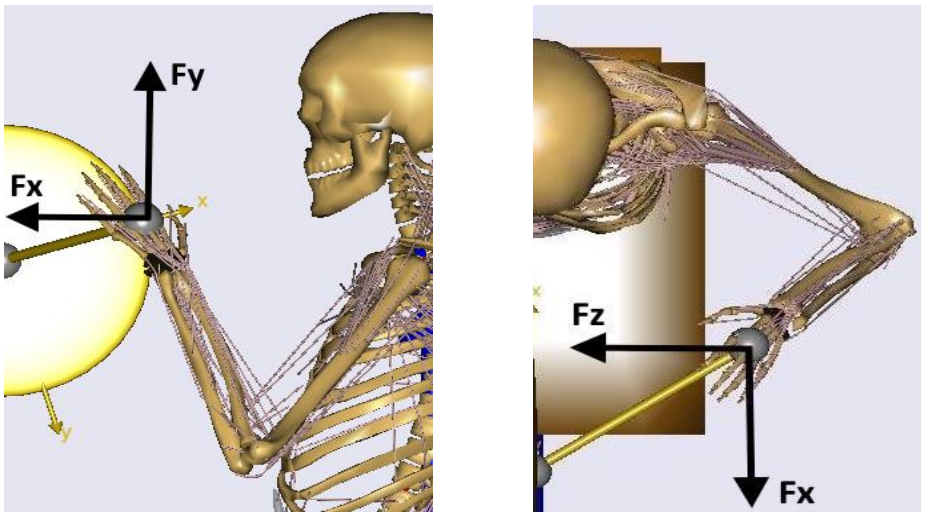

Figure 78 - Details from the side and above of the forces used in AnyBody

Obviously we had chosen the sign of the forces coherently with the reference frame of the model, that is different from the one of the laboratory, this will be evident analysing the results of inverse dynamic analysis in which the sign of the torques produced will be exactly the opposite of the ones resulting from the 2D *MATLAB* analysis.

So after having added also the forces we could start the whole study on the human model devised; thanks to the computing power of the *AnyBody Modeling System* the results obtained concern all the analysis accomplished also in 2D (chapter 5. MATLAB 2D MODEL), such as:

- The kinematic analysis: the results of which are the motions of the human body.
- The dynamic analysis: the results of which are not only the torques produced in the body's articulations, but also the internal forces and loads within the joints.
- The muscles analysis: it's contained in the dynamic analysis *AnyBody* command, but it concerns the muscular forces generated and the muscle activity (i.e. EMG).

We can from this moment, in the next subchapters, examine the results of the 3D complete study.

6.5 Kinematic and dynamic 3D results

In this subchapter we are going to describe and show the results obtained, as the title says, from the kinematics and dynamics carried out in *AnyBody* environment. All the following graphs are plotted in *MATLAB* from the data coming from *AnyBody* resolutions, just to have a uniform method of results representation and even more to ease the comparison between the two models developed. The description and analysis accompanying the images will concern just the mere results shown in the figures, the comparison with the 2D analysis will be conducted in the next chapter (7. MODELS COMPARISON).

We'll start with the inverse kinematic analysis:

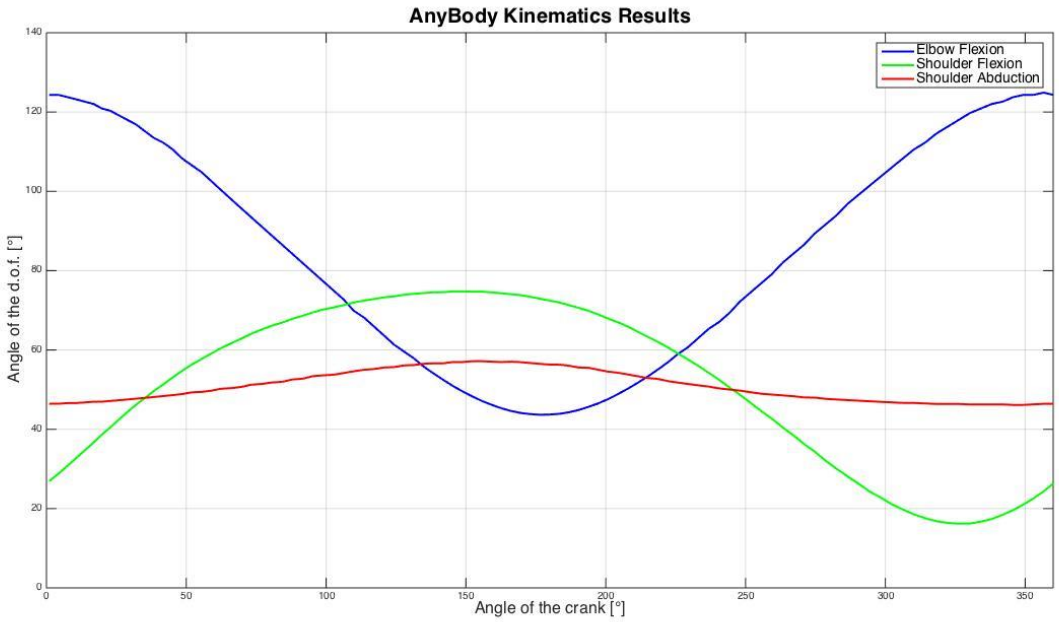

Figure 79 - Results of inverse kinematic analysis in function of the crank position

The Figure 79 shows the angle of flexion/extension of the elbow (in blue), the projection of the flexion/extension of the shoulder (in green) and the projection of the abduction/adduction movements (in red).

The shoulder angles are projections because, being a 3D articulation, the results of the kinematics are given in function of the axis of the reference frame to which they are related.

We have found the joint angles using a similar method to the one utilized in case of the markers positions (chapter 5.3 Kinematic 2D analysis), thanks to their projections along the reference axis, starting from the coordinated of elbow and shoulder in the main reference frame.

Looking at the next picture (Figure 80), we can see the reference frame of the *AnyBody* model.

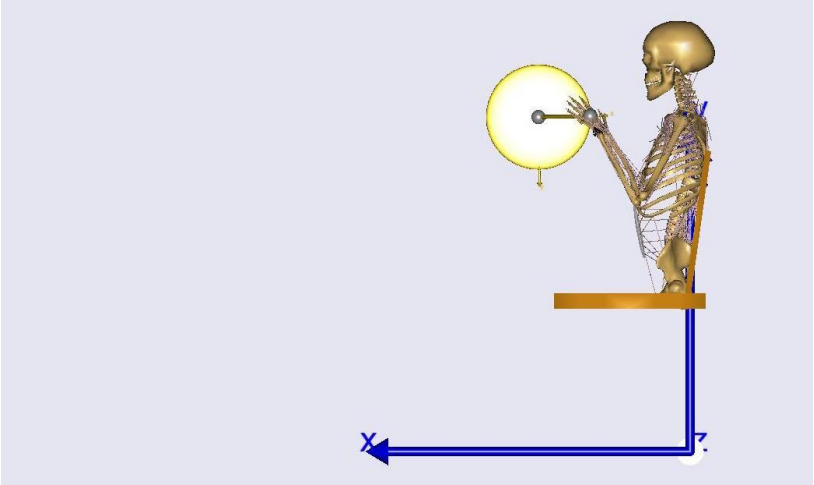

Figure 80 - Reference frame of the model

Considering the constraints on the backrest (outlined in the chapter 6.2 The model developed), the shoulder movements are all limited to the *glenohumeral articulation*, in this way the movements of the scapula along the thorax and between scapula and clavicle are limited like they are in the real situation.

Before showing the results of the inverse dynamics analysis, the plot containing the forces according to the reference frame of the 3D model will be illustrated:

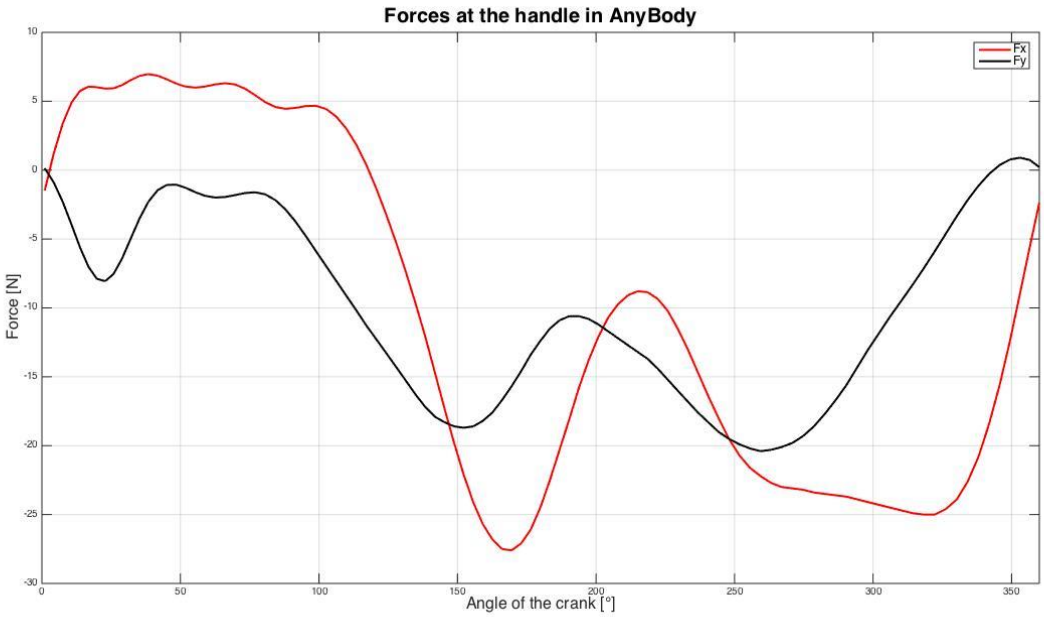

Figure 81 - Forces from AnyBody model: in red the F_X and in black the F_Y

Applying the forces to the contact point between the hands palms and the handles, and moving the whole model with the kinematics analysis, we have obtained the following results:

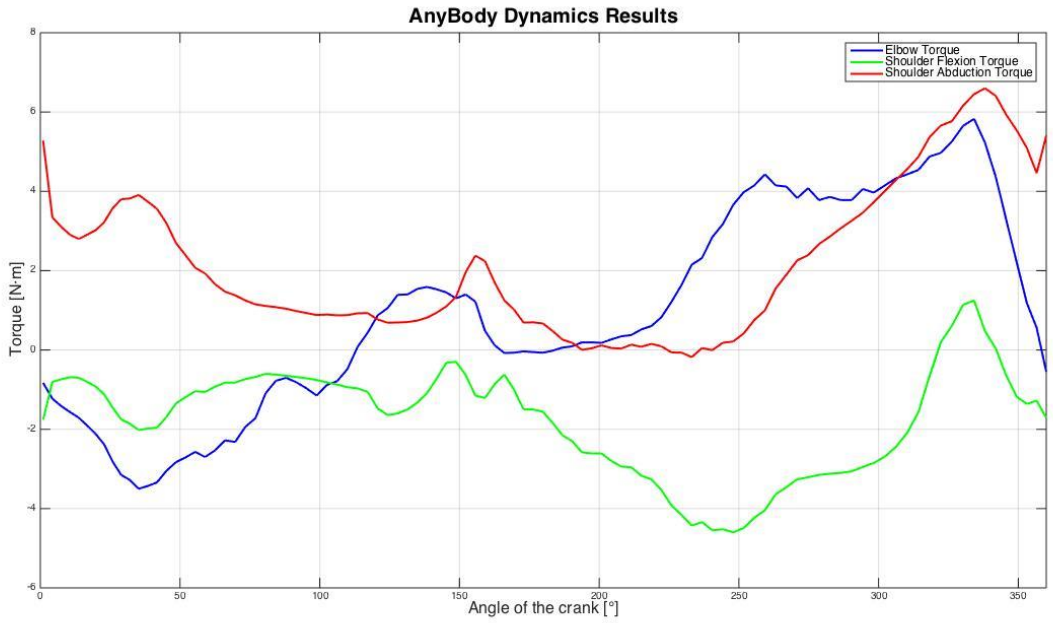

Figure 82 - Results of inverse dynamic analysis in function of the crank position

From the image above (Figure 82) we can easily recognise the different torques generated and examined in this thesis:

- The elbow torque (represented in blue): shows a clear change in sign, according to the coordinate system set in the *AnyBody* program (Figure 80).

- The shoulder flexion torque (represented in green): it is hard to compare and analyse the graphs regarding the shoulder articulation with the real behaviour of it, because differently from the elbow joint, the shoulder is a composition of three different rotations.

- The shoulder abduction torque (represented in red): it's the missing movement in the 2D analysis, however it influences the total behaviour of the shoulder joint.

The torques, like the angles, are calculated with the convention set by the coordinate system (Figure 80), the next subchapter (6.6 Muscles forces analysis) will be the last of the 3D analysis and will feature everything related to the analysis of muscle forces.

6.6 Muscles forces analysis

In this subchapter we'll show the behaviour of the main muscles of shoulder and elbow articulations.

All the data that we supposed in the 2D analysis, such as the *PCSA*, the *moment arm* and the *specific force of the muscular fibres (N/cm^2)* of each muscle, are already present in the complex environment of the *AnyBody* human body model. Every muscle results from a composition of fibres, each one with its own maximum force generable (consequently PCSA and specific force per cm^2), moment arm and length. Depending on the width and the shape of each muscle considered, the configuration of the fibres has been created, as well as their attachment on the bones, in order to approximate properly every muscle of the upper limbs.

We decided to plot, in each figure, just the forces generated by each group of fibres, because plotting the muscles all together without assemble the muscle fascicles with the closest ones, especially in the shoulder case, would have been just a chaos of coloured lines.

6.6.1 Elbow muscles study

In case of the elbow articulation, being few muscles controlling it, we can plot also several muscles forces (also in this case the sum of several fibres forces) in only one graph, to evaluate the effect of each muscle during the cranking activity and estimate possible coactivation.

Let's start showing the main elbow muscles:

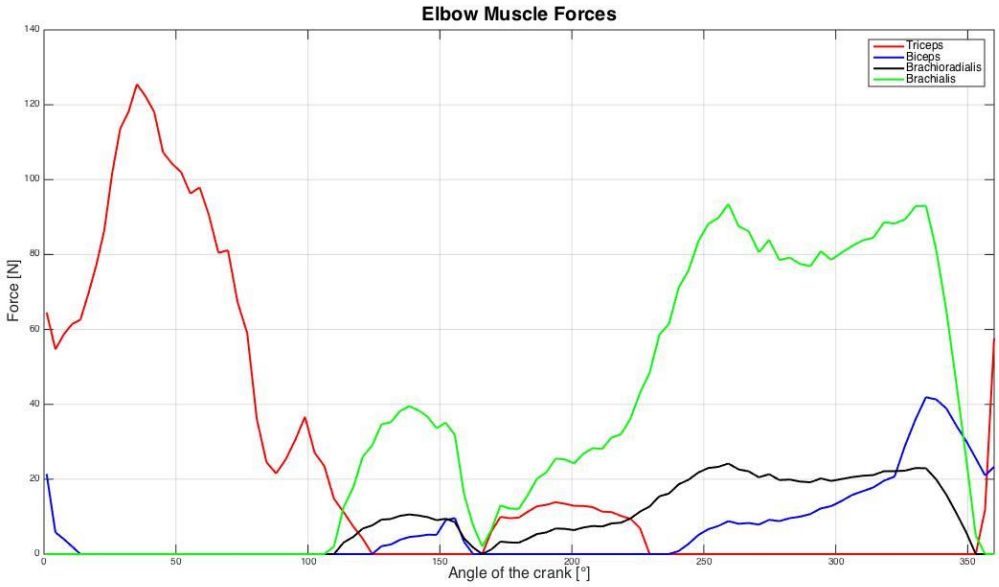

Figure 83 - Main elbow flexor/extensor muscles in function of the crank position

The previous image (Figure 83) contains the data regarding the main flexor and extensor muscles of the elbow articulation; it can be easily compared with the Figure 70, the equivalent result of the two-dimensional study. We have decided, referring to anatomical studies [1] [4], to select as the principal extensor the *triceps brachii* (in red), and as the main flexors: the *biceps brachii* (in blue), *brachialis* (in green) and *brachioradialis* (in black) muscles.

The previous plot can be viewed as a polar diagram, like in the analogous 2D (Figure 71):

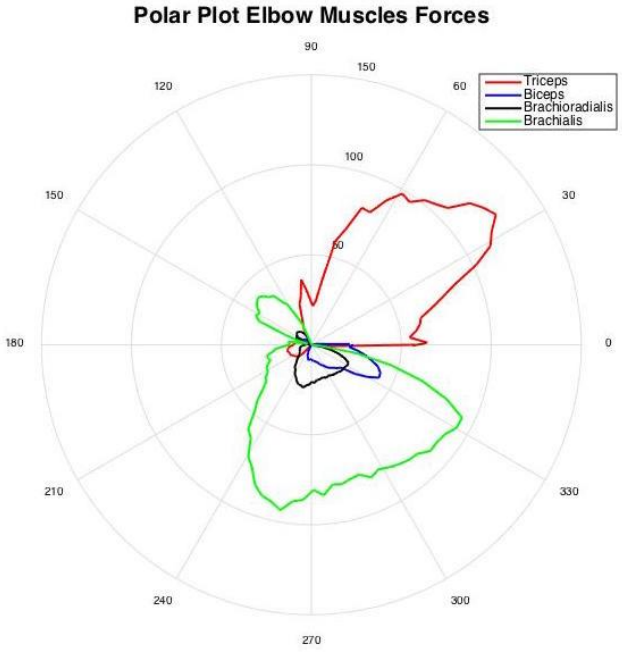

Figure 84 - Polar plot of elbow muscles forces: in red the force of the triceps, in blue the biceps one, in black the brachioradialis and in green the brachialis

The forces plotted in the previous two images (Figure 83-Figure 84), are the sum of the several fibres forces that compose the muscles in the human body model, for example:

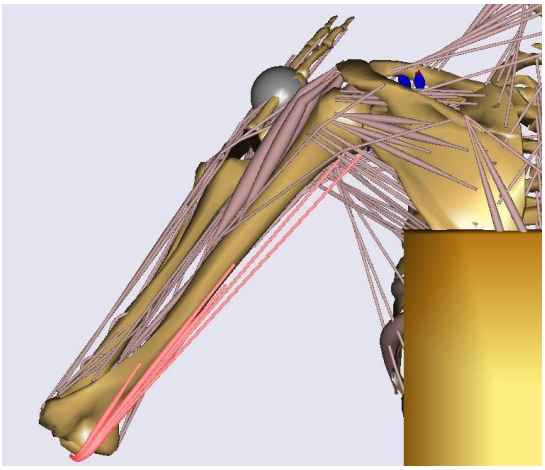

Figure 85 - Triceps divided into six fibres: two for the long, two for the medial and two for the lateral heads

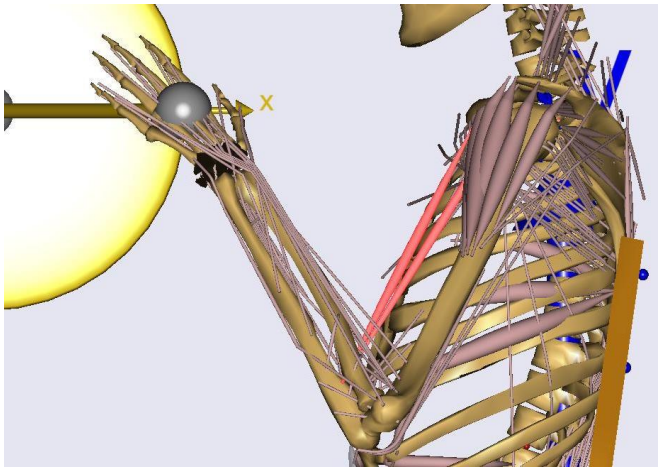

Figure 86 - Biceps divided into two heads: long and short

During the software simulation, the used muscles swells, in order to highlight the intensity of their activation:

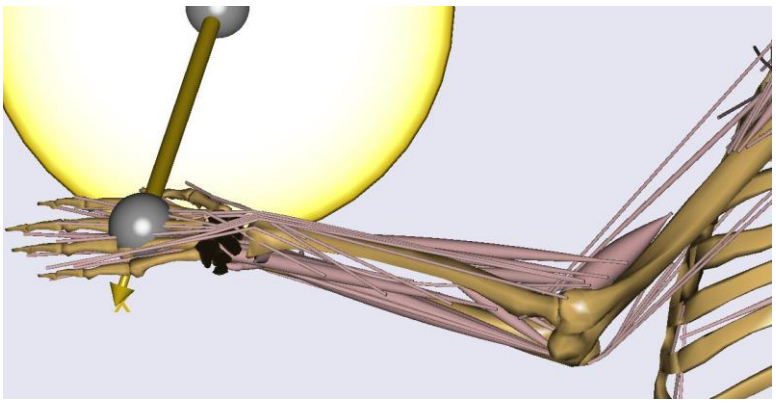

Figure 87 - A detail of the swollen muscles during the simulation: it's easy to notice that some muscles like the flexors are used in this case, whereas the extensors like triceps are relaxed

Other muscles cross the elbow joint, but their main function is normally aimed at the prono-supination movement or the flexion-extension/abduction-adduction of the wrist.
But in this case, not taking into account the wrist articulation, they affect also the forces of the main elbow muscles, so it's worth to take a look at their values:

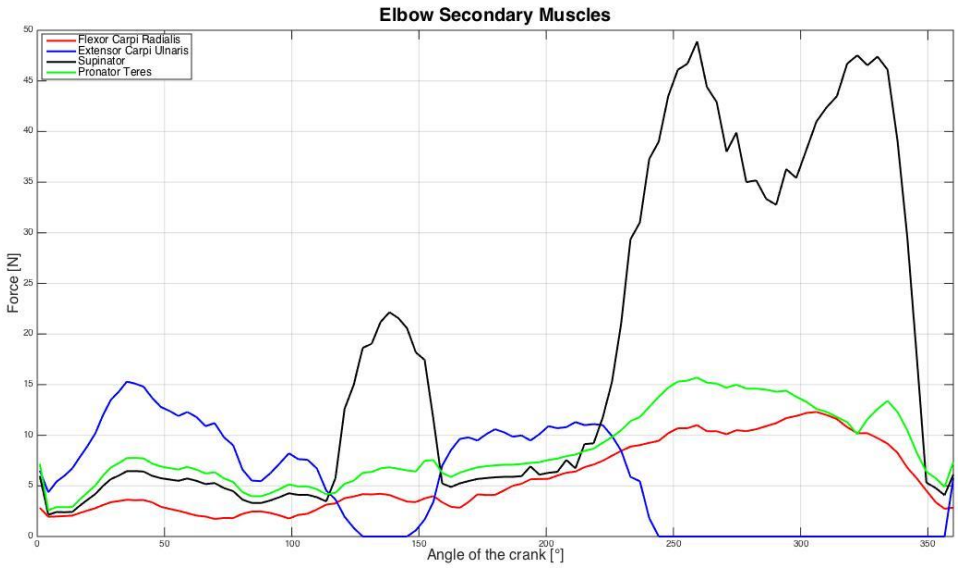

Figure 88 - Secondary elbow muscles in function of the crank position: in red the flexor carpi radialis, in blue the extensor carpi ulnaris, in black the supinator and in green the pronator teres muscle

The Figure 88 contains the force amount of four different muscles: a flexor-abductor of the wrist the *flexor carpi radialis* (in red), an extensor-adductor of the wrist the *extensor carpi ulnaris* (in blue), a forearm supinator muscle the *supinator* (in black) and a forearm pronator muscle the *pronator teres* (in green).

6.6.2 Shoulder muscles study

After the previous analysis of the elbow articulation, we'll now focus on the muscles surrounding and activating the shoulder joint.

We have selected the muscles that, from the bibliography and previous experiences of study on handcycling, result as the most important and used in this activity. Furthermore from the results obtained in *AnyBody* we could evaluate the force exerted by each muscle in order to select the principals to examine:

- The *deltoid* muscle is divided into three big parts:
    - *Anterior deltoid*: composed by the six fibres of the, so called in *AnyBody*, *clavicular deltoideus*. The fibres, like its name says, attach to the clavicle bone.
    - *Posterior deltoid*: composed by the first three fibres of the *scapular deltoideus*.
    - *Medial deltoid*: formed by the union of the last three fibres of the *scapular deltoideus.*

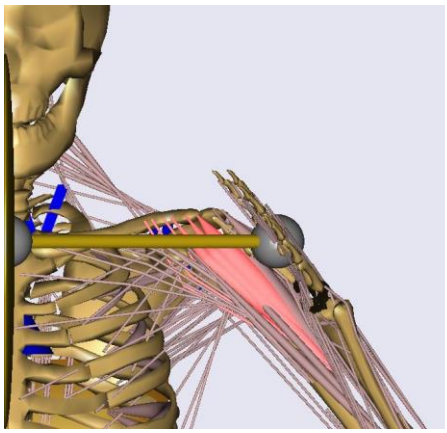

Figure 89 - Six fibres of anterior deltoid

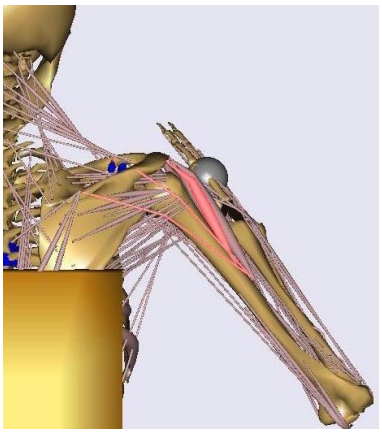

Figure 90 - Three fibres of posterior deltoid

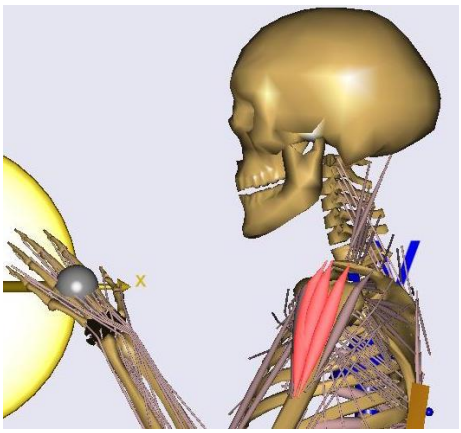

Figure 91 - Three fibres of medial deltoid

- The *trapezius* muscle is divided into two parts directly in *AnyBody human body model*:
    - The *scapular trapezius* is formed by six fibres and attached to the *scapula*.
    - The *clavicular trapezius* is again composed by six fibres but linked to the *clavicle.*

- The remaining muscles analysed are wide and divided into several fibres; they have been already described in the subchapter 2.3.1 Shoulder muscles:

    - *Infraspinatus*.
    - *Latissimus dorsi*.
    - *Serratus anterior.*
    - *Subscapularis.*
    - *Teres major.*

  In this case summing the forces of the several fibres, composing the whole muscles, doesn't make sense, because these muscles have a big area and each part of them can work in a different way during the cranking cycle, and particularly the fibres don't attach in the same tendon or in close positions, so the sum can't be considered a good approximation as for the elbow muscles.
  Anyway we'll provide a plot per muscle, leaving separated the fibres composing them.

Let's start plotting the deltoid muscle force:

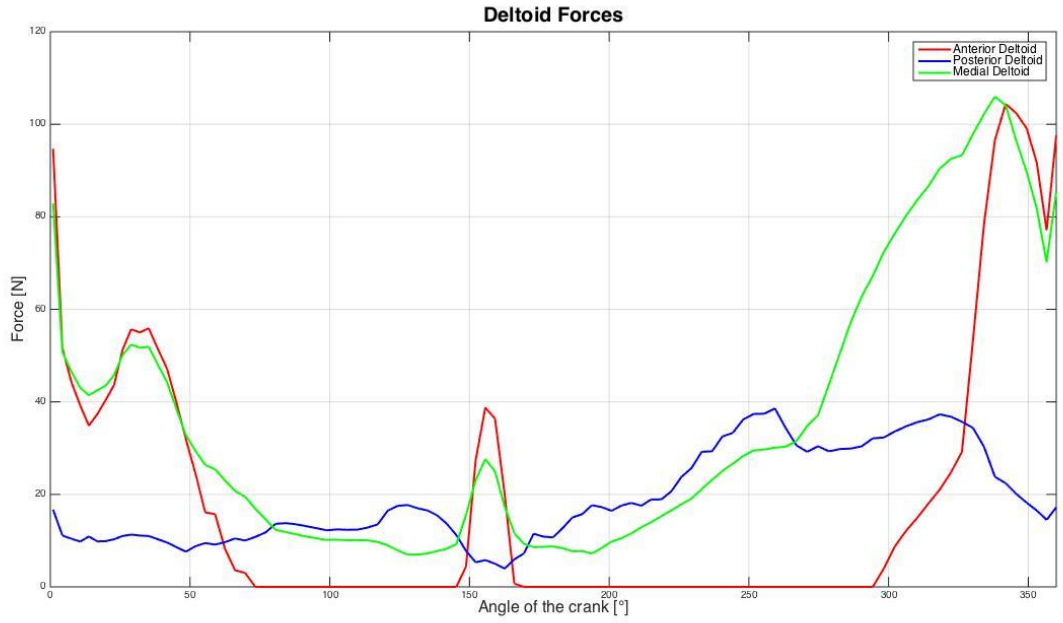

Figure 92 - Deltoid force in function of the crank position: in red the anterior deltoid, in blue the posterior deltoid and in green the medial deltoid

The Figure 92 contains the data regarding the three parts of the deltoid: anterior (in red), posterior (in blue) and medial (in green).

The second muscle described and divided into two parts is the *trapezius*:

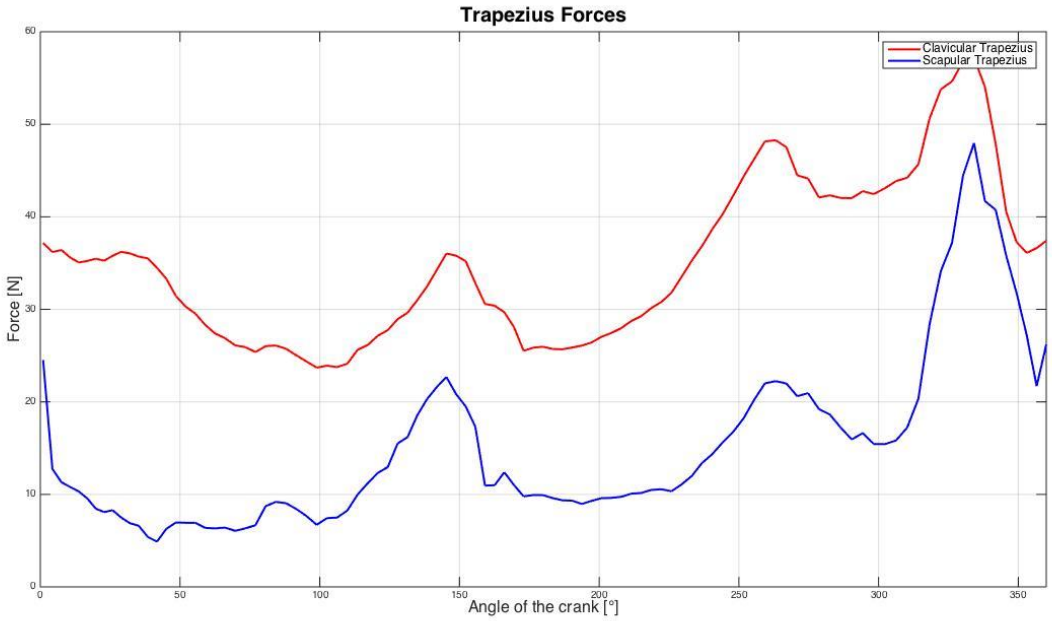

Figure 93 - Trapezius force in function of the crank position: in red the clavicular trapezius and in blue the scapular trapezius

The shapes of the forces of the two parts of the trapezius are similar: also in this case we summed the actions of the fibres composing both sections.

From the Figure 94 to the Figure 98 we will display the data relative to the muscles listed before:

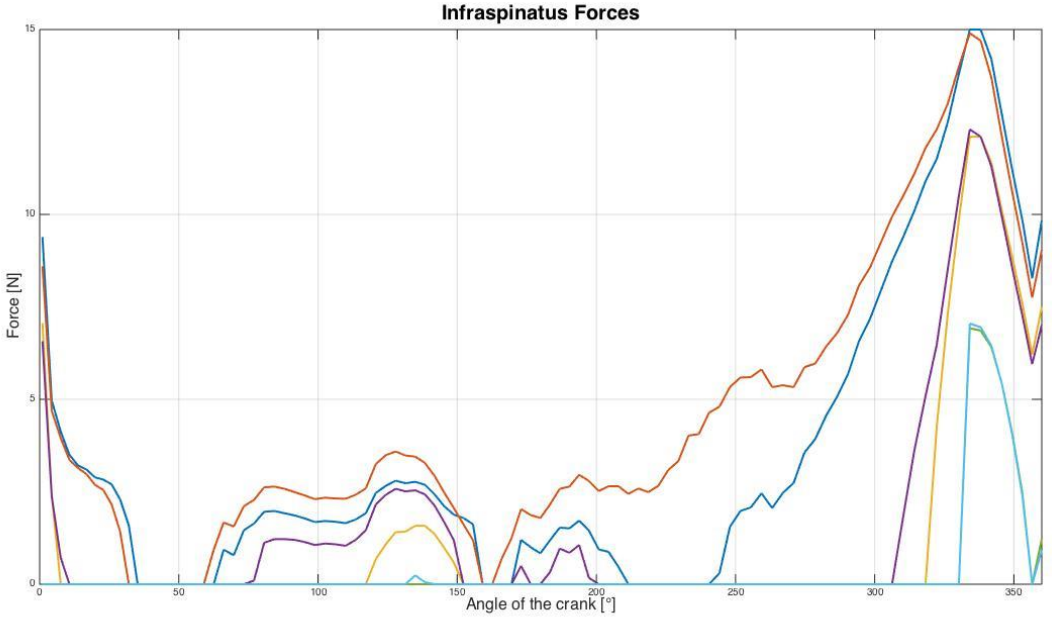

Figure 94 - Infraspinatus fibres forces

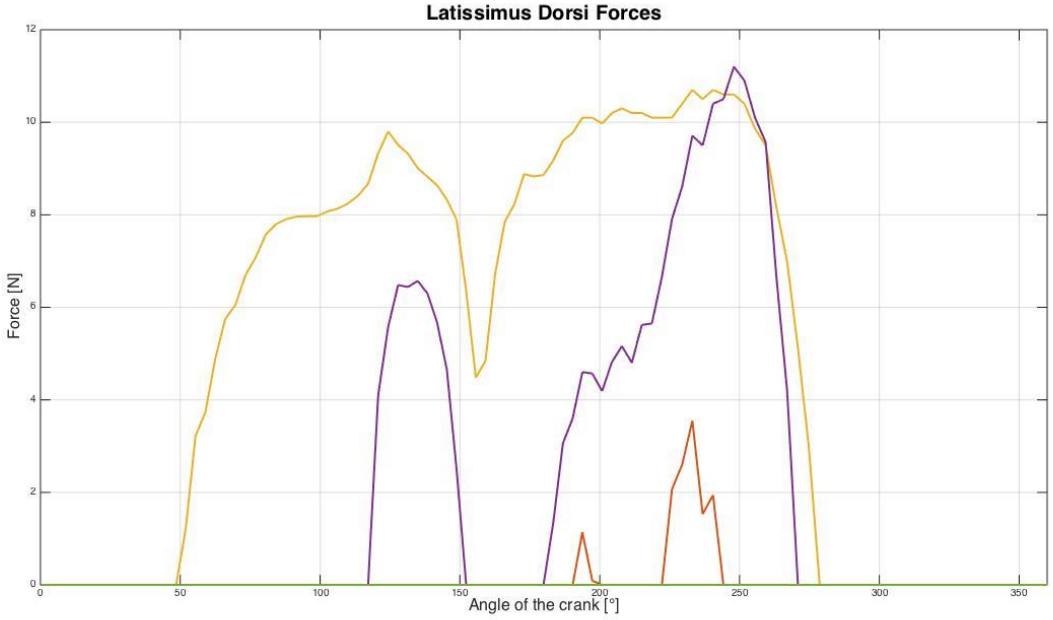

Figure 95 - Latissimus dorsi fibres forces

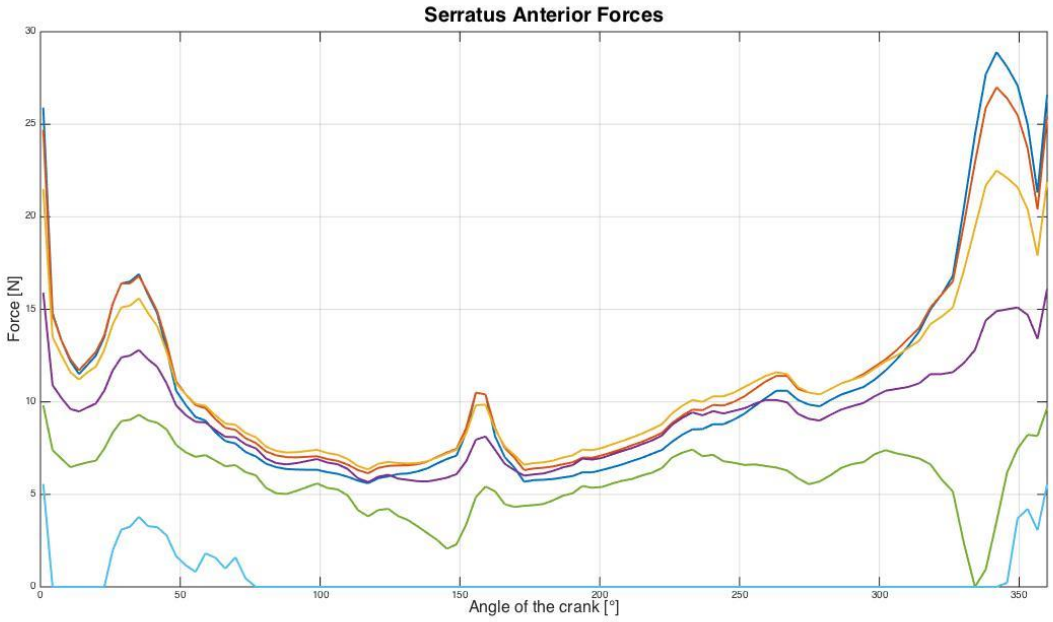

Figure 96 - Serratus anterior fibres forces

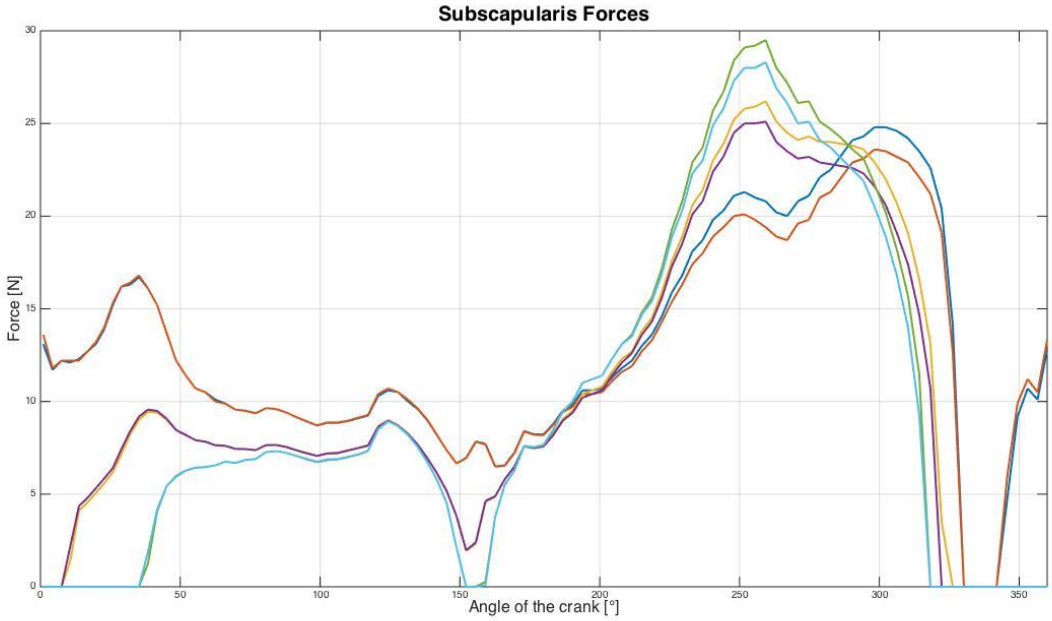

Figure 97 - Subscapularis fibres forces

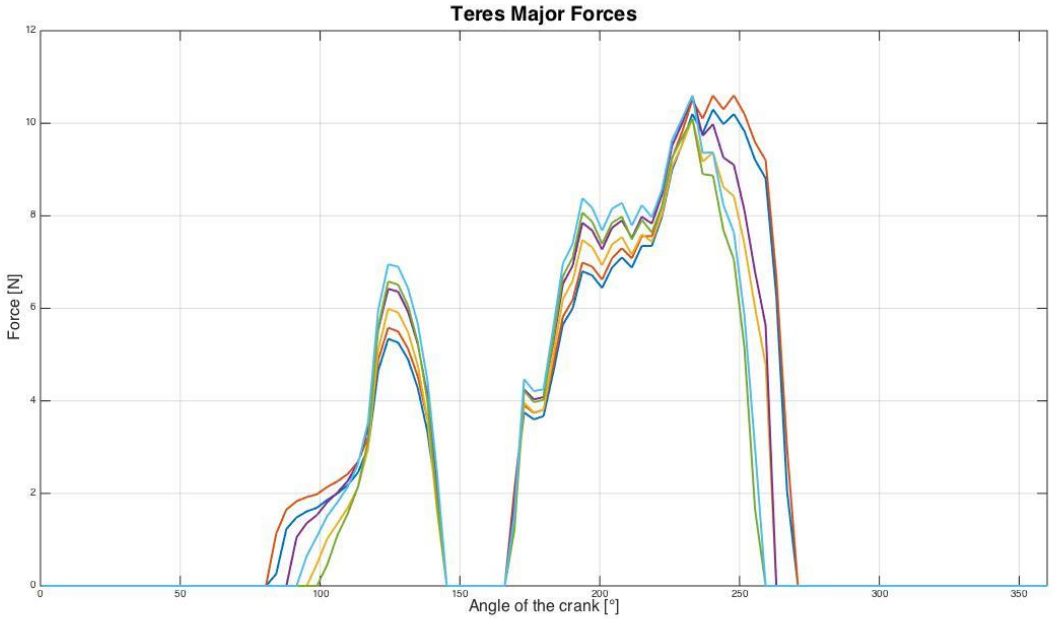

Figure 98 - Teres major fibres forces

The only consideration that can be done on the graphs contained in Figure 94, Figure 95, Figure 96, Figure 97 and Figure 98 is about the similarity of the forces exerted by each fibre; i.e. if in the same image the coloured curves (representing the forces of the several fibres constituting the whole muscle) have a similar behaviour, it means that the single parts are contemporary contracting or relaxing, therefore the muscle's functioning can be approximated as the one of a single fibre, whose force is the sum of the forces generated by the several parts.

7. MODELS COMPARISON

The graphical results, acquired and shown in the previous parts of the thesis, will be compared and examined in this chapter.

In particular we'll dwell on the comparison between the 2D and 3D models' kinematics, dynamics and muscular studies. We will take into account also the plots derived from the vision system and compare them to the ones resulting from the *AnyBody* model.

7.1 Kinematics

In the kinematics analysis, especially, we can contrast the 2D, 3D and also the experimental data, in order to have an index of the effectiveness of the approximations utilized to create the models.

Particularly we are going to compare the joints movements, or better their projections.

Let's start showing the elbow flexion/extension:

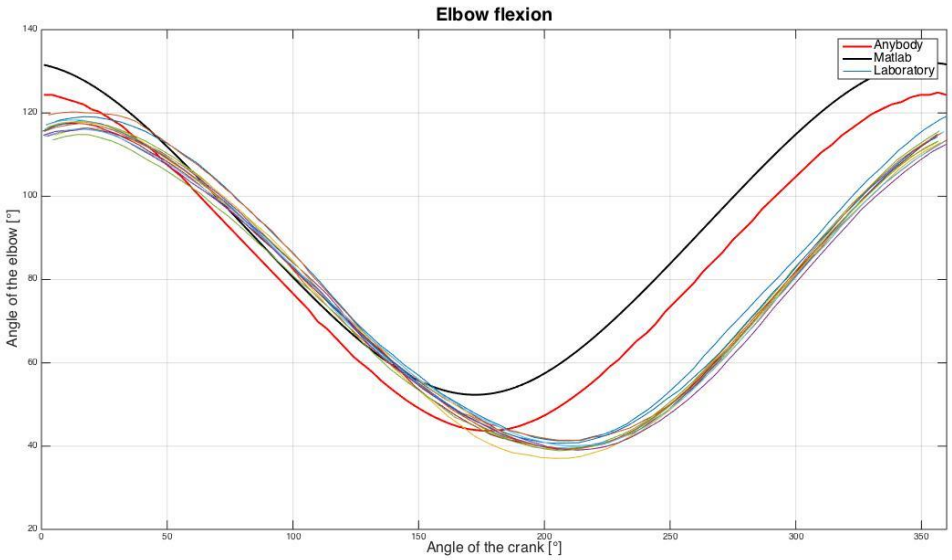

Figure 99 - Comparison of elbow flexion angles: in red the AnyBody result, in black the MATLAB one and with coloured lines the experimental data

In this case the three diagrams plotted are similar, this is due to the fact that the elbow articulation is two-dimensional, and therefore it's more easily reproducible in a model, even in 2D. Moreover, also in 3D, the elbow joint is directly connected to the handle through the forearm, consequently its angle can't change so much deriving directly from the crank's position.

It's a different matter for the shoulder flexion/extension:

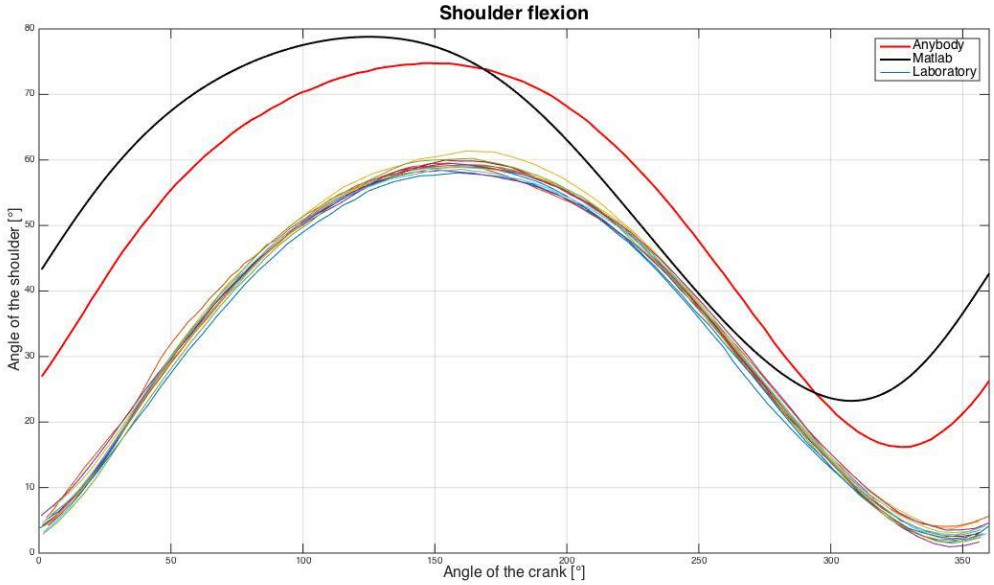

Figure 100 - Comparison of shoulder flexion angles: in red the AnyBody result, in black the MATLAB one and with coloured lines the experimental data

In this case the analysis is much more difficult than in the previous situation; the shoulder is a complex articulation that even in 3D can be described just with a lot of different degree of freedom. The complete movement is not only given by the rotation of the *humerus* inside the *glenohumeral cavity*, but also by the relative movements between *scapula* and *clavicle* bones.

The evident differences between the graphs are given by the approximations, or rather, neglects of a large part of the information regarding the shoulder.

Theoretically we should have started from markers positions and use them to move the *AnyBody* model thanks to the vision system's information and to obtain a very good approximation of the real movement; this is not possible due to the low number of reflecting markers used in the *LARIN* laboratory.

With the *AnyBody* simulation realized, we obtained a result (Figure 100: red curve) that it's more similar to the 2D model (Figure 100: black curve) than to the real behaviour of the shoulder articulation (Figure 100: coloured curves); another reason is the presence of constraints on the

spine in order to fasten the human body to the backrest of the 3D model and limit the use of the muscles of the trunk; this fact is creating a more simple situation, which however is not fully comparable to reality, because indirectly it adds constraints on the shoulder bones, and then restricts the joint movements.

The last analysis about kinematics has been done regarding the shoulder abduction/adduction:

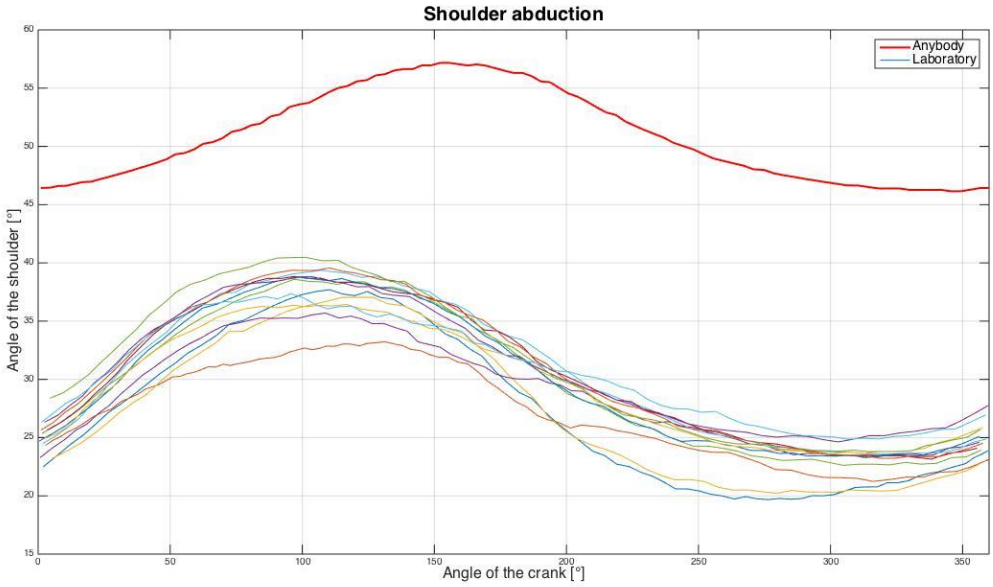

Figure 101 - Comparison of shoulder abduction angles: in red the AnyBody result and with coloured lines the experimental data

In this case the difference between the simulated motion and the real one is even clearer, the main problem with the abduction/adduction movement is that it's not really linked to the motion of the crank, that is in the plane X-Y, or better it is less influenced by the handle position, it depends more on the way of cranking of the subjects.

Anyway the width of the range of motion of the two graphs is similar and comparable, also the shape of the curves; the fact that the red diagram (*AnyBody* model) is positioned on the plot a lot upper than the experimental data curve, may be due to the fact that the starting position (i.e. the initial conditions) is different from the real one, because differently from the elbow and shoulder flexion/extension is not directly depending on the handle position. The abduction/adduction movement is in the frontal plane of the body, where the position of the crank changes just in one coordinate, on the contrary the shoulder flexion/extension is in the sagittal plane, the exact plane of motion of the crank, this is the main reason why the abduction is less depending on the cranking activity.

7.2 Dynamics

In this subchapter we'll compare the results of the dynamics studies in 2D and in 3D, particularly starting from the same forces, we'll analyse the differences of the generated torques.

In the dynamic case it will be even more complex analysing the diagrams and extract some considerations.

The Figure 102 shows the forces applied in the two models.

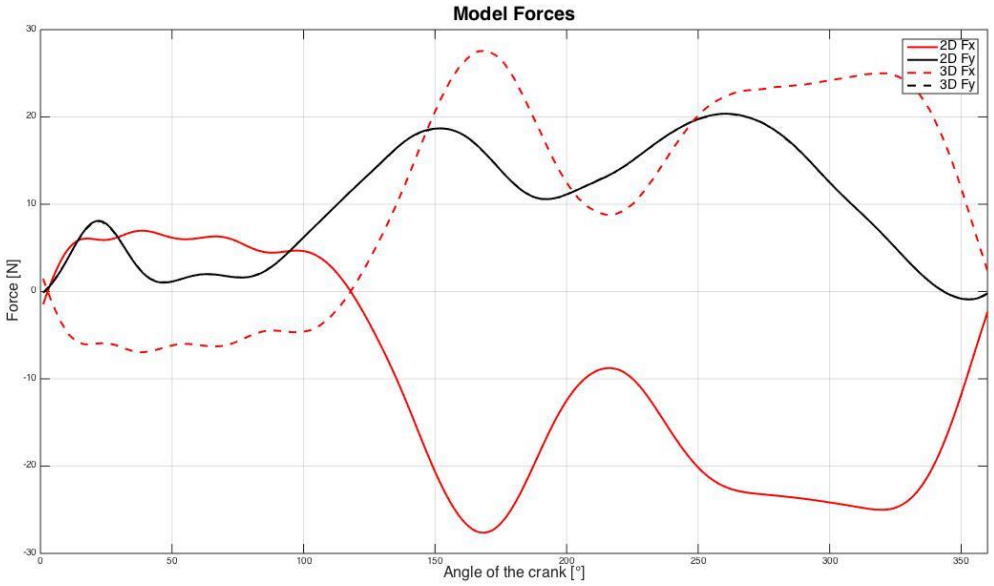

Figure 102 - Comparison between handle forces used in the models

In the Figure 102 it's possible to notice that the different reference systems of the two models (*MATLAB* and *AnyBody*) has effects on the forces we set as input of the two analysis. The sign of the two F_X (continue and dashed red line) is opposite, while the two F_Y (continue and dashed black line) are exactly the same.

From these force data, thanks to the inverse dynamics method we obtained the torques generated at the shoulder and elbow (Figure 103); like outlined before, the complex 3D analysis provided us the three components of the torque at the shoulder, whereas in the elbow case, having only one degree of freedom, just one torque resulted.

For what we need in this thesis we decided to plot the flexion/extension, abduction/adduction shoulder torques and the elbow moment (3D) in one diagram, together with the two torques resulting from the *MATLAB* dynamic study.

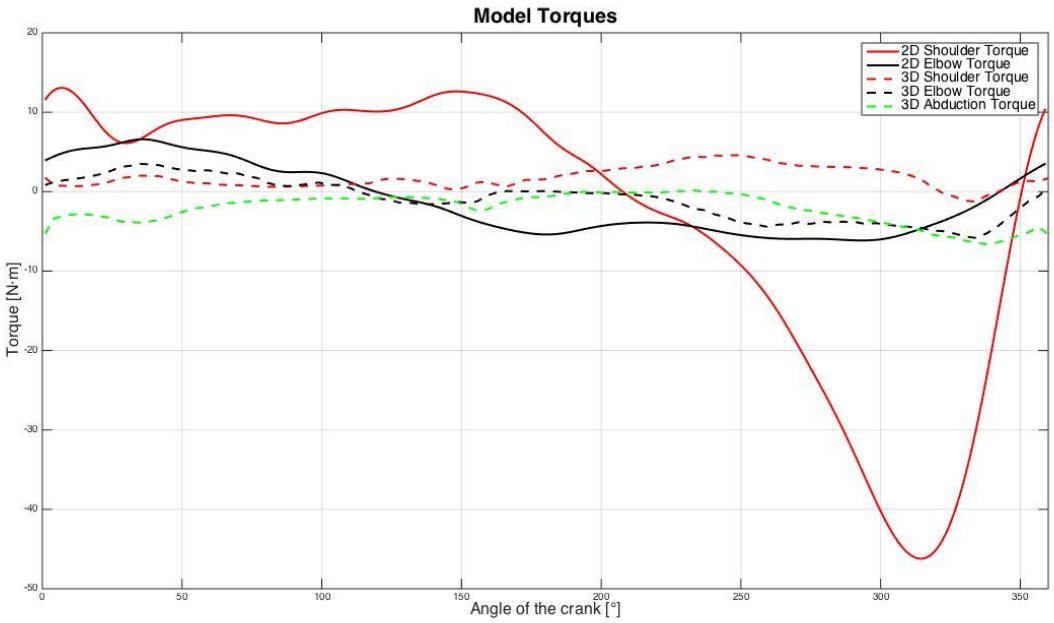

Figure 103 - Torques comparison

In Figure 103 the results of the 2D analysis are displayed with continue lines: elbow (black) and shoulder (red); on the contrary the 3D torques are represented with dashed lines: elbow (black), shoulder flexion (red) and shoulder abduction (green).

Obviously, as in the force image (Figure 102), also in this case the different configurations of the reference frames have to be taken into account, to better contrast the results we have represented the torques of Figure 103, as if they had the same coordinate reference system.

It's really hard to compare the results obtained, especially for what concerns the shoulder joint; at the elbow we can see that the two torques (black curves) are similar in shape, intensity and also sign so the approximations done by the 2D can be considered as valid.

Analysing the shoulder articulation we notice really big differences not only in the amount of torque generated, but also in the sign of it; from these results we can say that it's really hard to simplify the shoulder joint in 2D, at least for what concern the dynamic problem.

Anyway between the two methods there are a lot of approximations and differences that, calculation after calculation, can affect a successive confrontation of the results; the main estimations refer to: the inertial parameters, the angular joint velocities ($\dot{\alpha}$ and $\dot{\beta}$) and accelerations ($\ddot{\alpha}$ and $\ddot{\beta}$), but especially the lack of information about the shoulder and its limitation of movements.

So far we analysed only one test of the same subject at a mean power of 40 W, the Figure 104 will show the changes of the forces components during the cranking cycle in three different tests at power of 0, 40 and 80 W.

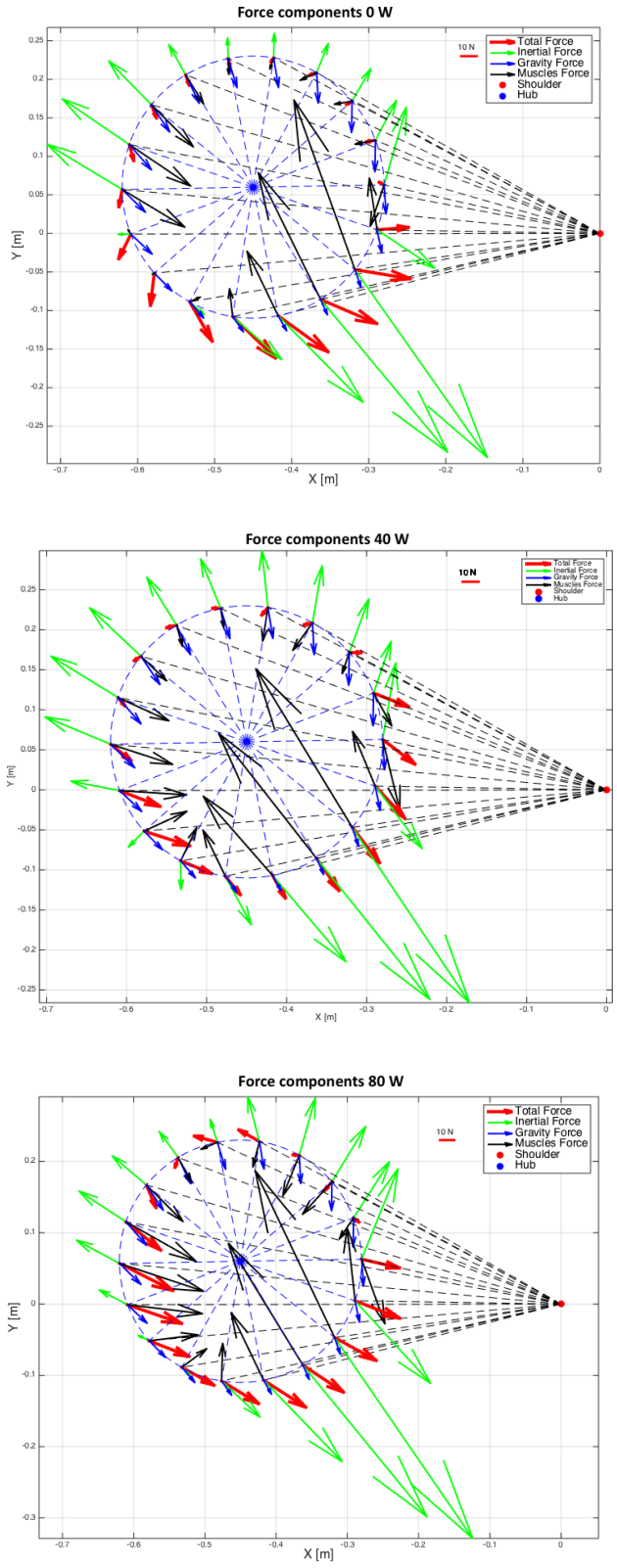

Figure 104 - Force components of tests at 0, 40 and 80 W: in red the total force, in blue the gravity component, in green the inertial part and in black the muscular force

7.3 Muscle forces

The last subchapter contained in the chapter 7. MODELS COMPARISON, regards the muscle forces analysis; the muscles examined in the two-dimensional *MATLAB* code are just the ones crossing the elbow, so also from the *AnyBody* output we chose just the main four elbow muscles: *triceps brachii, biceps brachii, brachialis* and *brachioradialis*.

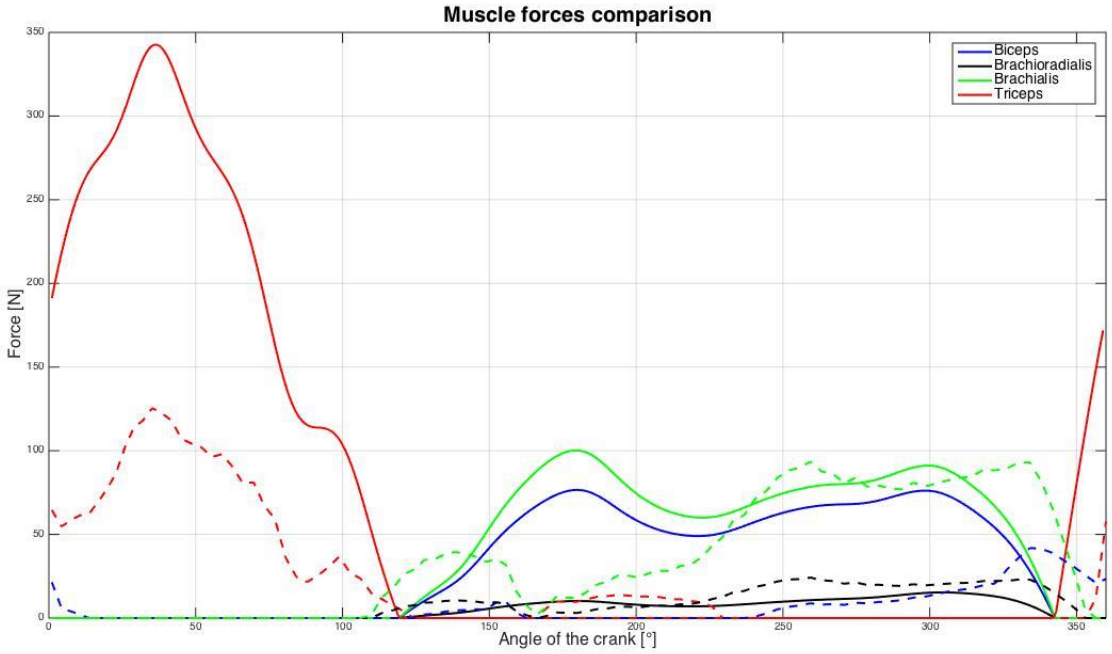

Figure 105 - Muscle forces comparison between the two models

The Figure 105 supply a useful analysis to evaluate the level of approximation of the 2D model, we plotted the muscular forces in function of the crank position, in order to evaluate their activities during the pedalling cycle.

The continue lines represent the *MATLAB* results, whereas the dashed curves stand for the 3D outputs; the different colours display the four muscles, in particular: the red is the *triceps brachii*, the blue the *biceps brachii*, the green the *brachialis* and the black the *brachioradialis*.

Analysing the graph we can say that the period of activation/utilization of the muscles is more or less the same in both models, the differences are in the intensity of forces, especially in case of triceps and biceps muscles.

This is probably due to the fact that both are biarticular muscles: i.e. they are composed by two (biceps) or three (triceps) muscular heads and in the first case both heads attach to the scapula,

for the latter just one attach to that bone; anyway the activities and forces of these two muscles affect not only the elbow joint, but also the shoulder one.

When we have minimized the overload function in *MATLAB* to obtain the muscular forces, we considered all the four muscles as they were acting just on the elbow, this may be correct for the *brachialis* and *brachioradialis* which actually act only on the elbow articulation, but not for *biceps* and *triceps*, like just explained.

Another reason, as anticipated in the chapter 5.6 Muscles forces, can be that the muscles considered in 2D are not the only muscles that actually cross the elbow, and even some muscles, whose main activities are linked to the wrist, can indeed influence the motion of the elbow (Figure 88).

Regarding the muscle analysis we supposed a lot of parameters: *PCSA, specific force* and *moment arm*, all these assumptions obviously influenced the result of the 2D study, especially considering that in *AnyBody* each muscular fascicle has its own set of parameters (*PCSA, specific force* and *moment arm*). The last two problems that may affect the comparison are: the fact that anyway the results of the inverse dynamics (generated torques) are different, this clearly changes the force intensity of the muscles considered; another important thing is that, for instance, contrary to popular belief, the biceps brachii is not the most powerful flexor of the forearm, its function is primarily as a powerful supinator of the forearm; in the 2D model we select as a factor of minimization the ratio between the muscular forces and the maximum tensions generable, without using a *weight parameter* in order to select how much the single muscles take part in the total action produced, considering their main normal function. Consequently the dissimilarities represented in Figure 105 can be attributed to all the causes listed above.

From the observation of the Figure 105 we can also examine the coactivation of some muscles during the handcycling, this is not present in 2D analysis because we select the sign of the torque as the discriminant factor to activate flexor or extensor muscles.

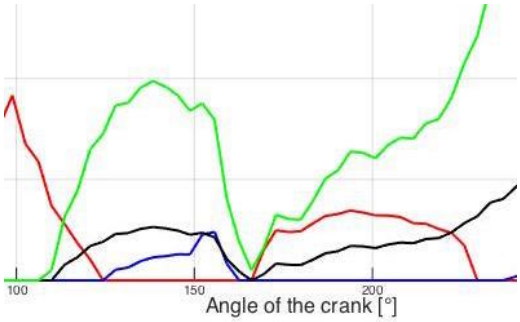

Figure 106 - Detail of the coactivation of some muscles in 3D result

The last confirmation about the muscles can be done comparing the experimental EMG and the results obtained at the elbow joint in *AnyBody*, for *biceps* and *triceps brachii*.

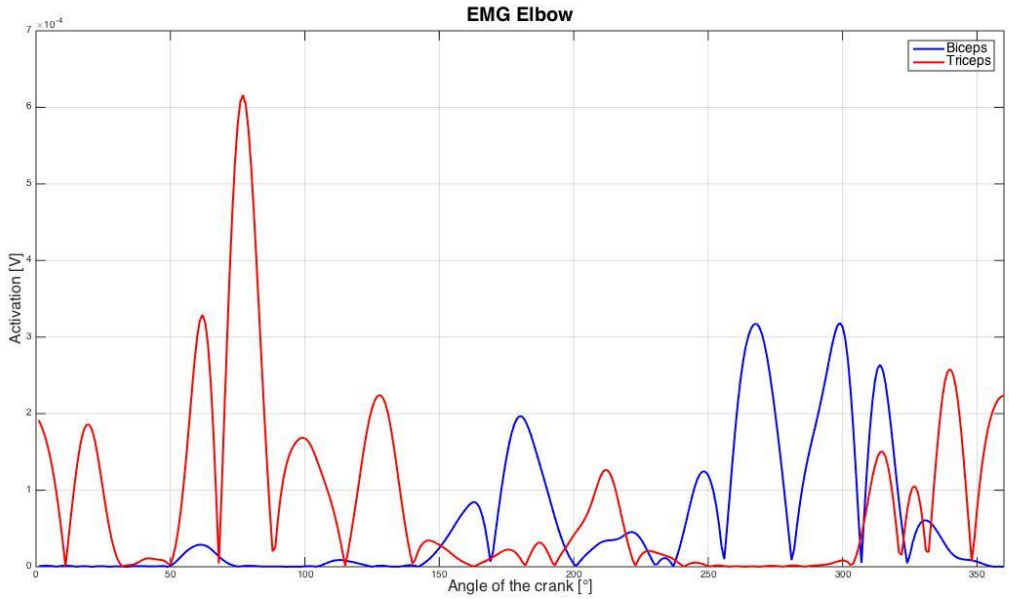

Figure 107 - EMG of biceps (blue) and triceps (red) in function of the crank position

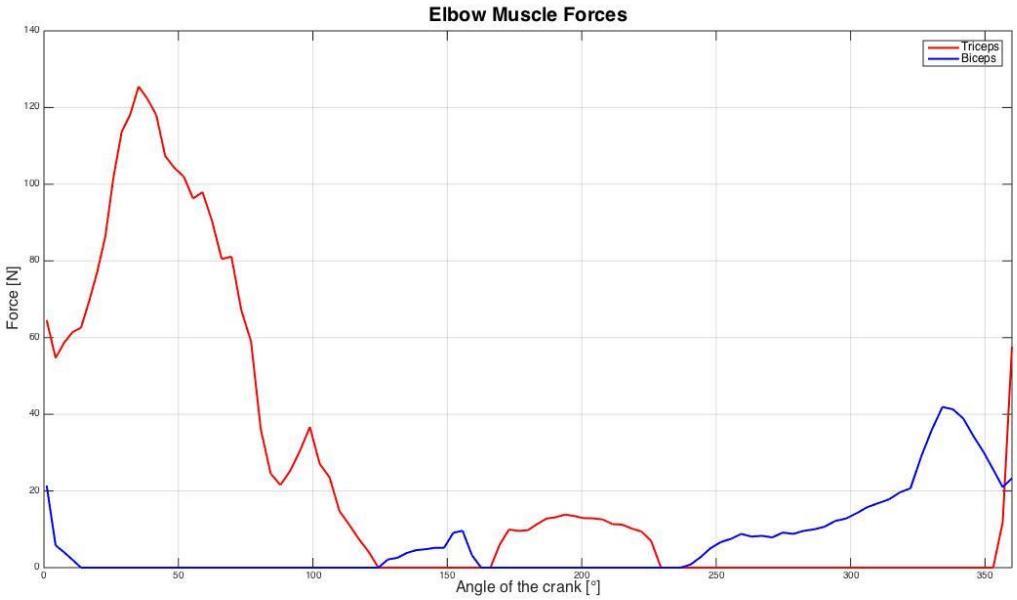

Figure 108 - Biceps (blue) and triceps (red) forces in function of the crank position

In Figure 107 and Figure 108 we can compare the EMG experimental data with the 3D results of the muscles analysis and we can say, that for what concerns the elbow articulation, there is a good correspondence between the real muscle activations and the one simulated in *AnyBody.*

An analogous comparison can be done with the other EMG data collected, regarding the three parts component the *deltoid* muscle: anterior, middle and posterior.

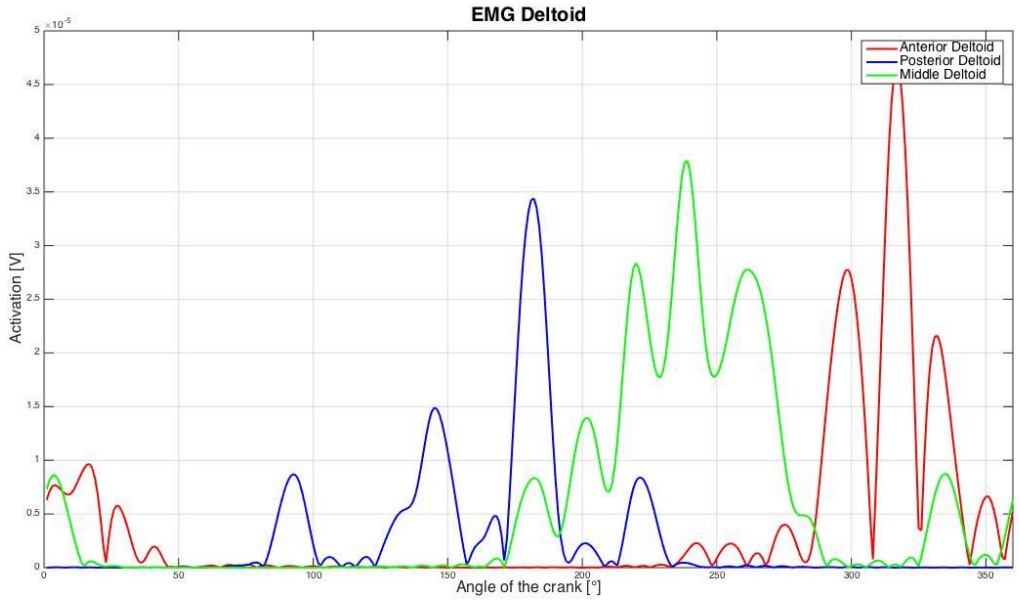

Figure 109 - EMG of anterior (red), posterior (blue) and middle (green) deltoid in function of the crank position

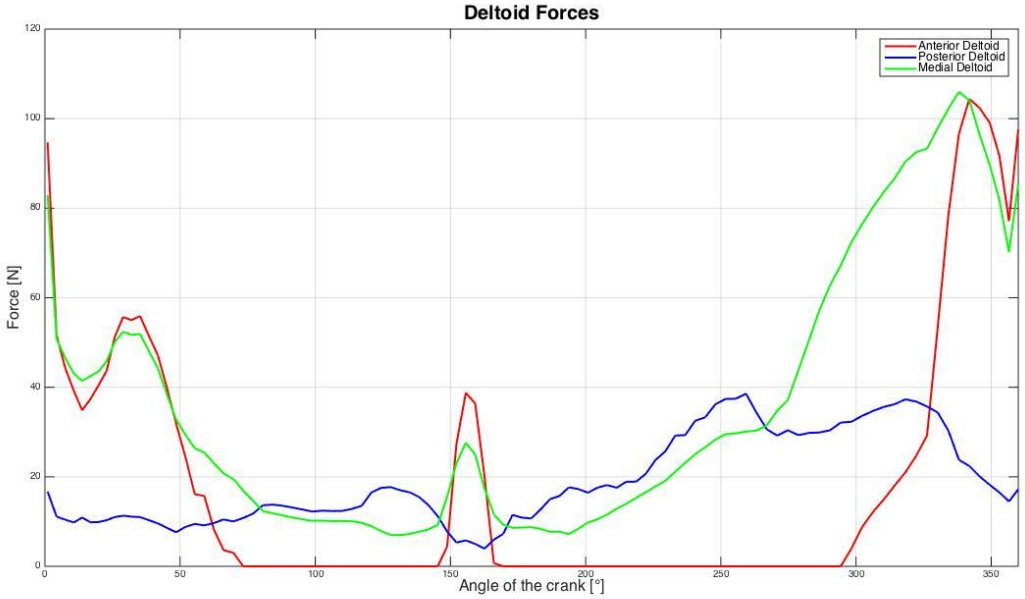

Figure 110 - Anterior (red), posterior (blue) and middle (green) deltoid forces in function of the crank position

In Figure 109 and Figure 110 we can see a good correspondence between the real *deltoid* behaviour and the 3D simulation; the approximation is less valid than the elbow one, because of the reasons that we've listed previously regarding the shoulder motion simplifications adopted, particularly it must be said that the deltoid is the principle abductor muscle of shoulder.

8. CONCLUSIONS & FUTURE DEVELOPMENTS

In this chapter we'll draw the conclusions of the whole work described in this thesis, particularly we'll provide an evaluation of the two models elaborated, finding which one is more adapt to a simplified study of the human handcycling activity. Afterwards we'll supply some advices and plausible improvements that could be useful in a future development of the work.
From the results obtained we can say that:

- The 3D *AnyBody* model created can provide a good approximation of the real movement acquired in the laboratory test, this is confirmed by the kinematics from the collected markers position and muscular EMG; with some improvements it will faithfully reproduce the real behaviour of the upper limb.

- The 2D *MATLAB* model can be considered a usable approximation for what concern the elbow kinematics and muscle analysis; in shoulder case, like outlined several times before in the thesis, the two-dimensional model contains simplification that are too important to maintain a good description of the articulation motions.

- Comparing the two models we can thus say that to have a real complete prospect of the kinematics, dynamics and muscular activities of the upper limb, we need a complete 3D study like the one that a complex software as *AnyBody* can provide.
  The developed 2D *MATLAB* model is a starting point for future developments in studying the human body biomechanics, especially regarding the elbow articulation, but it's too superficial to describe completely and thoroughly the upper limb behaviour.

The advices that, at the end of the work carried out, could be proposed to improve the results of the two models are:

- Firstly and most importantly, we should increase the number of markers applied on the subject, in order to obtain more information from the vision system, and move properly the 3D model, thanks to the potentialities of *AnyBody*.

- We should consider the wrist articulation and its muscles, also in 2D model, even if it would add some degree of freedom, especially in muscular analysis it's not totally negligible.

- In order to obtain a complete set of the forces exchanged at the handle we should add another strain gauge, so as to have not only F_X and F_Y but also F_Z.

- Talking about the 2D *MATLAB* model, if we'd like to achieve a better approximation of the real human body, we should have more in-depth studies on muscles features: especially on their *PCSA* and *moment arm*, in order to use several muscles also in the elbow study.

- In case of disabled patients, we should find a way to estimate their physical parameters similar to the anthropometric tables used with healthy people. Also in case of trained people we should find a way to discover the muscular features, that can't be considered as the average ones of the population.

- Have a big group of subjects different in age, sex and size, in order to better appreciate the results and try to find some common features, or some characteristics clearly depending on each subject particularity.

- Lastly, like outlined in chapter 7.3 Muscle forces, we should consider not only the minimization of the overload function, depending on the maximum forces generable, but also somehow a possibility of weighting the action of each muscle depending on the degree of freedom we are taking into account (i.e. if a muscle takes part in several actions in the body motion, we should weight its force depending on its main function).

9. REFERENCES

[1] *http://teachmeanatomy.info/upper-limb/*

[2] *http://en.wikipedia.org/wiki/*

[3] G. Legnani; G. Palmieri, 2016 - ***Fondamenti di Meccanica e Biomeccanica del Movimento*** - *Città Studi*

[4] A.I. Kapandji, 2011 - ***Anatomia funzionale I - Arto superiore*** – *Monduzzi*

[5] David A. Winter, 2009 - ***Biomechanics and Motor Control of Human Movement, Fourth Edition*** - *University of Waterloo, Ontario, Canada*

[6] *http://www.btsbioengineering.com/it/prodotti/cinematica/bts-smart-dx/*

[7] G.C. Santambrogio; A. Aliverti; G. Andreoni; C.Gabardi, 1996 - ***Analisi Motoria: Esercizi Svolti e Commentati*** - *Progetto Leonarso*

[8] Vickey Goosey-Tolfrey, 2010 - ***Wheelchair Sport: A Complete Guide for Athletes, Coaches, and Teachers*** - *Loughborough University*

[9] Arnaud Faupin, PhD; Philippe Gorce, PhD; Christophe Meyer, MS, 2011 - ***Effects of type and mode of propulsion on hand-cycling biomechanics in nondisabled subjects*** - *journal od Rehabilitation Research & Development Volume 48, 9, 1049-1060*

[10] U. Arnet; S. van Drongelen; M. Schlüssel; V. Lay; L. H. V. van der Woude; H. E. J. Veeger, 2014 - ***The effect of crank position and backrest inclination on shoulder load and mechanical efficiency during handcycling*** - *Scandinavian Journal of Medicine & Science in Sports 25, 386-394*

[11] Marco Ometto, 2010 - ***Sistemi e modelli per la biomeccanica del corpo umano*** - *Tesi di dottorato di ricerca in meccanica applicata, Università degli studi di Brescia*

[12] Giovanni Legnani, 2003 - ***Robotica industriale*** - *CEA*

[13] *http://it.mathworks.com/*

[14] Wendy M. Murray; Thomas S. Buchanan; Scott L. Delp, 2002 - ***Scaling of peak moment arms of elbow muscles with upper arms bone dimensions*** - *Journal of Biomechanics 35, 19-26*

[15] Arnaud Faupin; Philippe Gorce; Eric Watelain, Cristophe Meyer, Andre Thevenon, 2010 - ***A Biomechanical analysis of Handcycling: A Case Study*** - *Journal of Applied Biomechanics 2, 240-245*

[16] Wendy M. Murray; Thomas S. Buchanan; Scott L. Delp, 2000 - ***The isometric functional capacity of muscles that cross the elbow*** - *Journal of Biomechanics 33, 943-952*

[17] Rositsa Raikova, 1996 – ***A model of the flexion-extension motion in the elbow joint*** - ***some problems concerning muscle forces modelling and computation*** - *Journal of Biomechanics Volume 29, 763-772*

[18] Pascale Pigeon; L'Hocine Yahia; Anatol G. Feldman, 1996 - ***Moment arms and lengths of human upper limb muscles as function of joint angle*** - *Journal of Biomechanics Volume 29, 10, 1365-1370*

[19] W. Maurel; D. Thalamann; P. Hoffmeyer; P. Beylot; P. Gingins; P. Kalra; N. Magnenat Thalmann, 1996 - ***A Biomechanical Musculoskeletal Model of Human Upper Limb for Dynamic Simulation*** - *Computer Animation and Simulation - Springer-Verlag*

[20] *http://www.anybodytech.com/*

[21] Paul M. Smith; Mark L. Chapman; Kathryn E. Hazlehurst; Mark A. Goss-Sampson, 2008 - ***The influence of crank configuration on muscle activity and torque production during arm crank ergometry*** - *Journal of Electromyography and Kinesiology 18, 598-605*

[22] Sarah R. Sullivan; Noshir A. Lagrana; Sue Ann Sisto, 2005 - ***Multibody computational biomechanical model of the upper body*** - DETC2005-84809, *ASME 2005 International Design Engineering Technical Conferences & Computers and Information in Engineering Conference, September 24-28, 2005, Long Beach, California*

[23] http://wiki.anyscript.org/

AKNOWLEDGEMENTS

In conclusione di questo lavoro di tesi sento il dovere, ma soprattutto ho il piacere, di rivolgere un pensiero e un ringraziamento ad alcune persone che hanno fatto in modo che potessi intraprendere questo lungo cammino formativo e mi hanno accompagnato fino al suo compimento. Inizierei perciò ringraziando il professor Giovanni Legnani, mio relatore di tesi che mi ha seguito e aiutato durante tutto il percorso che ha portato alla stesura di questo lavoro, ma anche responsabile del progetto di doppia laurea che ha fatto sì che potessi vivere a Parigi, per sei mesi, un'esperienza indimenticabile. Rivolgo inoltre un ringraziamento sincero anche ai dottorandi Majid e Ghazaleh, che mi hanno supportato nel lavoro di tesi svolto.

Un pensiero va anche ad altri docenti che nei cinque anni passati hanno fatto in modo che potessi partecipare a due importanti progetti all'estero: vorrei quindi ringraziare i professori Antonio Visioli e Manuel Berenguel Soria per i sei mesi trascorsi in Spagna e le professoresse Véronique Perdereau e Viviane Pasqui, oltre al già citato Giovanni Legnani, per il periodo passato in Francia.

Un enorme ringraziamento va a tutti i miei familiari; ma il più grande, il più sentito, va ai miei genitori e mia sorella, che mi hanno sempre supportato e sopportato (e anche finanziato) durante questi lunghi anni di studio e sostenendomi costantemente hanno fatto in modo che potessi migliorarmi come studente, come uomo e come figlio, crescendo giorno dopo giorno.

Desidererei anche citare, ma soprattutto dire grazie, a tutti i compagni di studio che mi hanno accompagnato lungo questo incredibile cammino condividendo con me difficoltà e gioie; un pensiero speciale va quindi a Jac, Manni, Frax, Fabius, Pasi, Tine, Fero e Cappis, senza i quali questa esperienza non sarebbe stata così divertente e indimenticabile.

Ultimi, ma non meno importanti, vorrei ringraziare i miei amici, i soliti, gli storici compagni di mille avventure: Dassa, Dawson, Pisi, Zazza e Ema che ci sono sempre stati, in ogni momento, in tutti questi anni.

Infine rivolgo un pensiero altrettanto sincero, in questo giorno speciale, alla mia ragazza Serena e a tutte le persone che gioiranno con me nel vedermi tagliare questo importante traguardo.

UNIVERSITÀ DEGLI STUDI DI BRESCIA
UNIVERSIDAD DE ALMERÍA

Resumen/Abstract

The aim of the thesis consists in creating an upper limb biomechanical model useful for analysing the handcycling activities.In particular two models have been realized: one 2D and one 3D, to verify which was the best compromise between simplicity and completeness of representation.

The two-dimensional model has been developed in *MATLAB* software environment; instead the 3D one has been accomplished thanks to the *The AnyBody Modeling System:* a musculo-skeletal modelling system for biomechanical simulations, that analyses the reactions within the human body or between the human body and an environment.

Thanks to the agreement between the University of Brescia and the hospital *"Domus Salutis"* in Brescia, it was possible to use advanced instrumentations and collect data from experimental trials, in order to produce the sofyware models.

Doble TítuloUNIBS-UAL

Mechatronics for Industrial Automation

Ingegneria dell'Automazione Industriale

Grado en Ingeniería Electrónica Industrial

Curso 2015/2016